MSc Thesis

Dynamic simulation of pantograph catenary interaction by means of finite elements and a reduced order model

Ferd Smits

TU Delft

MSc Thesis

Dynamic simulation of pantograph catenary interaction by means of finite elements and a reduced order model

by

Ferd Smits

to obtain the degree of Master of Science
at the Delft University of Technology,
to be defended publicly on Friday April 13, 2018 at 13:00.

Student number:	4136365	
Project duration:	June 7, 2017 – April 13 , 2018	
Thesis committee:	Dr. ir. R. Happee,	TU Delft, chairman
	Dr. ir. D. de Klerk,	TU Delft, supervisor
	Dr. B. Shyrokau,	TU Delft
	Ir. R. Volgers,	Ricardo Nederland B.V.

TU Delft

Preface

Before you lies the Thesis: ”Dynamic simulation of pantograph catenary interaction by means of finite elements and a reduced order model”. It has been written to fulfill the graduation requirements of the master Mechanical Engineering, track Vehicle Engineering at the Technical University Delft.

This work is the result of the thesis assignment executed at Ricardo Nederland BV for the department Infra Interface. During which I have developed a simulation methodology for Pantograph-Catenary interaction. This simulation methodology has been validated according to European standard EN50318:2002. And will therefore provide a useful tool for further use by Ricardo Nederland BV. Throughout this work several subjects are discussed. From numerical analysis, to transient solution procedures, up to model order reduction methods. It has been a pleasure to search and identify useful techniques and to apply these techniques onto my simulation model.

This work would not have been possible without the input of several people. I would like to thank my company supervisor Ramon Volgers, who has provided me with his insights and reviewed the work, thereby bringing this work to the next level. Moreover, I thank my TU Delft supervisor Dennis de Klerk for his input and for guiding me through this project by providing insights and every now and again steering me in the right direction. Lastly, I thank Eline Kruithof, Roy Smits and Arnout Zwartbol for reviewing the work.

Ferd Smits
Delft, March 2018

Abstract

As train speeds continue to increase, the dynamics of the interface between train and infrastructure is an increasingly important factor in current collection performance. European legislation prescribes that assessment of the quality of the current collection system shall be performed according to measurements and/or simulations. Due to the increase in computer power in recent years, simulations have become increasingly attractive as an addition or replacement to real line measurements.

The goal of this work is to judge current collection quality through dynamic time-history simulations of the pantograph-catenary interface. First, the current state-of-art is reviewed, subsequently a simulation approach is determined, applied and tested to the norm EN50318:2002. Based on simulation results and comparison to measured values, the simulation approach is validated according to the norm EN50318:2002.

As a consequence of the large finite element models used in the valid model, a method for enhancing the simulation speed without losing non-linearities is determined. Changes in solver and contact model are identified as possible improvements, as is a modal reduction of the model. In order to apply the proposed solver improvements, a test model is built in Matlab. The valid Ansys model is used to test simulation times as different contact models are used. A modal reduction approach is implemented in Matlab.

It is found that as a consequence of solver changes, simulation times may improve by up to 40%. Furthermore, contact model changes may result in improvements of up to 77%. Modal reduction, when applied to the current model, has been found inefficient due to high amounts of interface DOF with respect to the full size of the model. Therefore, no results are presented for the modally reduced system.

Non-optimized simulations currently require around 24 hours of simulation time. It is to be expected that multiple simulations need to be executed in order to simulate all possible pantograph combinations, thus performing all simulations may require days to weeks. This situation is deemed undesirable. Based on the findings in this work, it is concluded that simulation times may improve by a ratio [6:43] if solver and contact model are chosen wisely. Therewith simulation times per simulation may be reduced to 3.4 hours.

Contents

Terms

AM Attachment Mode. 35

APDL Ansys Parametric Design Language. 12

auto-correlation Cross-correlation of the field/signal with itself. 32

DCSM Dual Component Mode Synthesis. 35

DOF Degree(s) of freedom. 25, 26, 31, 34, 37, 40, 41, 55, 69, 70, 102, 104

FD Finite Difference Method. 7

FE Finite Element Method. vii, 7, 11–13, 26, 31, 32, 35, 38, 40, 47, 49, 53, 68–70

KLD Karhunen-Loève decomposition. 32

LNM Linear Normal Mode. 31

LUMPM Lumped Mass. 7, 12

MBD Multibody dynamics. 7

MD Modal Derivative. 32, 36, 37

MOR Model Order Reduction. 25–27, 29

n Array index number. 15

PCA Principal Component Analysis. 31, 32

PMOR Parametric Model Order Reduction. 32–35

POD Proper Orthogonal Decomposition. 31–33

POM Proper Orthogonal Mode. 33

POV Proper Orthogonal Value. 33

RAM Residual Attachment Mode. 30, 34–37, 40, 104

RFFB Residual-Flexible Free-Interface. 30

SVD Singular Value Decomposition. 33, 43, 44

VM Vibration Mode. 34, 36, 37, 40, 104, 105

1 General Introduction

1.1. Research Goal / Context

The current work comprises 2 parts. These parts both focus on the Pantograph-Catenary interaction problem, which is best described as a calculation of the contact forces which exist between a train's pantograph and the overhead infrastructure whilst the train moves at high velocities. Several (proprietary) simulation models exist which simulate this problem, however, none of these is currently available at Ricardo Netherlands. Due to EU Legislation incorporated in Technical specifications for Interoperability, simulations are increasingly required in train or infrastructure certification procedures. Due to the lack of such a model, the simulation work must currently be outsourced. This is a situation Ricardo Netherlands would like to change, therefore the current work attempts to create such a simulation method. Validation of the simulation model will be based on the European norm EN50318:2002. This norm contains 2 validation steps, the first being a validation by means of a reference model and reference results, the second being a validation with real measured values. The research goal is therefore formulated as follows: *Build a Pantograph-Catenary interaction simulation model, which is valid according to EN50318:2002.*

Due to the extensive amounts of time required to perform a Pantograph-Catenary simulation, the research was extended to allow for a second research goal: *To find and apply a reduction method, which reduces computational effort whilst respecting dropper slackening, non-linear sliding contact and wave propagation.*

1.2. Thesis Outline

In order to clarify the contents of this thesis and the locations of the separate subjects, an outline of the thesis is written below. Furthermore, a visual representation of the thesis can be found in figure 1.1. The outline shows the chapters and their corresponding subject. Furthermore, it shows towards which of the goals the chapter is written.

Part I of this thesis is focused on the first goal. Firstly, chapter 2 introduces the Pantograph-Catenary interaction problem and the norm EN50318:2002. Secondly chapter 3 describes the modelling process. Lastly, chapter 4 contains the simulation results and the validation according to the 2 steps of EN50318:2002. Part II of this thesis is focused on the second goal. Firstly, chapter 5 introduces the simulation time improvement process. Secondly, chapter 6 identifies possible methods to improve simulation times and describes which methods are to be tested on the Pantograph-Catenary interaction problem. Thirdly, chapter 7 describes the simplified models, upon which the simulation time improvements are tested. Results for the improvement tests are then presented in both chapter 8 and 9. Lastly, chapter 10 contains the conclusion, discussion and recommendations for both the first and second goal.

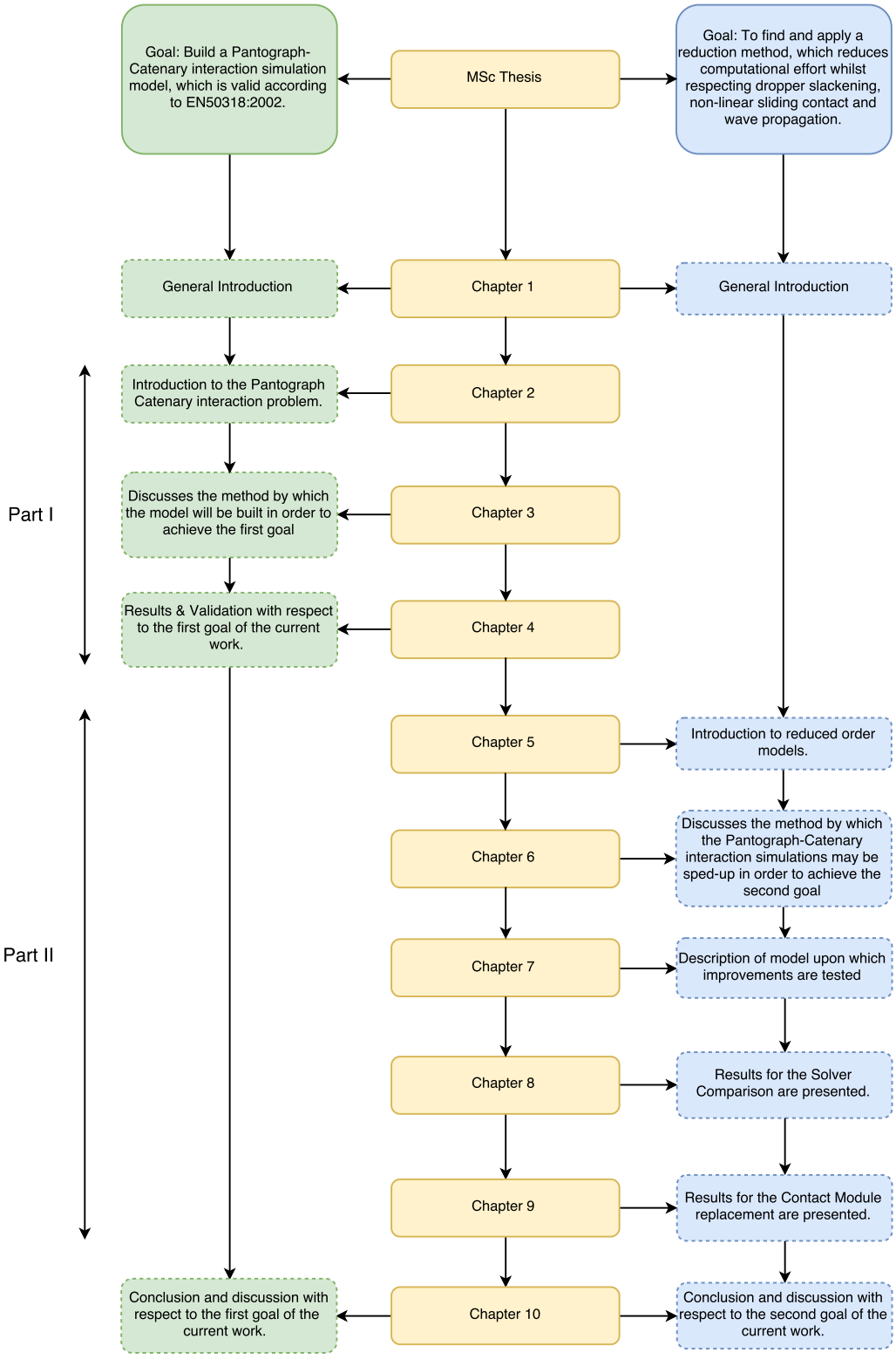

Figure 1.1: Visual representation of the Thesis Outline. Yellow blocks represent chapters, green blocks represent subjects related to the first goal, blue blocks represent subjects related to the second goal.

Part I: EN50318 Simulation Model

Part I contains the EN50318 modelling and simulation process, from identification of the requirements and mapping the current state of the art up to the validation of the model according to EN50318. This part is divided into three chapters. Firstly, chapter 2 introduces the Pantograph-Catenary system and its various parts. Secondly, chapter 3 describes the applied modelling approach. Lastly, chapter 4 contains the model validation according to EN50318.

Furthermore , chapter 10 contains the general conclusion, discussion and recommendations for both the first and second goal.

2

Introduction to Pantograph-Catenary simulation

2.1. Introduction

A robust current collection system is essential to a robust railway service. Sliding contact between the pantograph and the catenary makes robust current collection possible. The sliding contact however also induces wear. Increased amounts of wear may be introduced in the system when ill designed or ill built systems are in use. Increased wear can result in failure of either the pantograph or catenary (Figure 2.1). Failure results in service interruptions and high repair costs. In order to harmonize the performance of current collector and catenary, both infrastructure and rolling stock are subject to EU regulations. The European rail legislation is governed by the Technical Specifications for Interoperability [1]. A series of documents which provide specifications to which railway systems should be compliant, in order to create a standard in railway infrastructure, energy, rolling stock, signalling and traffic control systems. All toward improving the interoperability between the rail sectors in the separate EU countries.

As trains increase in speed, the dynamics of the interface become increasingly important. This, combined with the ever increasing computational abilities of computers, has provoked research into Pantograph-Catenary interaction simulations. These simulations are also an integral part of the EU regulations, and as such are incorporated in the TSI[1] Energy and the TSI LOC&PAS[2].

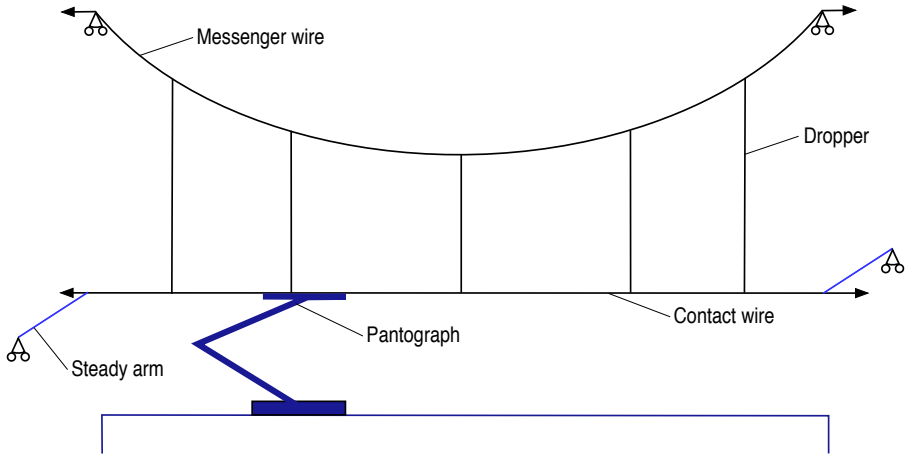

Figure 2.1: Image of the Pantograph-Catenary interface

[1]Technical specification for interoperability
[2]Locomotive and Passenger train

In the TSI Energy [1] in point 6.1.4.1 ”Assessment of dynamic behaviour and quality of current collection”, it is stated that assessment of dynamic behaviour should be done through measurement according to EN50317:2012 and through simulations according to EN 50318:2002[2]. The schematic in figure 2.2 shows the legislation regarding the European railways and where the Pantograph-Catenary interaction simulations originate.

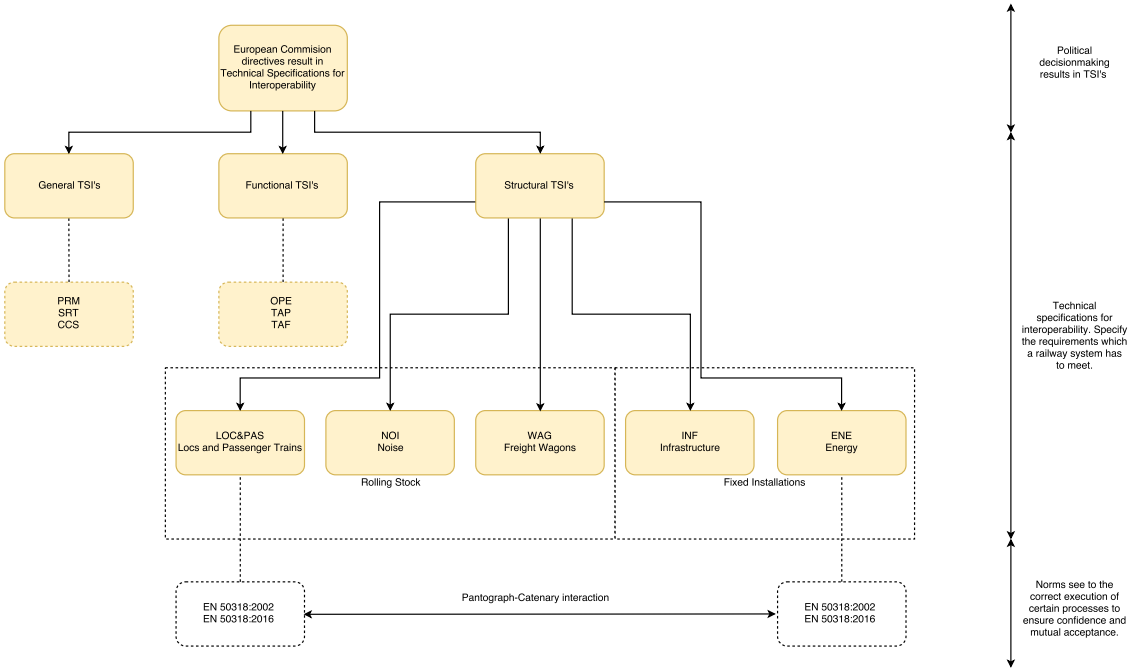

Figure 2.2: Schematic showing from which legislature the simulation requirement results[1]

2.2. State of the art simulation approaches

As the pantograph-catenary interaction is an important factor in the current collection system, it has been researched plentiful. The complexity of a pantograph-catenary system is increased due to nonlinearities such as:

- Non-linear contact
- Non-linear dropper stiffness[3]
- Geometric non-linearities [4]
- Electro-magnetic field influences

These influence the dynamic behaviour of the pantograph-catenary simulation[4]. Further research [5–13, 22, 24, 25] handles these complex factors differently, Kumaniecka & Snamina [5] do not incorporate dropper slackening and model the pantograph as a harmonically differing but uniformly moving force. This takes the wave propagation in account but leaves out the non-linearities. Further research such as Galeotti et al.[6, 7] assume the catenary system as a sinusoidal displacement/stiffness, which is an effective way of reduction in designing active pantograph systems. There are only a few methods in which the full response of the catenary is also taken into account. These methods are of interest. In Vehicle System Dynamics Vol 53no3 the pantograph-catenary interaction simulation methods, which are currently in use, are described and benchmarked in [14–24]. Three main methods can be derived from these simulation programs. 2D Finite difference Method[19, 20], 2/3D Finite Element method[14, 16–24] and 2/3D Finite element method combined with Multi body

dynamics[15, 20, 21]. Furthermore certain improvements may be implemented upon the original method such as described in [22]. Here a fine FE mesh moves along the catenary at the pantographs position to determine near field effects, far field has a much courser mesh. This allows for effective near field calculations whilst keeping computation times at a minimum. For a full review of the current state of the art refer to the benchmark by Bruni [24]. A comparative review of the methods which are in use can be found in table 2.1

Programme	Catenary	Pantograph
PrOSA	FD/FE	LUMPM/MBD[3]
PantoCat	FE	LUMPM/MBD
SPOPS	FE	LUMPM
CaPaSIM	FE	LUMPM
PCaDA	FE	LUMPM
Gasen-do FE	FD/FE	LUMPM
OSCAR	FE	LUMPM/MBD
TPL-PCRUN	FE	LUMPM/MBD
CANDY	FE	LUMPM
PACDIN	FE	LUMPM

Table 2.1: Methods applied for the current state of the art pantograph-catenary interaction programmes[14–24]

2.3. EN50318 validation criteria.

For the methods in table 2.1, all (excluding Gasen-do FE and TPL-PCRUN) are compliant with the EN 50318:2002 norm. The EN50318:2002 specifies functional requirements in order to ensure mutual acceptance of the in-and-output variables, a standardized subset of test results for evaluation of these simulation methods, comparison with measurements and comparison between simulation methods. The validation of simulation methods comprises of 2 steps:

1. Confidence is gained through simulation and validation of a reference model (figure 2.3).
2. A simulation representing a real stretch of track is validated through EN 50317:2012 measurement data of the same situation on the same track.

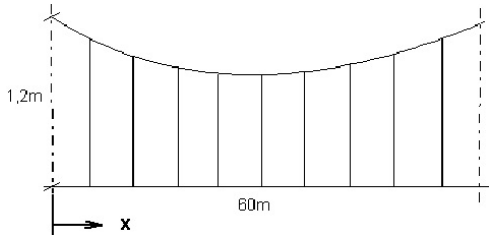

(a) Reference catenary [2]

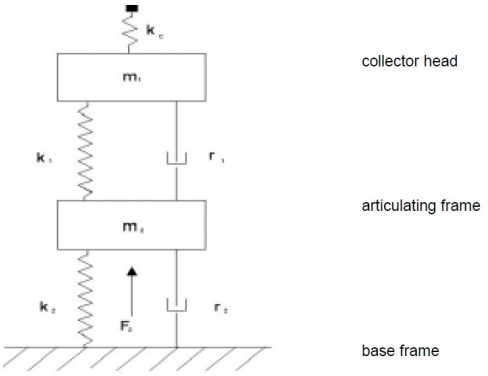

(b) Reference pantograph [2]

Figure 2.3: Reference model to be used in the first step of validation. source: [2]

The reference model consists of 10 spans of a simple overhead catenary and a 2 dimensional pantograph, represented by a lumped mass spring damper system, and which can be seen in figure 2.3a and 2.3b. The simulation is done at 250km/h and 300 km/h.

[3]Absolute Nodal Coordinate Formulation

Validation of the reference simulation happens through comparison of statistical values. All results should be within the ranges given in table 2.2. After this step is successfully passed the method will be compared to real measured values. If the simulated values are within the ranges in table 2.3 the simulation is validated. The complete process, from modeling to validation, is shown in figure 2.4.

	Reference Values	
Speed [km/h]	250	300
Fm [N]	110-120	110-120
σ (0-20Hz) [N]	26-31	32-40
Statistical maximum of contact force [N]	190-210	210-230
Statistical minimum of contact force [N]	20-40	-5-20
Actual maximum of contact force [N]	175-210	190-225
Actual minimum of contact force [N]	50-75	30-55
Maximum uplift at support [mm]	48-55	55-65
Percentage of loss of contact [%]	0	0

Table 2.2: Reference values for EN50318:2002 [2]

Parameter	**Required accuracy**%
Standard deviation of the contact force σ	$\pm$20
Maximum uplift at the support	$\pm$20
Range of vertical displacement of the point of contact	$\pm$20

Table 2.3: Validation through measured values [2]

2.4. Pantograph-Catenary simulation applications

Regulations are the main promoter of simulation efforts. They prescribe what has to be done to certify a new train on existing infrastructure and the other way around. If measurements can be shortened or replaced by simulation, a lot of money can be saved. There are however interesting applications beyond the regulatory simulations. Examples are:

- Upgrading: achieving higher operational speeds on current designs.
- Development: new (active) pantograph designs and new catenary designs.
- Failure prediction: as computational performance increases evermore, maintenance of infrastructure can be done based on information from simulations in combination with historical data. This way, capacity can be focused on the parts that need to be repaired.
- Capturing problems: in projects where a large investment (infra) has to be done, simulations can be done based on the design specifications to make sure the system does not have flaws. Ensuring no faulty design gets built.
- Resolving problems: If an unusual amount of issues surface in a certain location, but the problem is not directy visible, problem replication through simulations might provide important insights toward a solution.

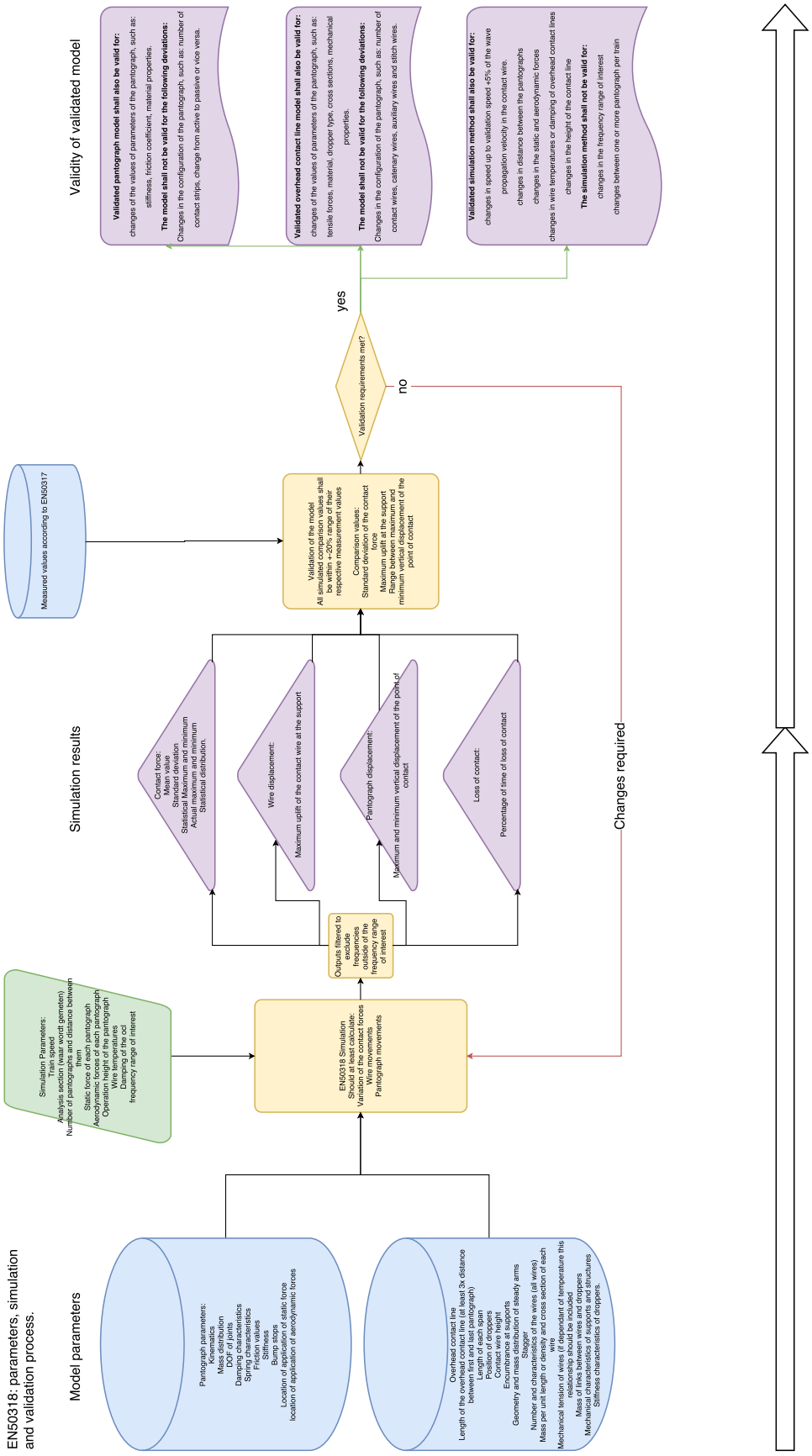

Figure 2.4: EN50318 modeling, simulation and validation process

3

Simulation model

3.1. Introduction

Based on the simulation models in table 2.1 and the simulation facilities at Ricardo, a method for simulation has to be chosen. Other important factors are the available software and the complexity of the method. The simulation process can be divided in three separate processes:

- Pre processing: determining material properties, geometrical lay out and loading.
- Solver: calculation of the predetermined model and load case.
- Post processing: interpretation and processing of solver results.

For each of these processes the best method is chosen through a weighted decision. All values arise from the basis that current state of art simulations use FE, therefore the methods which are capable of FE are valued higher. This decision is based on package availability, expected efficiency and if applicable, interface possibilities with the other processes,the actual ranking is based on the rank of the pre/post processor, combined with the rank of the solver[1]. Pro's and cons of certain methods, as well as decision values, are described in appendix A

		Solver / pre- and post-processor			
		C/C++/C#	Matlab[2]	Ansys	Simpack
Model definition and data analysis	C/C++/C#	2	2	4	1
	Matlab	4	4	6	3
	Ansys	-	-	5	-
	Simpack	-	-	-	0

Table 3.1: Decision table

From table 3.1 the combination of Matlab pre- and post-processing, combined with an Ansys solver emerges. This combination resulted in succesful EN50318[2] validation in prior research such as [17]. Other research uses Matlab for all three processes but may use additional non-standard toolboxes such as [20].

[1] A simple grading criterion is created, every method is awarded a grade for its usability as pre- and post-processor, as well as a grade for its usability as solver, in the current research.

- -, denotes a situation which can not exist.
- 0, is awarded if a method is not suitable for the desired purpose at all.
- 1, is awarded if a method might be suitable but might require additional modules, or programming.
- 2, is awarded if the method is suitable but might require more work than necessary.
- 3, is awarded if the method is suitable and efficient.

Adding both values for pre- and post-processor and solver results in the total value for all combinations, highest value is the 'best' method.

[2] Implementation of the Matlab solver may require an extra toolbox such as the SDTools Structural Dynamic Toolbox [20]

3.2. Catenary modelling

The Ansys program, in combination with a Matlab pre-processing code, allows for easy modelling and editing of models. Ansys provides a pre-existing contact model, removing the necessity for creating such model. Ansys can also run from code (APDL) allowing for automation. It is usable for all the above models, and allows for automation in future use. The Finite Element Method catenary model consists of the elements in table 3.2. The geometric layout of the catenary can be seen in figure 3.1. An explanation of the elements and their features resides in appendix B.

	Element type(s)
Contact wire Structural	BEAM188
Contact wire Contact	TARGE170
Messenger wire	BEAM188
Dropper	COMBIN39
Steady arm	BEAM188
Clamps	MASS21

Table 3.2: Catenary elements

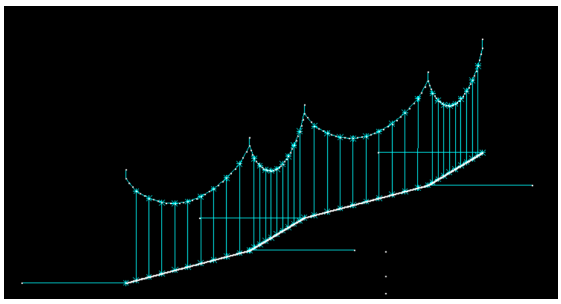

Figure 3.1: Catenary model in Ansys

3.3. Pantograph modelling

The pantograph is modeled as a 3D Lumped Mass model. This type of model is supported in the Ansys FE solver, and therefore does not require any interfacing or co-simulation. The Lumped Mass pantograph model consists of the elements in table 3.3. Figure 3.2 shows the model of the pantograph. The top horizontal line represents the contact element, the stars are MASS21 Elements and the vertical lines are COMBIN14 elements. An explanation of the elements and their features resides in appendix B.

	Element type(s)
Masses	MASS21
Springs	COMBIN14
Dampers	COMBIN14
Contact Elements	CONTA176

Table 3.3: Pantograph elements

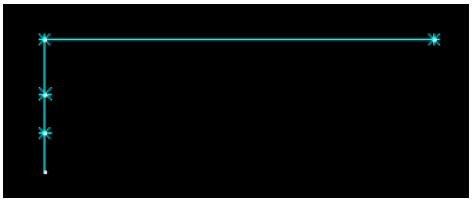

Figure 3.2: Pantograph model in Ansys

3.4. Augmented Lagrange method most suitable contact model

Since the solver in use is Ansys, the contact can be modeled through readily available elements. The pantograph-catenary interface is modeled through the CONTA176 element on the pantograph and TARGE170 element on the catenary. This contact pair allows for multiple contact algorithms such as pure penalty, augmented Lagrange and pure Lagrange. For this simulation the augmented Lagrange algorithm is chosen to ensure low penetration values and contact compatability.

The augmented Lagrange contact formulation adds an extra value λ, the Lagrange multiplier, to the penalty equation 3.1, resulting in equation 3.2. The extra value λ is calculated by the Ansys solver to reduce the penetration. This reduces the contact's sensitivity to the contact stiffness K. In comparison to the full Lagrange method, which calculates the Lagrange multipliers exactly. The augmented Lagrange method iteratively calculates multiple penalty method calculations and augments the λ in every iteration to reduce the penetration. This iterative process is repeated until a certain error/penetration threshold is reached [34].

$$\text{penalty function: } F_{contact} = K_{contact} * P_{Contact} \tag{3.1}$$

$$\text{augmented Lagrange function: } F_{contact} = K_{contact} * P_{Contact} + \lambda \tag{3.2}$$

Additionally the pure Lagrange method is available. This method calculates the exact λ and does not require the specification of a contact stiffness K. Result of the exact λ is that the exact solution is found and therefore zero penetration is enforced. The downside however is that finding the exact solution for λ is very computationally expensive.

3.5. Contact force errors due to FE discretization

Normally, good Ansys practice is to overlay the contact elements over the most flexible surface. In the case of a sliding non-linear contact however a discretization error occurs. In [20] it is described as an 'element passing' error. This error occurs when the contact between target and contact element slides over the interface between 2 or more contact elements.

The amount of elements in contact is always counted for the CONTA176 element, the TARGE170 element is only used as helper. Therefor, if a target element is used on the pantograph, it will move past the contact elements, at the interface of 2 contact elements, the algorithm may therefore find double contact, resulting in a force peak 2 times larger than the signal itself. In figure 3.3 the element passing issue is visualised.

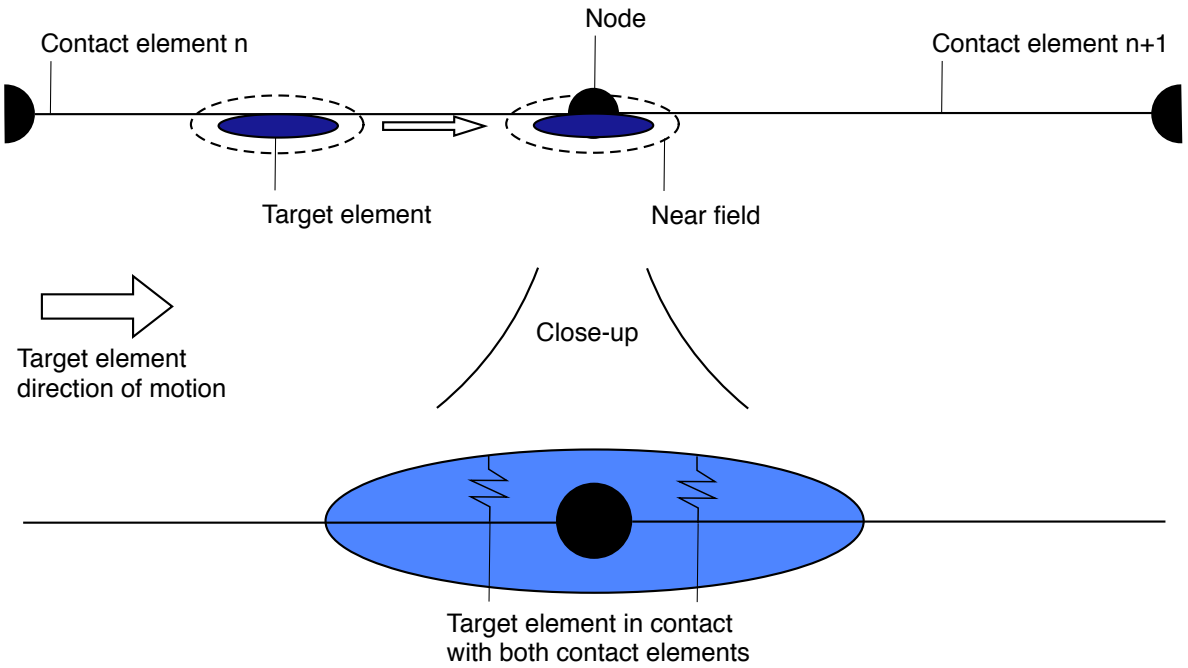

Figure 3.3: Element passing error visualisation

The element passing problem is solved through overlaying the TARGE170 over the catenary. Since these elements are never counted, the algorithm cannot find double contact.

3.6. Automated modeling/pre-processing

An efficient simulation method does not require a lot of time modeling every time a simulation is done. In order to simplify the modeling process, multiple matlab scripts automate the pre- and post-processing. The matlab script Preprocessor.m combines the catenary model and the pantograph model, which are defined in .MAT files, as well as reads simulation settings. This information is combined to create the simulation model and its loads. The process is described in figure C.10.

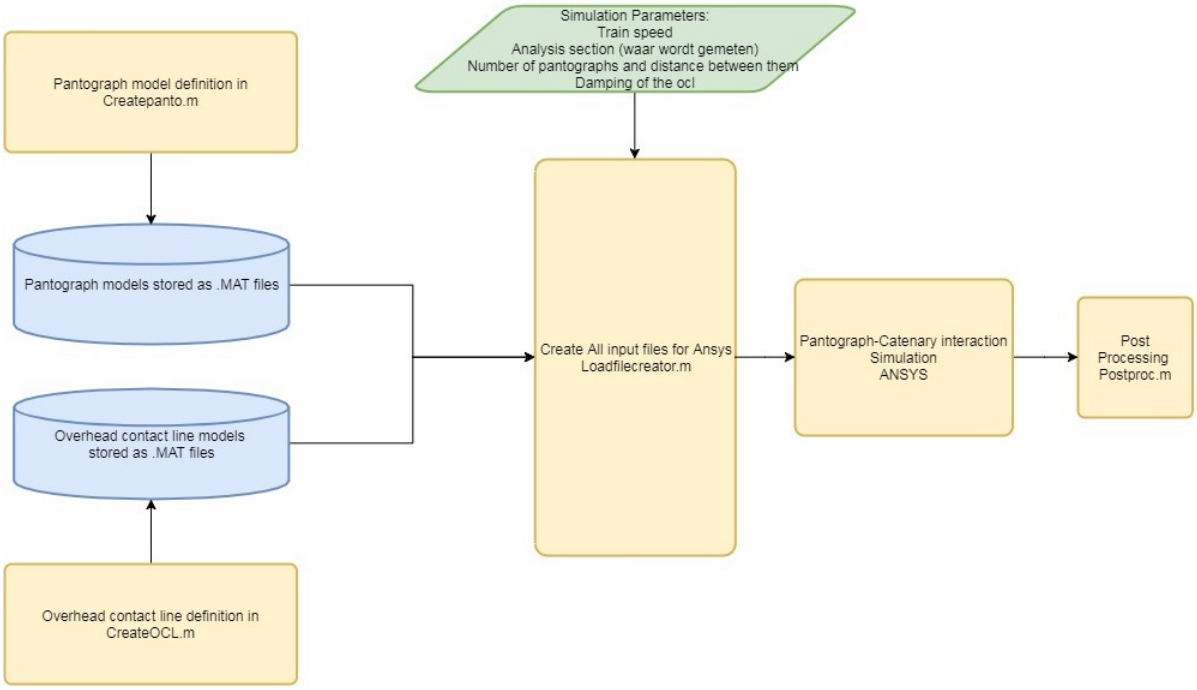

Figure 3.4: Automated simulation flow chart

3.7. Solving

For the time integration, an implicit Newmark method is used with time step: $\Delta t = 0.002s$, this represents 25 times the frequency range of interest, a severely oversampled system which allows the assumption that filtered results will not show aliasing. Integration parameters are chosen: $\alpha_N = 0.25250625, \delta_N = 0.505$, these are standard Ansys values. Damping coefficients are prescribed in EN50318 [2] $\alpha = 0.0125s^{-1}, \beta = 0.0001s$. The non-linear transient dynamic solver in Ansys is set to calculate the full matrices. Stiffness matrix K is updated every time step in order to incorporate the non linear droppers and contact elements. The solver convergence criteria in table 3.4 are chosen in such a way that models of over 20 spans will also converge without solver instabilities. These values are the result of an iterative process, in which the solver parameters were tweaked in order to ensure solver stability and accurate results. Furthermore, previous research such as [17] provided a good starting point for getting to the current values.

Label	Tolerance	Norm
F	1E-6	INF
U	1E-6	INF
M	1E-6	INF
ROT	1E-6	INF

Table 3.4: Solver convergence criteria

3.8. Post-processing

The post-processing script is a reasonably simple Matlab script. It's process is as follows:

- Load the .csv result files into 2 by n arrays.
- Resample the arrays to create uniform time steps at 500Hz .
- Perturb displacement and force values to make them a function of location, not displacement.
- Filter all results in the bands 0-20Hz, 0-5Hz, 5-20Hz.
- Cut results to respresent only the analysis section.
- Calculate all desired statistical values.
- Validate results or output which values are not within tolerance.

4

Results and Validation

4.1. Introduction

Now that the simulation method has been defined (chapter 3) the next step in the process is validation of the proposed simulation method. Validation of the Pantograph-Catenary interaction simulation method will be done by following the 2 steps, as described in the norm EN50318:2002 [2]. The first step entails the validation of the simulation method through building a reference model, defined in the norm EN50318:2002. The second step is to build a real-world model, the dutch Prorail B4+ Catenary in combination with a commonly used panto, this is explained in section 4.3.

4.2. EN50318 Validation of Step 1 / Reference Model Results

This reference model originates from the EN50318:2002 norm. The reference results, as described in the norm, as well as the results obtained by the simulation method developed in this work, can be found in table 4.1.

	Results		**Reference Values**	
Speed [km/h]	250	300	250	300
Fm [N]	116.4	116.3	110-120	110-120
σ (0-20Hz) [N]	29.9	33.4	26-31	32-40
Statistical maximum of contact force [N]	206.2	216.5	190-210	210-230
Statistical minimum of contact force [N]	26.6	16.0	20-40	-5-20
Actual maximum of contact force [N]	182.3	196.3	175-210	190-225
Actual minimum of contact force [N]	51.0	47.2	50-75	30-55
Maximum uplift at support [mm]	48.4-52.0	56.4-60.3	48-55	55-65
Percentage of loss of contact [%]	0	0	0	0

Table 4.1: Results for the EN50318:2002 reference model simulation

As can be concluded from the obtained results and the comparison to the reference values, the currently developed simulation method complies with Step 1 of the EN50318:2002 norm. Thus the method is deemed validated according to Step 1 of EN50318:2002. A visualization of the results can be found in figure 4.1 for the 250 km/h simulation and in figure 4.2 for the 300 km/h simulation. Based on the validation of Step 1, the models' methodology is deemed valid.

4.3. EN50318 validation of Step 2 / Real model results

Since step 2 validations depend on the data available, validations are done within the scope of this project to show that the simulation method is indeed applicable to real world situations. Further EN50318:2002 step 2 validations will be done in the scope of projects in extension to

the current project, for instance when less general models are required for simulation. Next to the EN50318 validation there will also be charts which show how the simulation values compare to a larger measurement set.

Step 2 validation has 4 requirements:

- Standard deviation of the contact force shall be within ±20% of the measured value.
- Uplift at the support shall be within ±20% of the measured value.
- Vertical displacement of the point of contact shall be within ±20% of the measured value. Note: This value is a common result from simulation methods, but is usually not measured in EN50317 measurements, if this value is not available, the validation is done based on the following value: $(U_{midsection} - U_{atsupport}) \pm 20\%$, where U is the uplift value measured.
- For the comparison the minimum length of the analysis section shall be defined, so that the results are representative for the behaviour of the overhead contact line.

4.3.1. Prorail B4+ Catenary, 1 Pantograph, 140 km/h

In this section the simulation method is validated for the situation where 1 Pantograph (Ricardo document:628573) moves below a Prorail B4+ catenary at 140 km/h. The simulation results and the measurement results with which the simulation is validated can be found in table 4.2. The analysis section is defined as the middle 2 spans, thus 114 m, to ensure no end effects are taken into account. A visual representation of the results can be found in figure 4.3. Figure 4.4 shows how the simulated standard deviation compares to the measured values, as well as to a competitive simulation package.

	Simulation Results	**Measured Values**			
Speed [km/h]	140	140	140	140	141
Fm [N]	139.3	131	131	137	132
σ (0-20Hz) [N]	25.6	22.6	30.1	26.4	23.8
Statistical maximum of contact force [N]	216.0	199	221	216	203
Statistical minimum of contact force [N]	62.6	63	41	58	61
Actual maximum of contact force [N]	215.3	-	-	-	-
Actual minimum of contact force [N]	76.4	-	-	-	-
Maximum uplift at support [mm]	19.7-20.6	19	19	19	19
Percentage of loss of contact [%]	0	0	0	0	0

Table 4.2: Results for the EN50318:2002 STEP 2 simulation [54]

Based on the norm EN50318:2002, the validation values are found to be within the allowed ranges. *Thus the method is deemed validated according to Step 2 of EN50318:2002, for 1 Pantograph at 141 km/h below a PRORAIL B4+ catenary.*

The method may therefore be used in the following simulations:

- 1 Pantograph, for allowed deviations see §10.2.1 of EN50318:2002 [2]
- Prorail B4(+) catenary or similar, for allowed deviations see §10.2.2 of EN50318:2002 [2]
- Speed; the validation speed + 5% of the wave propagation speed: 141 + 19.12 = 160.12 Km/h, §10.2.3 of EN50318:2002 [2].

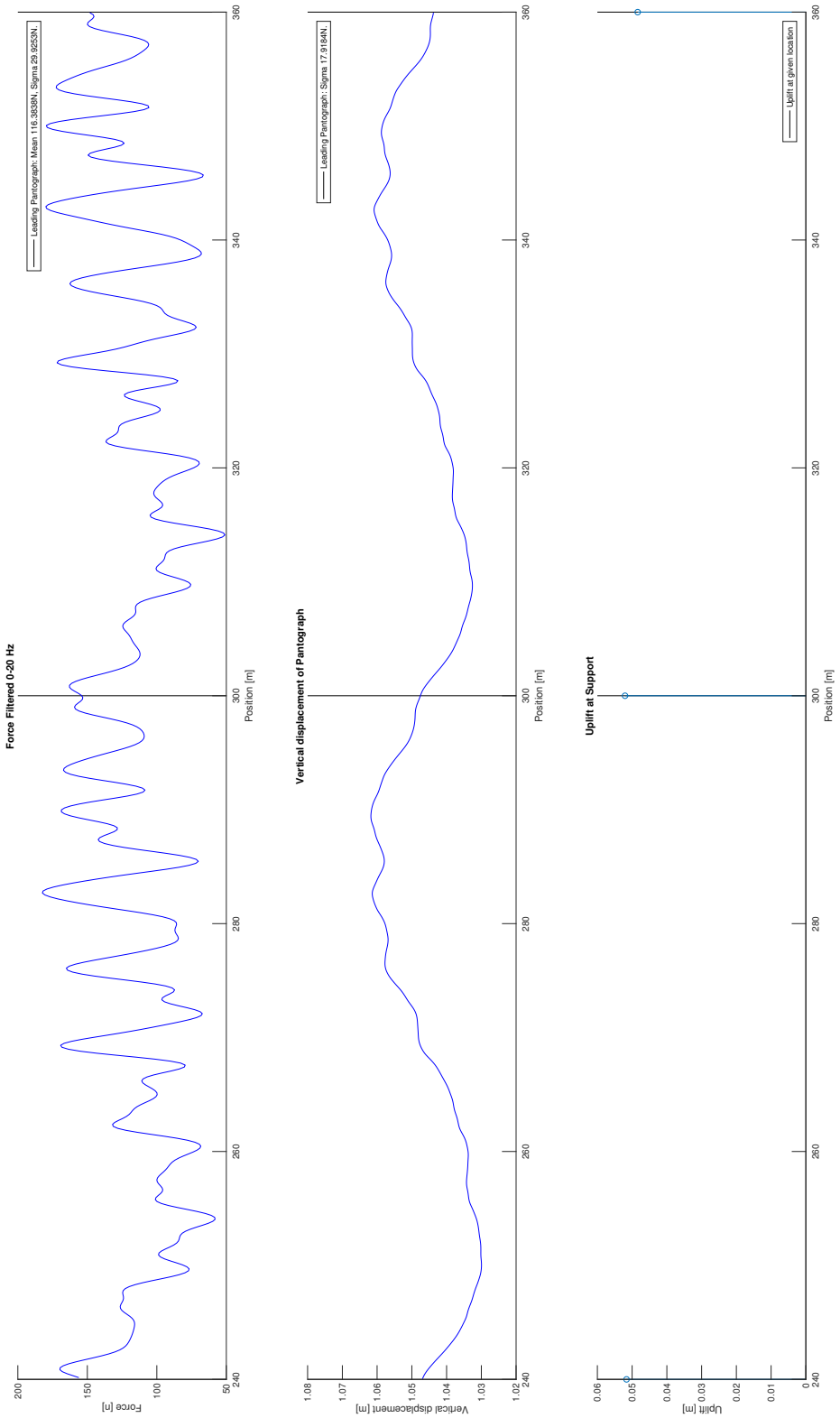

Figure 4.1: Valid en 50318:2002 simulation results at 250 km/h

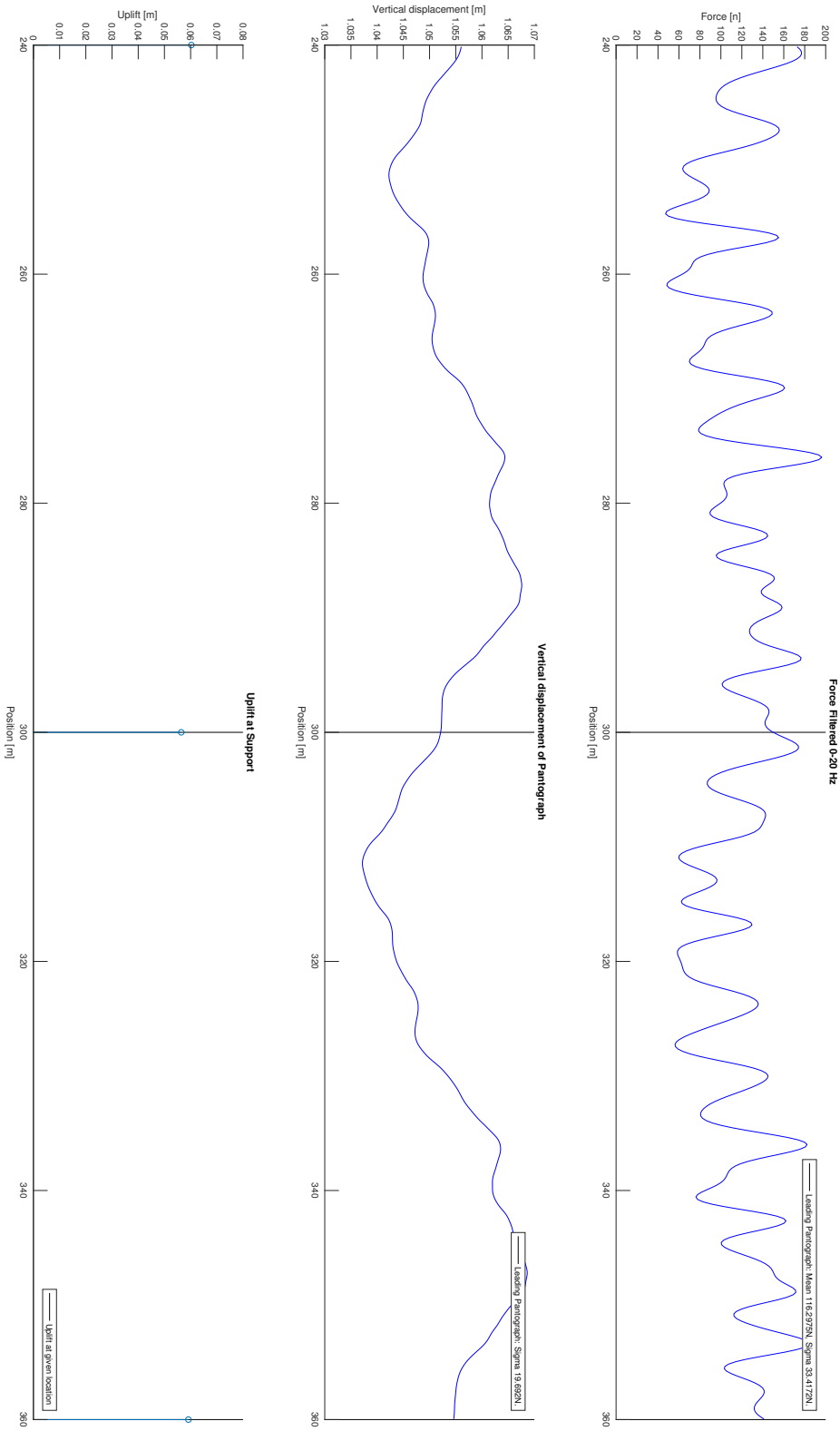

Figure 4.2: Valid en 50318:2002 simulation results at 300 km/h

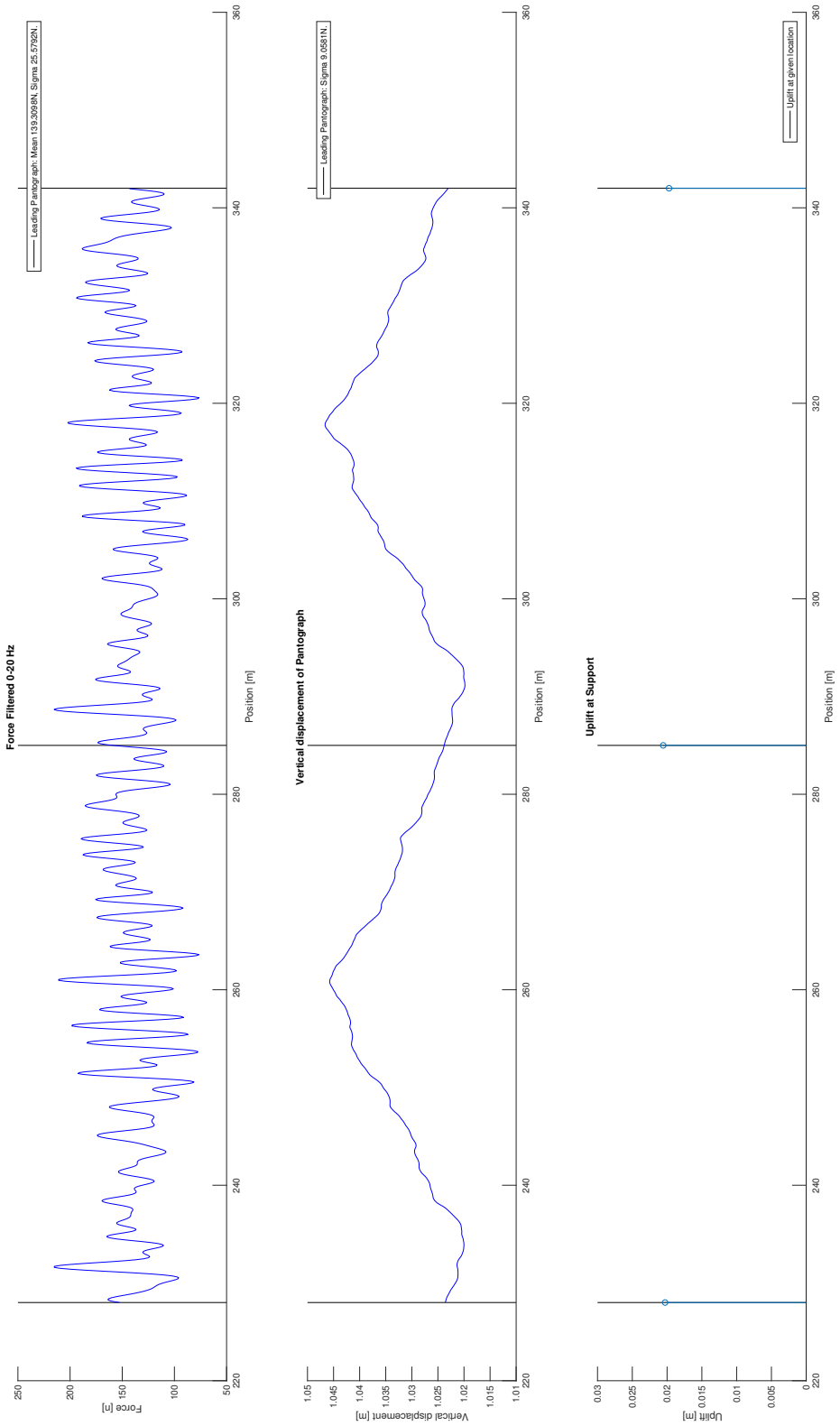

Figure 4.3: Valid en 50318:2002 step 2 simulation results at 140 kph

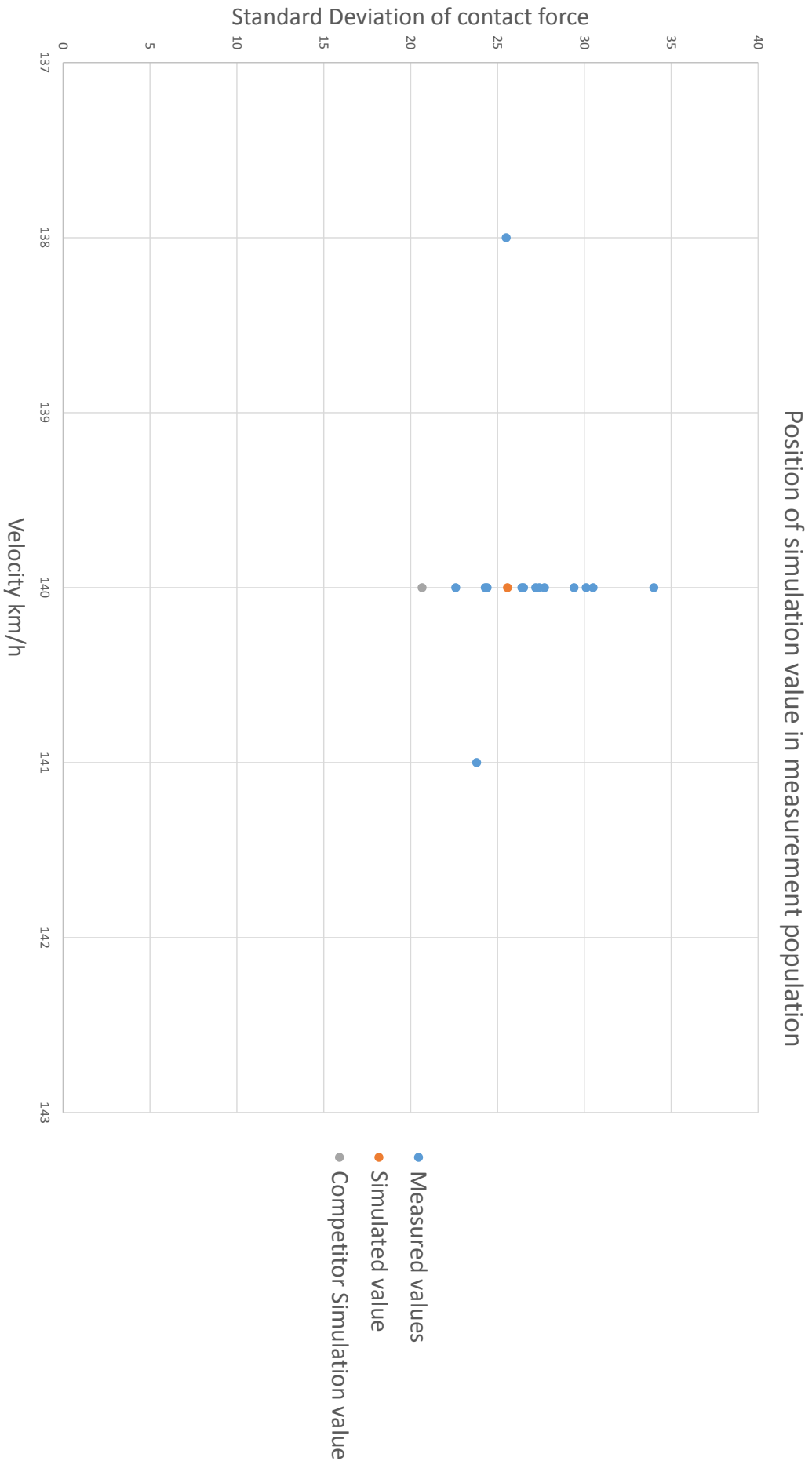

Figure 4.4: Valid en 50318:2002 step 2 simulation results at 140 kph SIGMA comparison

Part II: Model reduction for efficient simulation times

Part II describes the model reduction / simulation time improvement process. The process, from identification of possible improvements through the theoretical implementation up to the testing and concluding, is separated into 5 chapters. Firstly, chapter 5 introduces the simulation time improvement process. Secondly, chapter 6 identifies possible methods to improve simulation times and describes which methods are to be tested on the Pantograph-Catenary interaction problem. Thirdly, chapter 7 describes the simplified models, upon which the simulation time improvements are tested. Results for the improvement tests are then presented in both chapter 8 and 9.

Furthermore , chapter 10 contains the general conclusion, discussion and recommendations for both the first and second goal.

5

Introduction to Model Order Reduction

5.1. Introduction

A proper pantograph-catenary model can easily exist of more than 6000 elements [20] with 6 DOF's per element, resulting in 36000 DOF's in one model. The global sparse stiffness matrix K has size $m*m$ where m equals the total amount of DOF's in the system. An increase of the amount of nodes in the system by $\delta = 20\%$ results in $\delta*m = 0.2m\delta+m = 1.2m$ increases the size of the matrix K by $(\delta+m)^2 = 1.44*m^2$. Furthermore the pantograph-catenary system is non-linear. In order to remain in an acceptable region of accuracy, the stiffness matrix requires updating in every N^{th} substep.

It can be seen that the combination of a system with a high amount of DOF's and non-linear behaviour will become very time consuming to compute. Therefore, it is desirable to create a system which allows for accurate simulation as well as low computational effort. This means the model should be as small as possible, whilst remaining within a certain accuracy. This process, known as model order reduction, is a collection of methods with which a computationally expensive model is reduced to a less expensive model, while remaining in the acceptable accuracy range. Model Order Reduction is a way of removing all non-essential parts from a model, as they are just as expensive in computation times as essential parts. They do however not play a significant role in the outcome of the system. This interpretation is described by the first chapter of the book Model Order Reduction [26] where the process is described as: *"Model Order Reduction tries to quickly capture the essential features of a structure. This means that in an early stage of the process, the most basic properties of the original model must already be present in the smaller approximation. At a certain moment the process of reduction is stopped. At that point all necessary properties of the original model must be captured with sufficient precision."* A graphical representation of Model Order Reduction, also by [26] can be found in figure 5.1.

5.2. Proposed methods for reducing a Pantograph-Catenary model

MOR can be very effective, depending on the system and the desired results. For instance, linear systems might reduce very well by projection onto the modal basis. Resulting in a nearly perfect reproduction of results with big improvements in computation times. The model which is described in this work, is (partially) non-linear due to the dropper cables which slack under compression. The reduction of non-linear systems is less documented than the reduction of linear systems and, as stated in [28] and [29] (non-linear circuits) does not necessarily result in less computational effort. The reduction which is required for the system as described in this work should therefore be capable of accurately representing the non-linear behaviour of the catenary, as well as provide accurate contact behaviour.

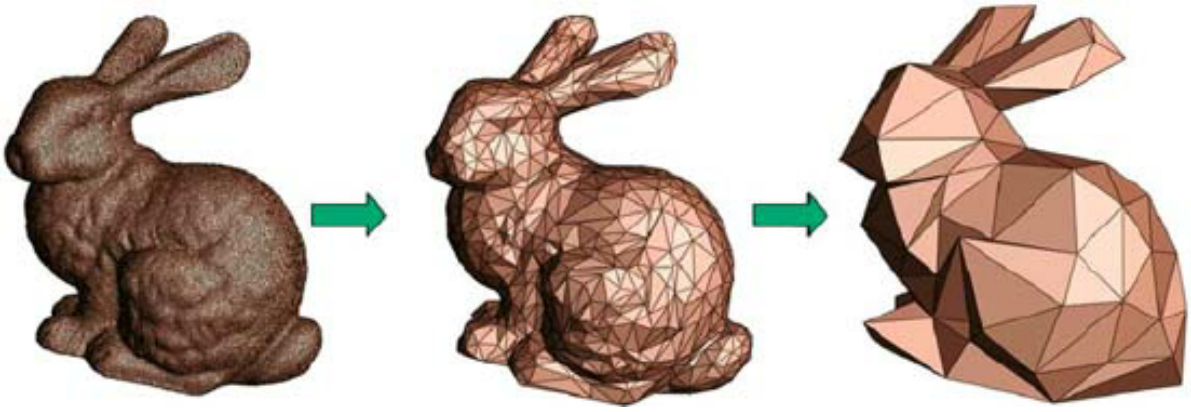

Figure 5.1: Graphical representation of Model Order Reduction source:[26]

For the pantograph-catenary interaction, a couple of reduction possibilities can be introduced:

- Physical reduction
  - Mesh coarsening
  - Localized mesh refinement/moving mesh
  - Dimension reduction 3D/2D
  - Splitting linear and non-linear parts, quasi-linear reduction.
- Projection
  - A priori methods, methods which require no information of the full model results
  - A posteriori methods, methods which require information of the full model results.

all of which provide their own challenges.

5.3. Rating criteria for reduction methods

Reduction of the model through actual reducing of the amount of DOF's, within the FE model, is the easiest way of reducing the system. A smart choice of simulation parameters could significantly reduce simulation times, without resulting in low accuracy. Projection based reductions however introduce a new basis which represents the model. These methods could describe the model behaviour accurately whilst greatly reducing the computational effort. Due to the non-linear behaviour induced by dropper slackening, as well as sliding contact, the applicability of certain methods might however prove to be difficult. Careful selection of Model Order Reduction methods is therefore necessary. The reduction sections of this research will therefore focus on finding applicable reduction methods. Keeping in mind the features which may not be lost in reduction:

- Dropper slackening / non-linear dropper behaviour
- Non-linear sliding contact
- Wave propagation.

When applicable methods are found, tests can be done to determine their accuracy and CPU time improvement. Furthermore the scalability of the methods can be determined. These tests ensure the reduction method provides accurate results as well as acceptable computational effort. Based on this the goal of the reduction is determined.

The main goal of the pantograph-catenary reduction:
To find and apply a reduction method, which reduces computational effort whilst respecting dropper slackening, non-linear sliding contact and wave propagation.

To achieve this goal, the reduction performance will be measured through:

- Computational time differences
- Reduction scalability.

A basic understanding of Model Order Reduction methods and their applicability is gained in chapter 6.

6

Methods for simulation time improvement

6.1. Introduction

The EN 50318:2002 simulations from chapter 3 are running on a laptop specified in table 6.1. Simulation times for a full EN 50318:2002 reference model take approximately 15-20 hours of CPU time.

Computer	MacBook Pro	
CPU	Core i7-4770HQ	2.20GHz 2(/4) Cores
Memory	1600MHz DDR3	8(/16)GB
Storage	WD Elements USB3.0	2TB
	WD Elements USB3.0	750GB
Extra	Running in Parallels	

Table 6.1: Computer spec for simulation

Improvement of the simulation times is necessary if multiple simulations runs need to be done in a timely manner. The options to this regard are:

1. Improve model efficiency; editing the model to reduce the computational effort required to perform simulation. The MOR methods are an example of this.
2. Improve computational power; this requires no changes to the model and might improve simulation times drastically.
3. Improve time integration/solver; Choosing a solver which is optimized for the problem at hand may improve simulation times.
4. Lower model criteria; using less stringent convergence criteria and lowering the result accuracy may improve simulation speeds.
5. Change interface algorithm / contact model; the built-in Ansys contact module encompasses a large module which is capable of many types of contact. Choosing a simplified contact method may improve simulation times.

all of which can be applied. Finding out whether or not these approaches work requires careful examination of the possibilities. In this chapter the possibilities for all three of these methods are explored. Model efficiency improvement is explored in section 6.3, computational power comparisons are not executed within the scope of this work. Furthermore, Time integration methods are proposed in section 6.4 and model criteria comparisons in subsection 6.4.4. Lastly, contact model improvements are proposed in section 6.5 First, however, the built-in Ansys reduction methods are discussed in section 6.2.

6.2. Ansys built-in reduction methods

The Ansys program, which is used as solver in this project, contains 4 different reduction methods. These reduction methods do not necessarily comply to the essential features as described in section 6.3. They might however prove useful for application in other applications. Thus they are briefly described in this section. The Ansys program provides, under the substructuring solver, options to reduce (substructure) the system. The methods which can be applied are:

- Static condensation / Guyan reduction [35]
- Fixed-interface CMS / Craig-Brampton reduction [36]
- Free-interface CMS / Herting reduction [37]
- Residual-flexible free-interface (RFFB) CMS / Martinez reduction [38]

The static condensation method is, as the name suggests, is useful in static reduction. It does not incorporate non-linear behaviour and does not provide useful vibration modes since it does not incorporate inertial terms [35]. Fixed interface CMS or Craig-Brampton reduction reduction determines the constraint modes, eigenvectors and eigen values with the master degrees of freedom constrained [33, 36], this method will provide incorrect modes due to the large amount of interfaces in the model. The free-interface CMS or Herting reduction determines eigenmodes and eigenvectors with the interfaces free (fixed interfaces possible through constraints) [33, 37]. The RFFB or Martinez reduction, contains Residual Attachment Modes which, in addition to the vibration modes capture the residual flexibility of the full system [33, 38]. The use of these modes is also observed in other work [27, 32], therefore the martinez reduction may provide an accurate reduced order model. It must however be stated, that for this model to work, the non-linear dropper behaviour should not be reduced with the system, this would result in a similar reduction method with respect to the proposed reduction method at the end of this chapter. The Martinez [38] reduction method has also proven useful in interfacing Ansys and SimPack. The linear reduced system can be imported into SimPack as flexible body through an .FBI file. For further research, such as active pantograph design. This interface could prove useful. These methods are not discussed in the remainder of this work since they are either not applicable, or they are incorporated in Ansys and require small changes which Ansys will not perform.

6.3. Model efficiency improvements

Improving the computational performance of the full pantograph-catenary interaction model through reduction would require significant time. Applying and reviewing reduction methods therefore requires a modified test-case: a model which contains all properties and non-linearities, only much smaller and easier to compute. The model visualized in figure 6.1 is used. In this model the upper wire is modeled as a rigid bar, non-linear springs are used to represent the droppers. Contact will be modeled through a pure penalty method. This method is implemented in matlab by checking the positions of the pantograph in X and Z direction. The position of the catenary is checked as well. If penetration is found, the force from equation 3.1 will be applied to both pantograph and catenary.

The testing model contains all the essential features for which the reduction method needs to be tested.

- Dropper slackening / non-linear dropper behaviour
- Sliding contact
- Wave propagation / dynamics

6.3.1. Dimensionality reduction

Dimensionality reduction is a widely used method in data processing, for instance in image classification. As large amounts of high dimensional data must be interpreted, the computa-

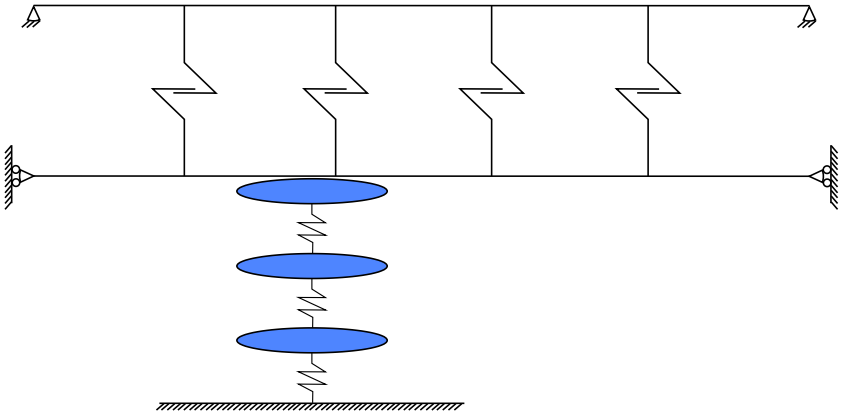

Figure 6.1: Example system for reduction testing.

tional effort to perform this interpretation becomes too high. In order to perform these interpretations, the dimensionality of the data is reduced. Simply removing dimensions however is bad practice. Through feature extraction techniques such as Principal Component Analysis (PCA), the dimensions which contain the largest variance remain [40], whilst the rest is removed, resulting in lower dimensional data. All reduction methods work towards lowering the dimensionality of the problem. Specifying a dimensionality reduction for the pantograph-catenary model by PCA involves projecting the data onto a new set of basis vectors. Reduction methods that project onto a new basis are described in section 6.3.3.

For the pantograph-catenary interaction model, with respect to the geometry, there are three dimensions. These dimensions have two DOF's each. The total geometric dimensionality of this system is therefore 6D. As might be recalled from section 5.1, the size of the stiffness matrix K has size $m * m$ with m being the amount of DOF's, subsequently $m = elementamount * DOF_{element}$. Computational effort is linked to the size of this vector. Reducing geometrical dimensions therefore reduces the computational effort.

6.3.2. Moving mesh reduction

Further reduction options include a dynamic/moving mesh [22], a model is created in which the far-field catenary is modeled with a coarse FE mesh. Whereas the near-field catenary is modeled with a much finer mesh. The fine mesh moves along the catenary together with the pantograph. This method is implemented in Matlab [22]. Due to the lack of a FE toolbox at Ricardo and the TU Delft, it is not possible to review this method within the scope of this project.

6.3.3. Projection based Non-linear structural dynamic reduction

As stated by Lülf et al. [30], there are many different bases upon which the full non-linear model can be projected. In [30] the methods which are described fall in one of 2 types: a priori or a posteriori. A priori bases do not require any information from the result of the full system. A posteriori reductions do require result information from the full system. Examples of the former are: Linear Normal Modes (LNM), Ritz-vectors, the A Priori Reduction and the Local Equivalent Linear Stiffness Method. Examples of the latter are: Proper Orthogonal Decomposition, Smooth Orthogonal Decomposition and Centroidal Voronoi Tesselation. Not all methods provide accurate results for all models, a clear choice has to be made based upon which reduction is interesting for our system. Based on the comparative study as described in [30], in which all the methods mentioned above are compared, a basic idea of which methods are usable and which are not, is gained. The method, as described in [30] should mainly be based on the type of excitation which is applied to the system. In our case this is the moving contact. From [30, 31], it is found that the Proper Orthogonal Decomposition method is the most accurate method of reduction of certain non-linear systems. From [30] however, it is also concluded that all methods, including the POD method, lack robustness to changing excitations, this is mostly applicable in the frequency range. Amplitude changes provide

better robustness. Also the robustness is better if, the bases are defined on the critical values and the changes in the excitation are less demanding (lower frequency or amplitude w.r.t. the original excitation upon which the basis was made). The methods provided by [30, 31] are, however, not the only applicable methods. Further research such as Tamarozzi [32] uses eigenmodes and residual attachment modes to describe the moving contact behaviour in a Parametric Model Order Reduction (PMOR). A more general review of PMOR applications, which may be applicable to the current work resides in Benner et al. [39]. The work by Géradin et al. [27] uses Rigid body Modes, Vibration Modes, Attachment Modes and Residual modes to create a nodeless superelement, with which the moving contact problem can be tackled, it is, however, applied to a linear FE model. Jain et al. [47] uses Vibration Modes and the derivatives of the eigenvalue problem of small undamped vibrations with respect to the modal amplitudes (Modal Derivative (MD)) to create a Quadratic Manifold, capable of describing geometric non-linearities in systems. All of these methods will briefly be discussed in this section, a small explanation of the theory will be given, as well as a preliminary judgment on whether the method seems applicable in the current work.

Proper Orthogonal Decomposition

The Proper Orthogonal Decomposition (POD) is a reduction method, also known as the Karhunen-Loève decomposition (KLD) or as Principal Component Analysis in statistical sciences [42]. As described in section 6.3.3, the POD is an a posteriori reduction method, it requires training data from the unreduced model to accurately represent the full model. It is particularly interesting since the prior application of POD in reducing non-linear structures, such as [42, 46]. The now following mathematical representation of the continuous POD as described in this work was taken from G. Kerschen et al.[42] and Chatterjee [41], additional content is based on [41, 42, 45].

Take $\theta(x,t)$ a random field on a domain Ω, it is decomposed into its mean and the time varying components, equation 6.1.

$$\theta(x,t) = \mu(x) + \vartheta(x,t) \tag{6.1}$$

At time t_k the system displays a snapshot $\vartheta^k = \vartheta(x,t_k)$. The POD will aim to fit the $\varphi(x)$ to a collection of snapshots $\vartheta(x,t)$, equation 6.2.

$$\text{Maximize } \left\langle |(\vartheta^k, \varphi^k)|^2 \right\rangle \text{With } ||\varphi||^2 = 1 \tag{6.2}$$

where

$$(f,g) = \int_\Omega f(x)g(x)d\Omega$$
$$\langle . \rangle = \text{Average}$$
$$||.|| = (.,.)^{\frac{1}{2}} = \text{Norm}$$
$$|.| = \text{Modulus}$$

The constraint $||\varphi||^2 = 1$ in equation 6.2 can be taken into account through a Lagrange multiplier, resulting in equation 6.3.

$$J_{[\varphi]} = \left\langle |(\vartheta, \varphi)|^2 \right\rangle - \lambda(||\varphi||^2 - 1) \tag{6.3}$$

In [45] it is shown that this condition results in the eigenvalue problem in equation 6.4.

$$\int_\Omega \left\langle \vartheta^k(x)\vartheta^k(x') \right\rangle \varphi(x')dx' = \lambda\varphi(x) \tag{6.4}$$

Where $\left\langle \vartheta^k(x)\vartheta^k(x') \right\rangle$ is the averaged Auto-correlation function. The solution to equation 6.2

is therefore the eigenfunction $\varphi_i(x)$ in equation 6.4.

$$\vartheta(x,t) = \sum_{i=1}^{\infty} a_i(t)\varphi_i(x) \tag{6.5}$$
$$\text{Where: } a_i(t) = (\vartheta(x,t), \varphi(x))$$

These eigenfunctions are the Proper Orthogonal Mode (POM). The corresponding eigenvalues λ_i are the Proper Orthogonal Value (POV). The POM's are used to decompose the original field $\vartheta(x,t)$, resulting in equation 6.5. The coefficients $a_i(t)$ are uncorrelated, meaning a_i is dependent of φ_i and no other φ.

In practice however, the data is not continuous but discretized. The application of the POD in a discrete way follows from [41, 42, 45, 46]. There are multiple methods with which the POM and POV's can be computed. The eigensolutions of the sample covariance matrix can be computed [42, 46]. The Singular Value Decomposition (SVD) can be computed [41, 42, 46]. This method gives an insight into system dynamics and plays a role in model updating for non-linear systems [44]. Due to this extra information, the SVD is interesting for the current reduction problem.

To ensure uniformity, the method used in Kerschen et al. [42] is followed again. The discretized data consists of n amount of observations with m dimensional data. The response matrix X in equation 6.6 is created.

$$X = \begin{bmatrix} x_1 & \dots & x_n \end{bmatrix} = \begin{bmatrix} x_1 1 & \dots & x_1 n \\ \dots & \dots & \dots \\ x_m 1 & \dots & x_m n \end{bmatrix} \tag{6.6}$$

The SVD of response matrix X is written as equation 6.7, alternatively 6.8.

$$X = USV^t \text{ Kerschen et al.[42]} \tag{6.7}$$
$$X = U\Sigma V^t \text{ Chatterjee. [41]} \tag{6.8}$$
$$\text{Where: } U = \text{an } m \times m \text{ orthonormal matrix}$$
$$\text{Where: } S \text{ and } \Sigma = \text{an } m \times n \text{ pseudo diagonal, semi-positive definite matrix}$$
$$\text{Where: } V = \text{an } n \times n \text{ orthonormal matrix}$$

The left singular vectors in the U matrix represent the Proper Orthogonal Mode's. Whereas the S matrix contains the singular values, which are the square roots of the eigenvalues of XX^T. These therefore represent the Proper Orthogonal Value's. The V matrix's columns contain the time modulation of the respective POM, normalized by the corresponding POV [46].

The Proper Orthogonal Decomposition is computed exclusively from the full system responses. Therefore the physical meaning of the POM's does not necessarily relate to the physical meaning of for instance the vibration modes. The POM's are orthogonal to each other whereas mode shapes are orthogonal w.r.t. the mass and stiffness matrix. Due to this orthogonality relationship, the only way the POM's and mode shapes are related is, if the mass matrix is equal to the identity matrix, or the system is resonating in one of its vibration modes [42].

Moving contact Reduction through a Parametric Model Order Reduction scheme

The reduction of a moving contact through a Parametric Model Order Reduction (PMOR) is discussed in Tamarozzi et al. [32]. An extensive review of PMOR applications resides in [39]. The PMOR method proposed in [32] aims to reduce the reduction space of dynamical and sliding contact problems by use of a time varying reduction space. The time-varying effect in the reduction space capture the different locations where contact can be expected. The following explanation follows the process of Tamarozzi et al. [32], sign conventions may differ from earlier theory references to follow the conventions in [32]. The general description of

the model in differential form is:

$$M\ddot{x} + C\dot{x} + Kx = Bu \tag{6.9}$$

Assuming Damping = 0

$$M\ddot{x} + Kx = Bu \tag{6.10}$$

Where x is the vector of nodal displacements, u is the vector of input values, $M \in \mathbb{R}^{n\times n}$ is the mass matrix, $K \in \mathbb{R}^{n\times n}$ is the stiffness matrix and $B \in \mathbb{R}^{n}$ is the input matrix. The system is projected onto its new basis by Galerkin projection with reduction space $V \in \mathbb{R}^{n\times m}$

$$V^T MV\ddot{x} + V^T KVx = V^T Bu \tag{6.11}$$

The reduced system has the same form as the full system in equation 6.10:

$$M_r\ddot{x}_r + K_r x_r = B_r u \tag{6.12}$$

Where $M_r \in \mathbb{R}^{m\times m}$, $K_r \in \mathbb{R}^{m\times m}$ and $B_r \in \mathbb{R}^{m}$. Up until this point the reduced model is defined by Galerkin projection of the original model by a reduced space V. This is applied in many different reduction methods, it performs the mapping from the full to the reduced basis. The accuracy and efficiency of the reduction method is dependent of the choice for V. In the PMOR scheme, the reduction space V is created by Vibration Mode's (VM) denoted as Φ, which describe the model dynamics, the dynamics that are included in the model are therefore accurate up to the eigen frequency of the largest VM. Inclusion of moving contact is added to the reduction space by adding Residual Attachment Modes (RAM) denoted as Ψ. These RAMs are dependent of a parameter p, which will later be used to include the time dependency of the corresponding RAM. The reduction space $V \in \mathbb{R}^{n\times m}$ becomes:

$$V = V(\mathbf{p}) = [\Phi\Psi(\mathbf{p})] \tag{6.13}$$

Where the matrix Φ contains all non-parametrized shape vectors, $\Psi(\mathbf{p})$ contains all parametrized shape vectors. The model may have multiple time dependent, location dependent or otherwise varying properties. These properties may all result in a parameter p_i and (multiple) corresponding shape vectors $\psi_i(p_i)$.

$$V = V(\mathbf{p}) = [\Phi\psi_1(p_1)\psi_2(p_2)..\psi_i(p_i)] \tag{6.14}$$

Alongside proposing a new PMOR scheme, the work in [32] also uses a method for comparison, where the reduction space consists of VM's and non-parametric RAMs, see equation 6.15.

$$V = \left[\Phi\psi_1\psi_2..\psi_j\right] \tag{6.15}$$

If the contact location is the only parameter i.e. p_1 in the PMOR scheme and all shape vectors ψ_j in equation 6.15 are residual attachment modes computed at locations where contact will occur, equation 6.14 reduces to:

$$V = V(p_1) = [\Phi\psi_1(p_1)] \tag{6.16}$$

If the original FE model uses linear shape functions, the parametric shape vector $\psi_1(p_1)$ now contains linear combinations of the RAMs from equation 6.15. This means that the amount of DOF's used for robust contact behaviour, are reduced drastically from j to 1. For systems with large amounts of contact locations, where j will indeed become large, the PMOR reduces the amount of unknowns and equations of motion drastically with respect to the non-parametrized method (equation 6.15). This results in significant speed improvements. For this to be the case, the value for p at a given time must, however, be known a priori, or calculated during time integration. The former results in the lowest computation times. The latter requires calculation of $P, \dot{P}$ and $\ddot{P}$ during time integration. The PMOR scheme is created for moving point loads and distributed loads, where velocities and amplitudes are defined a priori. It can, therefore, be concluded from the work in [32], that the PMOR reduction scheme

will provide accurate results for models under highly dynamic (known a priori) moving loads. Towards applicability in this work the only unknown that arises from this method is the following: How does the PMOR scheme proposed in [32] cope with loads from which the amplitude as well as frequency is not predetermined.

Moving contact Reduction through a Nodeless Superelement formulation

In Gèradin et al. [27] a method is proposed, where a linear FE subsystem is reduced through a nodeless superelement formulation. This method is applied in the context of flexible multibody dynamics, which is not the foreseen application of the current work. Nevertheless, the work in Gèradin et al. [27] provides some insights which may be applicable in the current work. The method, like the work in [32], uses residual attachment modes in order to correctly describe the contact which may occur. The application of this contact may be of interest in the current work. Therefore, the way the reduction space $V \in \mathbb{R}^{N \times n_u + n_v + n_a + n_r}$ (refered to as modal reduction matrix in [27]) is determined becomes of interest.

For reasons of brevity the general description of the model, as well as the Galerkin projection method are not repeated here, for a review of these, please see equations 6.9-6.12.

This reduction space V in [27] uses rigid body modes $U \in \mathbb{R}^{N \times n_u}$, vibration modes $\Phi_v \in \mathbb{R}^{N \times n_v}$, attachment modes $G_a \in \mathbb{R}^{N \times n_a}$ and residual modes $G_r \in \mathbb{R}^{N \times n_r}$. For the contact model, the modes which are of interest are the Residual Attachment Mode G_r. The reduction space V now looks as follows:

$$V = [U \Phi_v G_a G_r] \tag{6.17}$$

The vibration mode matrix Φ_v can vary in size, to include dynamics up to the highest corresponding eigen frequency. The RAMs are chosen to ensure a robust response to not fully predictable external actions on the model. In the current work, this unpredictable action will be the sliding contact between pantograph and catenary. In [27] the generation of the RAMs happens through the application of static loads $J_c \in \mathbb{R}^{N \times n_c}$ where $r \in c$ to a cloud of nodes. The nodes on which the load vector J_c is applied are chosen when contact is likely to occur at their location. The Attachment Modes (AM) G_a and RAMs G_c are computed as follows:

$$K\,[G_a G_c] = [J_a J_c] \tag{6.18}$$

Since the matrix K in [27] is singular, due to the chosen Dual Component Mode Synthesis method, equation 6.18 needs to be solved using a Moore-Penrose Matrix inverse K^+, which results in:

$$[G_a G_c] = K^+\,[J_a J_c] \tag{6.19}$$

In the current work, assuming the flexible bodies are constrained sufficiently during reduction, the matrix will not be singular. Therefore the inverse of matrix K can be computed, which results in:

$$[G_a G_c] = K^{-1}\,[J_a J_c] \tag{6.20}$$

In [27], the next operation would be a mass orthonormalisation procedure. This is not relevant in the current context of defining an applicable reduction subspace, since the final reduction method is not yet known. Furthermore the amount of RAMs is finally reduced from G_c to G_r with $n_r < n_c$. For the current work the amount of RAMs does not need to be truncated, since contact locations can be pre-computed and all n_c are relevant. This results in $n_c = n_r$ resulting in:

$$G_r = G_c \tag{6.21}$$

Furthermore assuming the rigid body basis $U = []$ since there is no rigid body motion in the system. The final reduced basis is:

$$V = [\Phi_v G_a G_c] \tag{6.22}$$

Note that the submatrices G_i in the work by Gèradin et al. [27] represent the same functions as the submatrices ψ_i in the work by Tamarozzi et al [32]. Assuming ψ_i in equation 6.15 can be an Attachment Mode, equations 6.15 and 6.22 are the same.

Quadratic manifold / Linear manifold + Modal Derivatives

The reduction of a structural/geometrical non-linear system is proposed by Jain et al. [47]. The proposed method uses Vibration Modes to describe the linear part of the system, as well as Modal Derivatives to describe the second order non-linearities of the underlying model. The method is applied to thin plate models with geometric non-linearities, there is little resemblance between the models in [47] and the models to be reduced in the current work. The method proposed in [47] will need to be extended in order to include sliding contact, for instance by additional RAMs such as in [27, 32]. Furthermore, the method proposed in [47] is capable of accurately describing second order non-linearities whereas the non-linearity in the current work is a discontinuity between 2 linear regions. These differences make the applicability of the method proposed by [47] to the current work questionable. Nevertheless the method is briefly discussed, since there are also large displacement (geometric non-linear) effects in the current model. These geometric non-linearities are not discussed in the remainder of the reviewed methods. The methods described in [27, 32, 43] use a 'linear' reduction space, spanned by for instance the Vibration Modes and Residual Attachment Modes. The method proposed in [47] also uses a reduction subspace containing the linear VMs, in addition to the VMs the method uses the Modal Derivatives (MD) of these VMs. These MDs are used to describe the geometric non-linear (large displacement) behaviour of the system. From [47] the following derivation of the modal derivatives is taken.

The system from which the MDs are derived is:

$$M\ddot{u}(t) + C\dot{u}(t) + f(u(t)) = g(t) \tag{6.23}$$

where

$$u(t_0) = u_0$$
$$\dot{u}(t_0) = v_0$$

this system can be linearized around $u_{eq} = 0$ which results in:

$$M\ddot{u} + C\dot{u} + K_{|eq}u = g(t) \tag{6.24}$$

where

$$K|_{eq} = \frac{\partial f(u)}{\partial u}\,|_{u=0} \tag{6.25}$$

this can be written as a combination of Vibration Modes and eigen values:

$$u(t) = \sum_{i=1}^{n} \phi_i \eta_i(t) = 0 \tag{6.26}$$

The vibration modes belonging to equation 6.24 are then calculated with the generalized eigenvalue problem.

$$(K|_{eq} - \omega_i^2 M)\phi_i = 0 \tag{6.27}$$

Here ω_i^2 is the eigenfrequency squared and $\phi_i \in \mathbb{R}^n$ are the eigenmodes of the full system. For responses which remain close to the linearization $u = 0$ the response of equation 6.24 is accurate. In a situation where dynamics up to a certain frequency are required, the VMs can be truncated to obtain the reduced order model.

$$u(t) \approx \sum_{i=1}^{m} \phi_i \eta_i = \Phi\eta(t) \tag{6.28}$$

where $m < n$. It can be seen that the Φ calculated here represent the same VMs as the Φ_v in Gèradin et al. [27] as well as Φ in Tamarozzi et al. [32]. These Φ are applicable for small displacements from the linearization point. The Modal Derivatives are employed to capture the non-linear behaviour when displacements are no longer 'small'. The stiffness matrix K_{eq}

in equation 6.24 is now replaced by the tangent stiffness matrix K, also known as Jacobi matrix. And differentiated with respect to η_j, where M is a constant mass matrix.

$$(K|_{eq} - \omega_i^2|_{eq} M)) \left.\frac{\partial \phi_i}{\partial \eta_j}\right|_{eq} + \left(\left.\frac{\partial K}{\partial \eta_j}\right|_{eq} - \left.\frac{\partial \omega_i^2}{\partial \eta_j}\right|_{eq} M \right) \phi_i|_{eq} = 0 \tag{6.29}$$

Here the MDs can be seen in $\frac{\partial \phi_i}{\partial \eta_j}$ which is the derivative of mode i in the direction of mode j. Physically this is the sensitivity of mode i in direction j. These Modal Derivatives are not simply obtained from the equation 6.29. The MDs are derived for a mass normalization:

$$\phi_i^T M \phi_i = 1 \forall i \in \mathbb{R}^m \tag{6.30}$$

is then differentiated with respect to the modal amplitude resulting in

$$\phi_i^T M \frac{\partial \phi_i}{\partial \eta_j} + \phi_i^T M^T \frac{\partial \phi_i}{\partial \eta_j} = 0 \forall i, j \in \mathbb{R}^m \tag{6.31}$$

Then the symmetry of M is used in combination with evaluation at the equilibrium position, resulting in

$$\phi_i^T|_{eq} M \left.\frac{\partial \phi_i}{\partial \eta_j}\right|_{eq} = 0 \forall i, j \in \mathbb{R}^m \tag{6.32}$$

The MDs can then be calculated directly from equations 6.29 and 6.32:

$$\begin{bmatrix} \left[K|_{eq} - \omega_i^2|_{eq} M\right]_{n\times n} & -\left[M\phi_i|_{eq}\right]_{n\times 1} \\ -\left[M\phi_i|_{eq}\right]^T_{1\times n} & 0_{1\times 1} \end{bmatrix} \begin{bmatrix} \left.\frac{\partial \phi_i}{\partial \eta_j}\right|_{eq} \\ \left.\frac{\partial \omega_i^2}{\partial \eta_j}\right|_{eq} \end{bmatrix} = \begin{bmatrix} -\frac{\partial K}{\partial \eta_j}\phi_i|_{eq} \\ 0 \end{bmatrix} \tag{6.33}$$

The resulting MDs $\left.\frac{\partial \phi_i}{\partial \eta_j}\right|_{eq}$ will then be part of a linear reduction space V in addition to the relevant Vibration Modes. This reduction space will then be:

$$V = \left[\phi_1|_{eq} \phi_2|_{eq} \dots \phi_m|_{eq} \theta_{ij}|_{eq} \dots\right] \tag{6.34}$$

where $\theta_{ij} = \left.\frac{\partial \phi_i}{\partial \eta_j}\right|_{eq}$ are the modal derivatives describing the non-linear behaviour.

The work by Jain et al. [47] then moves on from the linear mapping $u \approx Vq$ towards a quadratic mapping $u \approx \Phi q + \frac{1}{2}(\Omega q)q$. Both the results given by a linear mapping including MDs and the quadratic mapping provide accurate reductions of the non-linear example model. The quadratic mapping does, however, provide a significant improvement of the amount of DOF in the final reduced model, therefore resulting in lower computational effort. With respect to the methods employed in [27, 32, 43], the current method focuses on the internal effects of geometric non-linear behaviour. It does not take into account the effects which may occur when external loads are applied at unknown locations. The application of the method described in Jain et al. [47] to the current work is dependent of the chosen linearization point and the deviation from this point. If a linearization point can be chosen suc, that the stress-stiffening effects due to the large axial load are incorporated into the reduction space a linear reduction space, using only VMs and RAMs might suffice. If this is not the case, then the non-linear effects need to be incorporated using MDs. Furthermore, since RAMs are not incorporated to cope with the sliding contact, the method must be combined with, for instance, the work by [27, 32], which are part of a linear reduction space. The linear mapping is therefore, for now, the only method of interest.

6.3.4. Proposed reduction scheme

Based on the reduction problem as defined in section 6.3 and the methods of reduction described in the previous section 6.3.3 a reduction approach for the current work can be formulated. Three essential features were identified in section 6.3:

- Dropper slackening / non-linear dropper behaviour
- Sliding contact
- Wave propagation / dynamics

The proposed reduction method is first formulated, after which the inclusion of the three essential features is discussed.

The full non-linear FE model consists of three independent elements: contact wire, messenger wire and droppers, which mainly determine the dynamic model behaviour. In the reviewed literature, there is no mention of cable slackening effects, thus this effect will need to be implemented through a new method. The complete system will therefore first be substructured into the three elements. Elements such as the steady arm and clamp masses are also of importance, their masses will however, for reasons of simplification, be reduced with their respective cable. The substructuring process splits the model in three parts, figure 6.2 shows where the model is split.

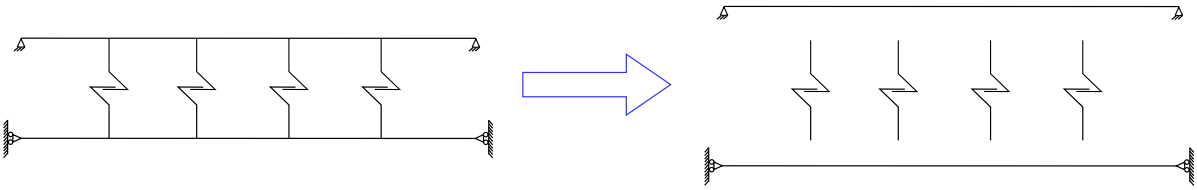

Figure 6.2: Substructuring process for 1 span

After this substructuring process, the relevant reduction spaces have to be defined for each substructure. The contact wire subspace will contain:

- Vibration modes Φ_i up to at least $\omega_i = 20$ Hz, evaluated at the static equilibrium position, in order to include geometric non-linear behaviour in the linearization. This ensures that wave propagation and dynamics up to 20 Hz are incorporated in the reduced order model.
- Residual attachment modes ψ_a to describe the support behaviour.
- Residual attachment modes ψ_d to describe the displacements resulting from dropper forces.
- Residual attachment modes ψ_c to describe the not fully predictable sliding contact.

it will therefore have the form:

$$V_c = [\Phi\psi_{ac}\psi_{dc}\psi_{cc}] \tag{6.35}$$

The messenger wire subspace will contain:

- Vibration modes Φ_i up to at least $\omega_i = 20$ Hz evaluated at the static equilibrium position, in order to include geometric non-linear behaviour in the linearization. This ensures that wave propagation and dynamics up to 20 Hz are incorporated in the reduced order model.
- Residual attachment modes ψ_a to describe the support behaviour.
- Residual attachment modes ψ_d to describe the displacements resulting from dropper forces.

and thus have form:

$$V_m = [\Phi\psi_{am}\psi_{dm}] \tag{6.36}$$

Since the non-linear dropper behaviour was not described in previous literature, this part will not be reduced. Each dropper will be represented by a stiffness K_d:

$$K_d = \begin{bmatrix} K_{d,1} & 0 & 0 & 0 \\ 0 & K_{d,2} & 0 & 0 \\ 0 & 0 & \dots & 0 \\ 0 & 0 & 0 & K_{d,i} \end{bmatrix} \tag{6.37}$$

During time integration all far-field $K_{d,i}$ are assumed to be in tension and therefore $K = 100000N/m$. This assumption results from the fact that the non-linear behaviour only happens to the droppers closest to the pantograph. Near field values are reviewed to check whether the corresponding dropper is in compression using the following scheme:

$$\begin{aligned} &\text{get } x \text{ position pantograph} \\ &\text{find closest dropper number } j \\ &\text{calculate } U_d = \left[\left(z_{1,j-2} - z_{2,j-2} - l_{d,j-2}\right) \dots \left(z_{1,j+2} - z_{2,j+2} - l_{d,j+2}\right)\right]^T \\ &\text{for each } U_{d,j} < 0 \rightarrow K_{d,j} = 0 \end{aligned}$$

Where $U_d \in \mathbb{R}^i$ is the strain vector, $z_{1,i}$, $z_{2,i}$ are the z positions of respectively messenger and contact wire at the dropper location. For a situation where $K_{d,j-1} \rightarrow K_{d,j+1} = 0$ the updated dropper stiffness matrix has the form

$$K_d = \begin{bmatrix} K_{d,1} & 0 & 0 & 0 & 0 & 0 & 0 & 0 & 0 & 0 \\ 0 & K_{d,2} & 0 & 0 & 0 & 0 & 0 & 0 & 0 & 0 \\ 0 & 0 & \dots & 0 & 0 & 0 & 0 & 0 & 0 & 0 \\ 0 & 0 & 0 & K_{d,j-2} & 0 & 0 & 0 & 0 & 0 & 0 \\ 0 & 0 & 0 & 0 & 0 & 0 & 0 & 0 & 0 & 0 \\ 0 & 0 & 0 & 0 & 0 & 0 & 0 & 0 & 0 & 0 \\ 0 & 0 & 0 & 0 & 0 & 0 & 0 & 0 & 0 & 0 \\ 0 & 0 & 0 & 0 & 0 & 0 & 0 & K_{d,j+2} & 0 & 0 \\ 0 & 0 & 0 & 0 & 0 & 0 & 0 & 0 & \dots & 0 \\ 0 & 0 & 0 & 0 & 0 & 0 & 0 & 0 & 0 & K_{d,i} \end{bmatrix} \tag{6.38}$$

from this updated stiffness matrix K_d and the strain vector U_d, the non-linear dropper force f_{nl} is calculated

$$f_{nl,i} = K_d U_d \tag{6.39}$$

$$\begin{bmatrix} f_{nl,1} \\ f_{nl,2} \\ \dots \\ f_{nl,j-2} \\ 0 \\ 0 \\ 0 \\ f_{nl,j+2} \\ \dots \\ f_{nl,i} \end{bmatrix} = \begin{bmatrix} K_{d,1} & 0 & 0 & 0 & 0 & 0 & 0 & 0 & 0 & 0 \\ 0 & K_{d,2} & 0 & 0 & 0 & 0 & 0 & 0 & 0 & 0 \\ 0 & 0 & \dots & 0 & 0 & 0 & 0 & 0 & 0 & 0 \\ 0 & 0 & 0 & K_{d,j-2} & 0 & 0 & 0 & 0 & 0 & 0 \\ 0 & 0 & 0 & 0 & 0 & 0 & 0 & 0 & 0 & 0 \\ 0 & 0 & 0 & 0 & 0 & 0 & 0 & 0 & 0 & 0 \\ 0 & 0 & 0 & 0 & 0 & 0 & 0 & 0 & 0 & 0 \\ 0 & 0 & 0 & 0 & 0 & 0 & 0 & K_{d,j+2} & 0 & 0 \\ 0 & 0 & 0 & 0 & 0 & 0 & 0 & 0 & \dots & 0 \\ 0 & 0 & 0 & 0 & 0 & 0 & 0 & 0 & 0 & K_{d,i} \end{bmatrix} \begin{bmatrix} U_{d,1} \\ U_{d,2} \\ \dots \\ U_{d,j-2} \\ U_{d,j-1} \\ U_{d,j} \\ U_{d,j+1} \\ U_{d,j+2} \\ \dots \\ U_{d,i} \end{bmatrix} \tag{6.40}$$

In comparison with the $K \in \mathbb{R}^{n \times n}$ matrix for a full model , the updating of matrix $K_d \in \mathbb{R}^{i \times i}$ is much less expensive since $i << n$ furthermore, due to assuming far field to remain in the linear region, the part of the matrix that must be edited contains only 5 unknowns. The final reduced model then contains three subsystems: the contact wire, is reduced by Galerkin projection:

$$\tilde{K_c} = V_c^T K_c V_c \tag{6.41}$$

$$\tilde{M_c} = V_c^T M_c V_c \tag{6.42}$$

$$\tilde{C_c} = \alpha \tilde{M_c} + \beta \tilde{K_c} \tag{6.43}$$

where $\tilde{C_c}$, the damping matrix is a weighted (α, β) linear combination of the mass and stiffness matrices. Similarly the messenger wire reduces to:

$$\tilde{K_m} = V_m^T K_m V_m \tag{6.44}$$

$$\tilde{M_m} = V_m^T M_m V_m \tag{6.45}$$

$$\tilde{C_m} = \alpha \tilde{M_m} + \beta \tilde{K_m} \tag{6.46}$$

note that the values α and β in equations 6.43 and 6.46 are the same, since damping is applied globally. The three essential features are all incorporated in this reduction space:

- Dropper slackening / non-linear dropper behaviour, as defined in this section the non-linear dropper behaviour is separated from the contact and messenger wire, therefore this part need not be reduced.
- Sliding contact, this is incorporated in the reduction space due to the Residual Attachment Modes
- Wave propagation, this is incorporated in the reduction space through the Vibration Modes.

The actual calculation of the reduction spaces V_c and V_m and the reduced order model parameters in equation 6.41 to equation 6.46 will be the subject of the subsequent thesis work. Different reduction spaces may be introduced to further improve upon the currently proposed space.

6.3.5. Assembly

Assembly of the full FE model can be achieved in a primal or a dual manner, both methods are described briefly and both methods have their own pros and cons. Furthermore the time integration method of choice further complicates the assembly method since it implies that the results are not only dependent of the stiffness matrix, yet also from the mass and damping matrices. Further on in the section this part will be discussed in full.

The full un-assembled system stiffness matrix consists of 2 different matrices. The block diagonal beam element stiffness matrix K_b which contains the Euler-Bernoulli beam stiffnesses and the geometric stiffness due to pre loading.

$$K_b = \begin{bmatrix} K_{b,1} & 0 & 0 & 0 \\ 0 & K_{b,2} & 0 & 0 \\ 0 & 0 & \dots & 0 \\ 0 & 0 & 0 & K_{b,i} \end{bmatrix} \tag{6.47}$$

Where $K_{b,i}$ is a 4 by 4 element stiffness matrix related to the elemental displacement vector $U_b = [u_{b,1}\theta_{b,1}u_{b,2}\theta_{b,2}]$. The block diagonal dropper element stiffness matrix K_d contains the dropper stiffness according to equation 6.38. The full un-assembled stiffness matrix K_{block} is then made by putting K_b and K_d on the diagonal.

$$K_{block} = \begin{bmatrix} K_b & 0 \\ 0 & K_d \end{bmatrix} \tag{6.48}$$

In order to assemble the full system, a signed boolean matrix B needs to be built, containing a constraint equation in each row which determines which DOF are constrained to eachother. This matrix is of size $c \times n$ where c is the amount of constraint equations and n the amount of DOF in the system.

The full system can be written as follows:

$$M_{block}\ddot{u} + C_{block}\dot{u} + K_{block}u = f + g \tag{6.49}$$

where M_{block} is the block diagonal mass matrix, $C_{block} = \alpha * M_{block} + \beta * K_{block}$, f is the external force vector and g is the internal force vector.

Primal assembly

In a primal assembly the assembled system retains only the active (non-constrained) DOF. Compatability is ensured by $Bu = 0$, equilibrium is obtained through $L^T g = 0$. In order to primally assemble the stiffness matrix, a boolean matrix $L = null(B)$ is built, L represents the null space of boolean matrix B and is of size $n \times (n - c)$. The global stiffness matrix is then assembled by pre- and post-multiplication of K_{block} by respectively $L^T and L$. This section is not a full derivation of the primal assembly method, it is meant to show how the current system can be assembled with this method which is described in de Klerk et al. [48].

$$K_{glob} = L^T K_{block} L \tag{6.50}$$

K_{glob} is of size $(n - c) \times (n - c)$ and is non-singular, whereas K_block was singular due to the dropper stiffness K_d. Similar to the assembly of K_{glob}, the assembled force vector and mass and damping matrices may be created

$$F_{glob} = L^T F \tag{6.51}$$

$$M_{glob} = L^T M_{block} L \tag{6.52}$$

$$C_{glob} = L^T C_{block} L \tag{6.53}$$

The full assembled system is now:

$$\begin{cases} M_{glob}\ddot{q} + C_{glob}\dot{q} + K_{glob} q = F_{glob} \\ L^T g = 0 \end{cases} \tag{6.54}$$

where $q = L^T u$.

Dual assembly

In a dual assembly all interface DOF are retained and equilibrium and compatability are satisfied a priori by choosing the internal forces [48] $g = -B\lambda$ and equilibrium $L^T g = 0$. As opposed to the primal formulation, no new system matrices need to be calculated, however, Lagrange multipliers need to be calculated or eliminated.

$$\begin{cases} M_{block}\ddot{u} + C_{block}\dot{u} + K_{block} u + B^T \lambda = F_{block} \\ Bu = 0 \end{cases} \tag{6.55}$$

6.4. Solver / time integration improvements

Time integration will be done using a Newmark-β method. The method explained here is a HHT-α method, which for $\alpha = 0$ reduces to the desired Newmark-β method. The difference between HHT-α and Newmark-β lies in the numerical damping, applied through changing the α As an extension to this Newmark-β time integration an HHT-α integration can be done. This method, as well as the Newmark-β method, is unconditionally stable. The finite difference approximations which hold for both method are as follows:

$$x_{i+1} \approx x_i + h\dot{x}_i + h^2 \left[\left(\frac{1}{2} - \beta \right) \ddot{x}_i + \beta \ddot{x}_{i+1} \right] \tag{6.56}$$

$$\dot{x}_{i+1} \approx \dot{x}_i + h\left[(1 - \gamma)\, \ddot{x}_i + \gamma \ddot{x}_{i+1} \right] \tag{6.57}$$

The HHT-α equation of motion is

$$M\ddot{x}_{i+1} + (1 - \alpha) C\dot{x}_{i+1} + \alpha C\dot{x}_i + (1 - \alpha) K x_{i+1} + \alpha K x_i = (1 - \alpha) f_{i+i}^{ext} + \alpha f_i^{ext} \tag{6.58}$$

This equation is unconditionally stable when

$$0 \leq \alpha \leq \frac{1}{3}$$

$$\beta = \frac{(1 + \alpha)^2}{4}$$

$$\gamma = \frac{1}{2} + \alpha$$

Substitution of the Newmark-β finite difference approximations 6.56 and 6.57 in to equation 6.58 and grouping terms

$$\begin{aligned}\left[M + h(1-\alpha)\gamma C + h^2(1-\alpha)\beta K\right]\ddot{x}_{i+1} + \\ \left[h(1-\alpha)(1-\gamma)C + h^2(1-\alpha)(\frac{1}{2}-\beta)K\right]\ddot{x}_i + \\ \left[C + h(1-\alpha)K\right]\dot{x}_i + \\ Kx_i \\ = (1-\alpha)f_{i+i}^{ext} + \alpha f_i^{ext}\end{aligned} \tag{6.59}$$

For $\alpha = 0$, $\beta = \frac{1}{4}$ and $\gamma = \frac{1}{2}$ this formula reduces to

$$\begin{aligned}\left[M + \frac{hC}{2} + \frac{h^2K}{4}\right]\ddot{x}_{i+1} + \\ \left[\frac{hC}{2} + \frac{h^2K}{4}\right]\ddot{x}_i + \\ \left[C + hK\right]\dot{x}_i + \\ Kx_i \\ = f_{i+i}^{ext}\end{aligned} \tag{6.60}$$

Rearranging results in

$$\left[M + \frac{hC}{2} + \frac{h^2K}{4}\right]\ddot{x}_{i+1} = f_{i+i}^{ext} - \left[\frac{hC}{2} + \frac{h^2K}{4}\right]\ddot{x}_i - \left[C + hK\right]\dot{x}_i - Kx_i \tag{6.61}$$

This can be solved for $\ddot{x}_{i+1}$, from the finite difference equations $\dot{x}_{i+1}$ and x_{i+1} can then be calculated.

6.4.1. Direct Newmark, with iteration matrix updates

The main issue of solving for $\ddot{x}_{i+1}$ is solving the equation of motion. The exact solution can be found by inverting the full system matrices and solving the equilibrium equation. In such a way the new equation of motion becomes

$$\ddot{x}_{i+1} = \left[f_{i+i}^{ext} - \left[\frac{hC}{2} + \frac{h^2K}{4}\right]\ddot{x}_i - \left[C + hK\right]\dot{x}_i - Kx_i\right] * \left[M + \frac{hC}{2} + \frac{h^2K}{4}\right]^{-1} \tag{6.62}$$

solving this equations requires computation of the inverse of $\left[M + \frac{hC}{2} + \frac{h^2K}{4}\right]$ multiple times as the K matrix changes during integration. This generally requires a lot of computational effort as the system matrices K, C and M become large. To improve the efficiency of this calculation, a preferable method is calculation of the inverse once, prior to time integration, after which small, computationally efficient updating is applied. The method to achieve this starts with the inverse to be calculated at time 0, for ease of use the inverse of $\left[M + \frac{hC}{2} + \frac{h^2K}{4}\right]$ will be compacted to L^{-1}.

$$L_0^{-1} = \left[M_0 + \frac{hC_0}{2} + \frac{h^2K_0}{4}\right]^{-1} \tag{6.63}$$

Where all stiffnesses are in the linear domain, since M does not change, K does and $C = 0.0125 * M + 0.0001 * K$ is a linear combination of both, the inverse is split in 2 parts, the changing and the non-changing part

$$L_0^{-1} = \left[\left(1 + \frac{0.0125 * h}{2}\right)M_0 + \left(\frac{h^2}{4} + \frac{0.0001 * h}{2}\right)K_0\right]^{-1} \tag{6.64}$$

accepting that a value for h is chosen prior to time integration, the inverse is now of a form

$$L_0^{-1} = [aM_0 + bK_0]^{-1} \tag{6.65}$$

the change in matrix K is allways of rank 1 since a dropper element stiffness

$$K_{d,i} = \begin{bmatrix} 100000 & -100000 \\ -1000000 & 100000 \end{bmatrix} \tag{6.66}$$

is of rank 1, the difference between the previous and current stiffness matrix is thus

$$K_{diff} = K_{previous} - K_{current} = \begin{bmatrix} 0 & 0 & 0 & 0 & 0 & 0 & 0 & 0 & 0 & 0 \\ 0 & 0 & 0 & 0 & 0 & 0 & 0 & 0 & 0 & 0 \\ 0 & 0 & \dots & 0 & 0 & 0 & 0 & 0 & 0 & 0 \\ 0 & 0 & 0 & 0 & 0 & 0 & 0 & 0 & 0 & 0 \\ 0 & 0 & 0 & 0 & 0 & 0 & 0 & 0 & 0 & 0 \\ 0 & 0 & 0 & 0 & 0 & 0 & 0 & 0 & 0 & 0 \\ 0 & 0 & 0 & 0 & 0 & 0 & 0 & 0 & 0 & 0 \\ 0 & 0 & 0 & 0 & 0 & 0 & 0 & K_{d,i} & 0 & 0 \\ 0 & 0 & 0 & 0 & 0 & 0 & 0 & 0 & \dots & 0 \\ 0 & 0 & 0 & 0 & 0 & 0 & 0 & 0 & 0 & 0 \end{bmatrix} \tag{6.67}$$

where $rank(K_{diff}) = 1$ and thus

$$L_{diff} = \left[aM_{previous} + bK_{previous}\right] - \left[aM_{current} + bK_{current}\right] \tag{6.68}$$

where $aM_{previous} - aM_{current} = 0$

$$L_{diff} = b\left[K_{previous} - K_{current}\right] = b\left[K_{diff}\right] \tag{6.69}$$

since b is a scalar it is clear that $rank(L_{diff}) = 1$ In which case the Sherman-Morrison [49] formula for rank-1 updates may be applied.

$$\left(L_{prev} + uv^T\right)^{-1} = L_{prev}^{-1} - \frac{1}{1 + v^T L_{prev}^{-1} u}\left(L_{prev}^{-1} uv^T L_{prev}^{-1}\right) \tag{6.70}$$

to compute uv^T we need to take into account that:

$$uv^T = L_{diff} \tag{6.71}$$

and since the Singular Value Decomposition of L_{diff}

$$USV^* = L_{diff} \tag{6.72}$$

combining equations 6.71 and 6.72 and taking note that due to rank of $L_{diff} = 1$, the SVD reduces to 1 singular value and 2 single-column vectors, and $real(V^*) = V^T$.

$$uv^T = S_{(1,1)} U_{(:,1)} V_{(:,1)}^T \tag{6.73}$$

resulting in

$$u = S_{(1,1)} U_{(:,1)} \;\; \& \;\; v^T = V_{(:,1)}^T \tag{6.74}$$

The rank 1 updating equation 6.70 now reads

$$L_{curr}^{-1} = \left(L_{prev} + S_{(1,1)} U_{(:,1)} V_{(:,1)}^T\right)^{-1} = L_{prev}^{-1} - \frac{1}{1 + V_{(:,1)}^T L_{prev}^{-1} S_{(1,1)} U_{(:,1)}}\left(L_{prev}^{-1} S_{(1,1)} U_{(:,1)} V_{(:,1)}^T L_{prev}^{-1}\right) \tag{6.75}$$

It can be checked that, for all matrices of rank 1, equations 6.74 and 6.75 hold, also after modal reduction, where the rank of the matrix is not easily observed as 1, yet is definitely of rank 1.

This method delivers an exact solution $\ddot{x}_{i+1}$ to equation 6.62, the accuracy of the result is based on the (finite difference) approximations on which the equation relies. Due to the low rank updating of the matrix inverse, time can be saved. The SVD decomposition of the full matrix however is time consuming. This is compensated by the fact that only the first column needs to be computed, nevertheless this means that for large systems, the currently proposed method delivers faster results, whereas small systems are better off by simply calculating the inverse. That being said, the currently proposed method will be applied to larger systems, and will therefore provide improved performance. Furthermore, in situations like equation 6.67, where the majority of the difference matrix is zero, a SVD of the 2×2 matrix $K_{d,i}$, combined with an index search operation to determine the placement of the SVD results.

6.4.2. Direct Newmark, without iteration matrix updates

The direct Newmark solver, which does not update the iteration matrix, corresponds to the Newmark solver for linear systems. The catenary system, on which the solver is applied, is mainly linear. Some non-linearities exist in the beam elements, such as stress-stiffening, may be pre-calculated by means of the geometric stiffness matrix (equation 7.2). Furthermore, the dropper decoupling, is a fairly straightforward matrix operation. Resulting in a near-linear system which may be solved using a linear solver.

First an estimate of the state is done using the following predictor formulae:

$$U^*_{n+1} = U_n + h * \dot{U}_n + (\frac{1}{2} - \beta) * h^2 * \ddot{U}_n \tag{6.76}$$

$$\dot{U}^*_{n+1} = \dot{U}_n + (1 - \gamma) * \ddot{U}_n \tag{6.77}$$

After this the value for $\ddot{U}_{n+1}$ is calculated by solving:

$$\left[M_{glob} + h * \gamma * C_{glob} + h^2 * \beta * K_{glob}\right] \ddot{U}_{n+1} = F_{glob_{(n+1)}} - C_{glob} * \dot{U}^*_{n+1} - K_{glob} * U^*_{n+1} \tag{6.78}$$

lastly the predicted values are updated:

$$U_{n+1} = U^*_{n+1} + \beta * h^2 * \ddot{U}_{n+1} \tag{6.79}$$

$$\dot{U}_{n+1} = \dot{U}^*_{n+1} + \gamma * h * \ddot{U}_{n+1} \tag{6.80}$$

This solution procedure entails calculating the inverse of the iteration matrix $\left[M_{glob} + h * \gamma * C_{glob} + h^2 * \beta * K_{glob}\right]$. The choice is made to refrain from updating this matrix, which allows the inverse to be pre-calculated, thereby improving the in-loop computational effort. Note that this method is identical to the method proposed in chapter 6. The difference is the formulation of the equations due to the updating of the iteration matrix. For a linear solver, this only works if the variational formulation is used.

6.4.3. Iterative Newmark + Newton-Rhapson, with and without iteration matrix updates

In order to provide a correct comparison between the proposed solvers and the current Ansys solver it is essential to build a representative Ansys solver. Based on the Ansys theory reference [50], the following solver is built.

First an estimate of the state is done using the following predictor formulas:

$$U^*_{n+1} = U_n + h * \dot{U}_n + (\frac{1}{2} - \beta) * h^2 * \ddot{U}_n \tag{6.81}$$

$$\dot{U}^*_{n+1} = \dot{U}_n + (1 - \gamma) * \ddot{U}_n \tag{6.82}$$

$$\ddot{U}^*_{n+1} = 0 \tag{6.83}$$

Where h denotes the time step, $\ddot{U}_n$, $\dot{U}_n$ and U_n the acceleration, velocity and displacement at time n, whereas U^*_{n+1} and its derivatives denote the predicted value at time $n+1$. Next the residual value is calculated:

$$R(\ddot{U}^*_{n+1}, \dot{U}^*_{n+1}, U^*_{n+1}) = F_{glob} - M_{glob} * \ddot{U}^*_{n+1} - C_{glob} * \dot{U}^*_{n+1} - K_{glob} * U^*_{n+1} \tag{6.84}$$

The value of $||R(\ddot{U}^*_{n+1}, \dot{U}^*_{n+1}, U^*_{n+1})||$ ($||*||$ denotes the norm of $*$) is compared to a convergence value $err = ||\eta * F_{glob}||$ where η is a value chosen to ensure the converged solution is close to the actual solution.

The iterative solution is triggered through the comparison: while $||R(\ddot{U}^*_{n+1}, \dot{U}^*_{n+1}, U^*_{n+1})|| >= ||\eta * F_{glob}||$. The following updating / correction procedure is started and will iterate until the residual norm is below the err value:

the following equation is first solved for δU^*_{n+1}

$$\left[\frac{1}{\beta * h^2} * M_{glob} + \frac{\gamma}{\beta * h} * C_{glob} + K_{glob}\right] * \delta U^1_{n+1} = F_{glob_{(n+1)}} - M_{glob} * \ddot{U}^*_{n+1} - C_{glob} * \dot{U}^*_{n+1} - K_{glob} * U^*_{n+1} \tag{6.85}$$

then the values for $\ddot{U}^*_{n+1}, \dot{U}^*_{n+1}, U^*_{n+1}$ are updated. To clarify, the * superscript denotes the iteration number, thus the first correction results in the values:

$$U^1_{n+1} = U^*_{n+1} + \delta U^1_{n+1} \tag{6.86}$$

$$\dot{U}^1_{n+1} = \dot{U}^*_{n+1} + \frac{\gamma}{\beta * h} * \delta U^1_{n+1} \tag{6.87}$$

$$\ddot{U}^1_{n+1} = \ddot{U}^*_{n+1} + \frac{1}{\beta * h^2} * \delta U^1_{n+1} \tag{6.88}$$

After the solution is converged, the process is repeated until the solution is finished. This solver is used for systems, with and without matrix updates. The solution of equation 6.85, only differs through the updating of the left hand side of the equation.

The solver as proposed here is one of the solvers available in Ansys when non-linear effects are to be taken into account. There are some minor differences between this solver and the Ansys solver which need to be taken into account:

- Ansys allows multiple convergence criteria, the currently proposed solver does not implement this functionality.
- The prediction and correction functions here might differ slightly from the functions used by ansys. This is due to the fact that these are not explicitly mentioned in the Ansys theory reference. This is however only a matter of form, the solution algorithm is the same.

6.4.4. Convergence criteria comparison

The optimization of model criteria, in essence, means loosening the convergence criteria to improve computation times. This method, which can only be applied when the current simulations return a stable catenary, improves computation times at the expense of solver stability. The requirement of stable catenary simulations means this method can only be implemented at the end of this project, thus, this method will be explored after the validated simulations are completed. This will be tested together with the solver improvement tests, to see how the proposed solvers scale as convergence criteria become stringent.

6.5. Contact method improvements

The contact methods are compared to each other, however, they can not just be compared based on one model. As described in chapter 8, it is important to change relevant variables. Furthermore, the analyses are done with changing frequencies, thereby taking into account scaling with time step. Moreover, velocity scaling is introduced by performing a second analysis at 10 times the speed. The scaling with respect to the size of the model shall be investigated through the addition of 2 and 4 spans at the end of the model, which are not loaded. This will show whether the improvement scales in unison with the size of the model, or whether it is absolute and therefore diminishes as the size of the model increases.

6.5.1. Contact module

The contact module as used in the EN50318 validated model, is a penalty based beam-to-beam contact model, in which the penalty stiffnesses and penetration are all governed automatically by the solver. This is expected to cause high computational effort, thereby resulting in prohibitive simulation times. In highly complex models where the contact compatibility is very important, a lot of elements are in contact simultaneously and results are not filtered afterwards. This may be a trade-off worth making. However, in the current work this is not the case. The contact exists between 2 elements, it will always be found at the current position of the pantograph and penetration is allowed as long as the contact force is correct. Furthermore, in low frequency situations the module may lose contact if the time step results in over penetration of the catenary. It is expected that use of the contact module results in increasingly difficult convergence behaviour as well as longer simulation times.

6.5.2. Direct Application

The direct application of forces onto the model requires multiple load steps to be defined. This has to be implemented prior to the solution process, thereby it does not allow for calculation of forces between steps. However, since an improved solution procedure will most likely be executed outside Ansys, this is not an issue. For the sake of comparison, a constant force will suffice. The Direct Application method is expected to be the faster contact method, first of all due to the lack of force calculations, more so due to the lack of all contact module overhead. Adversely, the method requires that every time the load moves a new load step must be solved, this will slow down the calculation of the results slightly. In order to show the effect this has, the Contact model simulation will also be calculated with multiple load steps.

6.5.3. Validation of Comparison

The contact model has been modeled as a rigid rod with 14kg mass and an average upward force of 150n whereas the Direct application has been modeled as an upward force of 150n at all times. This entails that the loads applied on the system, when comparing the Direct Application method and the Contact Module method are not completely equal. This is a necessary evil however, since the contact element needs to be modeled with significant mass to reduce the accelerations and respectively velocities on the element. The contact models, therefore, do not result in an exact same situation. The settings in the contact module represent the best case scenario when working with Ansys. However, at lower analysis frequencies, the model still does not converge correctly and becomes unstable. This is mainly the result of the element passing problem (see section 3.5). On the other hand, the Direct Application method is the best case scenario for the other simulation methods. In order to be able to put all these simulations in perspective, it is important to check the influence of the added mass to the simulation results. To that extent the Contact Module simulation is performed once, with a 14kg rod, and another time with a 7.5kg rod. The values in table 6.2 are the results of these control simulations.

	Contact Module 14kg	Contact Module 7.5kg	Improvement in %
500hz, 0.1m/step	483.05	483.69	0.13%

Table 6.2: Control simulation to check mass influence on simulation time, by simulation time [s]

Based on the values in table 6.2 it is concluded that the mass does not influence the simulation time. Therefore, when Contact Module and Direct Application are compared, the difference in simulation times can reliably be related to the used contact model.

6.6. Conclusion

Based on reviewed literature, a new reduction method is proposed. This reduction method contains all required features defined in the beginning of this chapter. It does not employ new or unproven techniques, only different applications of currently available methods. Therefore there is significant confidence that the method will provide accurate results, whilst being applicable to the current model. Inclusion of the non-linear dropper effect in time integration is ensured due to decoupling of the spring stiffness as the droppers are loaded in compression. Inclusion of this effect in the modal domain provides some questions which still need answering. Even though deducting a dropper stiffness in the modal domain is as easy as it is in the physical domain. The modes with which it is multiplied do not accommodate high movements at the dropper location, therefore the reduction space V will also need to be adapted. Several methods for improvement of time integration have been proposed. In the remainder of this research, these methods will be applied, tested and improved upon if possible.

In order to achieve the second goal of this research, as defined in chapter 1: *"To find and apply a reduction method, which reduces computational effort whilst respecting dropper slackening, non-linear sliding contact and wave propagation."*. The following questions are formulated:

- Does replacing the Ansys iterative solver by a direct solver which uses Iteration matrix updates, result in lower simulation times, and do these represent a significant improvement with respect to the Ansys method. Furthermore, how do these improvements relate to other common solver types.
- Does replacing the Ansys contact module by another contact method result in lower simulation times, and do these represent a significant improvement with respect to the Ansys method .
- Does replacing a physical Finite Element Method model by a Reduced Order Model through Modal Reduction improve simulation times, and do these represent a significant improvement with respect to a full physical Finite Element Method model.

7

Model for improvement tests

7.1. Introduction

This chapter focuses on creating a simplified FE model in Matlab, upon which spring decoupling, solver improvements and contact model improvements can be applied. These improvements will be described in chapters 8 and 9.

The remaining model building and decoupling process is as follows:

- Create simplified catenary Finite Element Method model.
- Write time integrator based on the Newmark - β or HHT-α solvers, ensuring unconditional stability.
- Perform decoupling procedure
- Extend Finite Element Method model to incorporate messenger wire

The model, upon which the reduction process is applied is a very simplified version of the full model. It consists of the basics which determine a catenary: Contact wire and droppers. This model is built to test which improvements can be done to improve upon the Ansys version of the model and to be able to judge these improvements in an inexpensive (time) manner. Later, the model is extended to include the messenger wire in order to gain a complete model upon which the solver can be executed.

7.2. Simplified model

To gradually create a more extensive catenary model, the first model that is built represents a system as can be seen in figure 7.1. This model does not include the pantograph. In its place a discrete moving load is applied. This helps isolating the simulation times as well as convergence issues arising from the catenary system, which is one of the goals of this work.

7.2.1. Element choice and Matrix generation

The contact wire is a long slender beam, whose bending stiffness is based on both the bending stiffness of the material and geometrical properties of the beam, as well as on the pre-tension applied to this beam. Based on the loading of the beam occuring predominantly in the bending domain, the axial degrees of freedom will not be taken into account in the simplified model. The bending stiffness of the matrix is based on the Euler-Bernoulli beam element. The stiffness matrices belonging to these phenomena are as follows:

$$Z_{Euler-Bernoulli} = E_b * I_{yy,b} \begin{bmatrix} \frac{12}{L^3} & \frac{6}{L^2} & \frac{-12}{L^3} & \frac{6}{L^2} \\ \frac{6}{L^2} & \frac{4}{L} & \frac{-6}{L^2} & \frac{2}{L} \\ \frac{-12}{L^3} & \frac{-6}{L^2} & \frac{12}{L^3} & \frac{-6}{L^2} \\ \frac{6}{L^2} & \frac{2}{L} & \frac{-6}{L^2} & \frac{4}{L} \end{bmatrix} \tag{7.1}$$

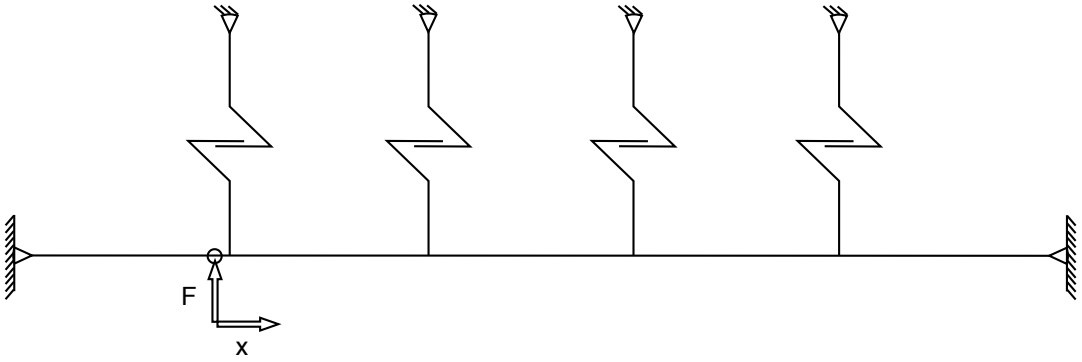

Figure 7.1: Simplified catenary system

Which represents the bending stiffness of an Euler-Bernoulli beam, with E_b is Young's modulus, $I_{yy,b}$ is bending moment of inertia and L is length of the beam element.

$$Z_{geometric} = \frac{N}{L}\begin{bmatrix} \frac{6}{5} & \frac{L}{10} & \frac{-6}{5} & \frac{L}{10} \\ \frac{L}{10} & \frac{2*L^2}{15} & \frac{-L}{10} & \frac{-L^2}{30} \\ \frac{-6}{5} & \frac{-L}{10} & \frac{6}{5} & \frac{-L}{10} \\ \frac{L}{10} & \frac{-L^2}{30} & \frac{-L}{10} & \frac{-2*L^2}{15} \end{bmatrix} \tag{7.2}$$

Which represents the geometric stiffness of the beam under tension N in newton, where L is length of the beam element. The dropper stiffness are defined as in equation 6.66. Assembly of the system is performed using the Primal assembly method provided in section 6.3.5. This results in assembled stiffness- mass- and damping matrices.

7.2.2. Decoupling procedure

The decoupling procedure as described in section 6.3.4 is applied through the following pseudo script:

- ***if*** dropper force >=0 && previous dropper force <0
  - Calculate block-diagonal stiffness matrix difference with 1 dropper removed
  - Assemble stiffness matrix difference
  - Compute new Assembled stiffness matrix
  - Compute new Assembled damping matrix
  - ***if*** Rank 1 updating of the tangent stiffness (equation 6.63) inverse is desired
    - Execute equation 6.64 to 6.75
  - ***end if***
- ***else if*** dropper force <=0 && previous dropper force >0
  - Calculate block-diagonal stiffness matrix difference with 1 dropper reattached
  - Assemble stiffness matrix difference
  - Compute new Assembled stiffness matrix
  - Compute new Assembled damping matrix
  - ***if*** Rank 1 updating of the tangent stiffness (equation 6.63) inverse is desired
    - Execute equation 6.64 to 6.75
  - ***end if***
- ***end if***

7.2.3. Load application and Time integration

The simplified model is loaded by a constant force. The location of this force changes based on the velocity input. This is implemented by continuously updating the load step to represent the new load case, whilst performing the time integration. In future work this will also entail the calculation of the amplitude of the force, based on the desired contact module as well as the chosen pantograph model.

7.3. Extended model

The extension of the simplified model entails the addition of a second cable, the messenger wire. The definitions of the wires can be reviewed in figure 2.1. The dropper stiffnesses have to be disconnected from the 'world' and connected to the messenger wire. A visual representation of this system can be seen in figure 7.2.

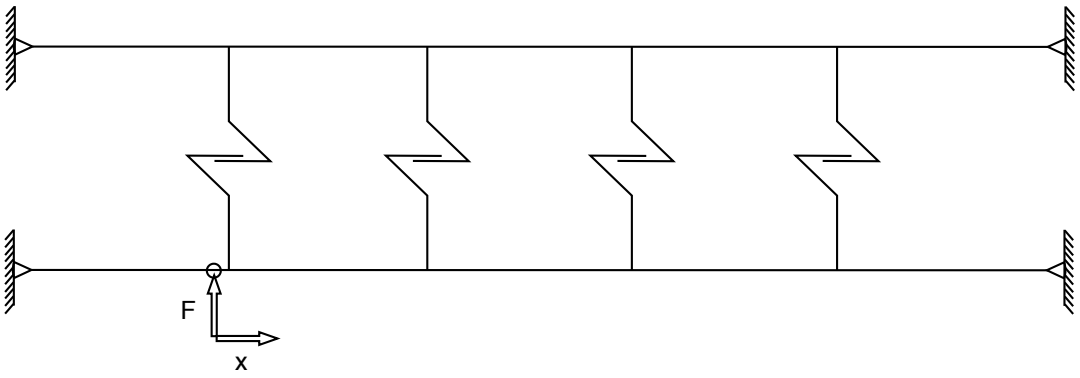

Figure 7.2: Extended catenary system

To move from the system in figure 7.1 to the system in figure 7.2 the system matrices will need to be changed in order to accompany the extra wire. Furthermore there will need to be minor changes to the boolean matrix B, to accompany the dropper stiffnesses to attach to the messenger wire correctly. The messenger wire stiffness matrix is constructed in a similar manner to the contact wire, see equations 7.1,7.2. The stiffness matrix lay-out now becomes:

$$Z_{system} = \begin{bmatrix} Z_{contact} & 0 & 0 \\ 0 & Z_{messenger} & 0 \\ 0 & 0 & Z_{dropper} \end{bmatrix} \tag{7.3}$$

Mass and damping matrices' lay-out will be comparable to the stiffness matrix lay-out. Furthermore the decoupling procedure now requires the displacements of both contact wire as well as catenary wire in order to correctly determine the moment of decoupling.

7.4. Modally reduced simplified model

The proposed substructuring method in chapter 6 is performed in Matlab r2017b. The modal reduction which was proposed here, has already in an early stage not resulted in simulation time improvements. This is mainly due to the large amount of interface locations and as a consequence, a large amount of modes need to be kept in the system. Furthermore, the load vector needs to be projected onto the modal domain every time-step, as physical model sizes remain large, this means this a reasonably inefficient procedure. This results in less simulation time improvement. Therefore, the decision has been made to not go too far into detail in the main body of this work. The process however, has been recorded and can be referenced in appendix D.

8

Solver Implementation results

8.1. Introduction

In the previous chapters the possibility of improving the simulation time has been discussed thoroughly. These improvements are tailored specifically to the problem at hand in this simulation method, which can be described as a largely linear system with very local non-linearities and pre-calculable stress-stiffening terms. This model, which is full of non-linear elements, can be solved by multiple methods. These can be split in Implicit and Explicit methods. Furthermore the system can be solved in a direct manner by solving the equation of motion, or the system can be solved in an iterative manner by calculating the residual and updating the guess. In general it can be stated that linear solvers usually entail a direct solver, whereas non-linear solvers usually entail an iterative solver. The proposed solver enhancements are to be tested on the simplified Finite Element Method model, this model is described in chapter 7.

Linear solvers usually entail direct solvers whereas iteration matrix $\hat{K}$ as well as the System matrices K, C and M are not updated. On the other hand, non-linear solvers usually entail an iterative solution procedure where the system matrices are updated. In these iterative solvers, the iteration matrix is not part of the solution and can therefore only improve the convergence behaviour. In methods like the one proposed in this work, differences in the iteration matrix are small, whilst updating this matrix requires high computational effort. This may lead to the decision to refrain from updating this matrix in-loop. The four solvers that will be tested are all Implicit solvers. The nature of the model has proven to be best with implicit solution procedures, whereas the explicit solutions are unstable. Therefore the solvers that are compared are as follows.

1. Iterative Newmark + Newton-Rhapson, with iteration matrix updates and K, C and M updates, ”Ansys” solver.
2. Iterative Newmark + Newton-Rhapson, without iteration matrix updates but with K, C and M updates.
3. Direct Newmark, with iteration matrix updates and K, C and M updates. (variational form)
4. Direct Newmark, without iteration matrix updates but with K, C and M updates.

8.2. Solver scaleability results

In order to compare the solving times qualitatively, the scaleability of a few important settings can be tested:

- Mesh size; as the amount of dof's increases the system matrices scale quadratically.
- Time step; lowering the time step causes more iteration steps, therefore increasing solution times. However, in iterative solvers, the amount of equilibrium calculations may be reduced.
- Pantograph velocity; increased velocities induce larger displacements, thus complicating equilibrium calculations, this effect should be less visible in the direct solver
- Convergence criterion; large models may or may not converge correctly when loose convergence criteria are used, resulting in solver instability.

The main value of interest is the scaleability of the Ansys solver, versus the scaleability of the fast, linear direct solver. The main interest here is to see which solver provides the best results at different mesh sizes, in order to determine how the solution times scale with mesh size.

8.2.1. Mesh Scaleability

The solvers have all been used to solve the exact same model. Changing mesh sizes allows for an initial comparison and an indication of the scaleability of the solvers as well. Solver efficiency can be measured in many ways. In this chapter the solving time is used as the value for efficiency. The values presented in table 8.1, as well as in figure 8.1 are averaged values, each value is based on at least three simulations. The simulations values are collected in a worksheet, parts of which can be found in appendix E.

	Solver			
Number of Elements	Iterative, no upd	Iterative, upd	Direct, no upd	Direct, upd
200	5.36	5.31	3.33	5.33
400	19.61	21.78	12.11	26.70
600	53.00	51.65	25.36	58.33
800	103.43	106.14	43.15	125.05
1000	206.44	213.54	75.80	225.87
1200	309.26	309.77	134.84	354.25
1400	460.77	470.63	233.18	572.07

Table 8.1: Solver comparison by simulation time [s]

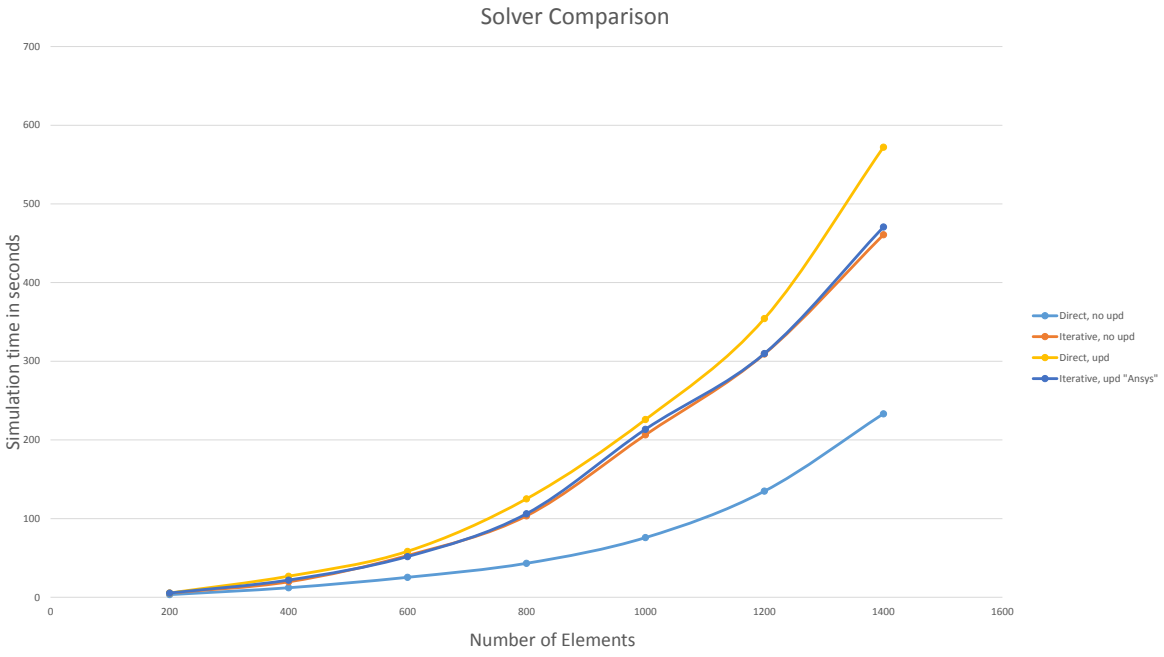

Figure 8.1: Solution times for all four solvers at different mesh sizes

Based on the graphical representation as show in figure 8.1, the simulation time increases quadratically with the size of the problem, intuitively this should also be the case due to the size of the matrices being DOF^2. The average improvement over all mesh sizes, when moving from Iterative, no upd to Direct no upd is: 54.41%. There is no clear trend in the improvement when related to the mesh size, it does however hover around 50% for all calculated result values.

8.2.2. Time Step Scaleability

Time step size can influence result accuracy significantly. Some solvers work well at high time steps, whereas other solvers require lower steps to provide the same accuracy. The time step size also affects the simulation times, as lowering the time step results in more calculations per unit of time. The resulting values are presented in table 8.2 and figure 8.2.

	Solver			
Time Step size	Iterative, no upd	Iterative, upd	Direct, no upd	Direct, upd
0.01	1.24	1.41	0.52	1.05
0.005	1.49	1.59	0.69	1.18
0.002	3.22	3.08	1.85	2.87
0.001	5.34	5.39	3.39	5.07
0.0005	10.22	10.21	6.67	10.02
0.0002	23.83	22.91	15.59	22.77
0.0001	60.11	46.33	30.37	44.15

Table 8.2: Solver comparison by simulation time [s]

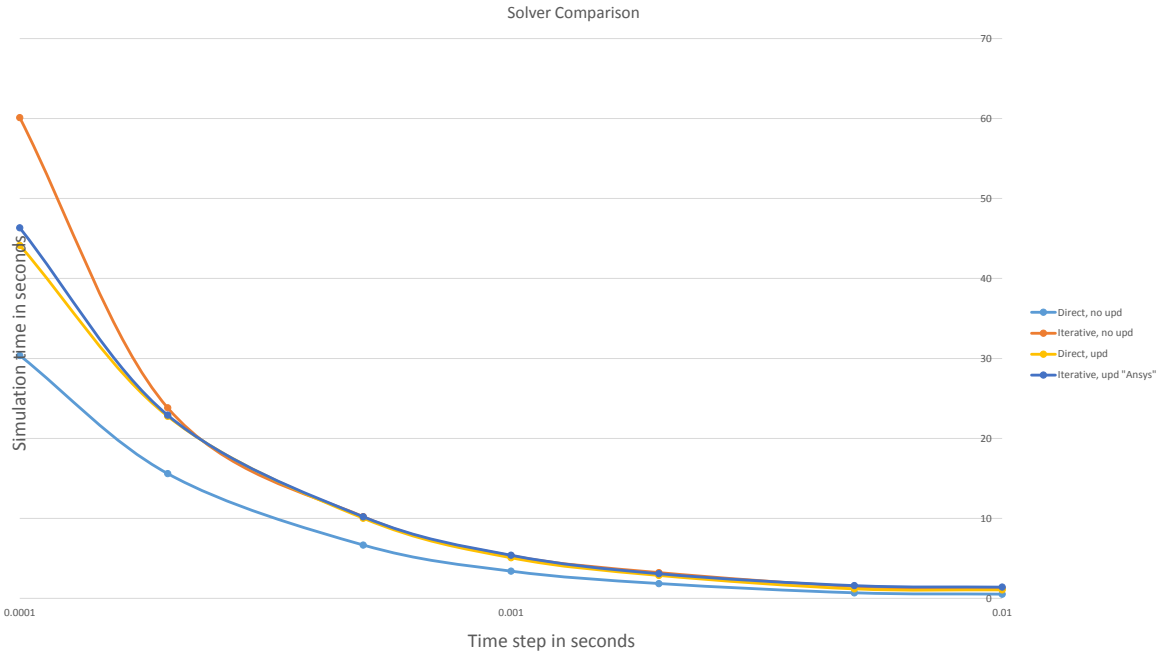

Figure 8.2: Solution times for all four solvers at different time step sizes (Logarithmic horizontal scale!)

When solving the same simulation problem, but at different time steps, the results show an increase in simulation times when time steps are lowered. The simulation times scale near-linear with the amount of calculations that are done, therefore the simulation times scale as

$$t_{sim} = \frac{a}{t_{step}} \tag{8.1}$$

a is a scalar factor which can be determined for every solver. The solutions for the Time step scaleability were gained using a 200 element mesh. The average improvement over all time step sizes, when moving from Iterative, no upd to Direct no upd is: 43.97%.

For the Ansys solver, as well as the Direct, no upd solver the a values have been calculated at every time step. The range of this value shows how close to linear the system behaves. Furthermore, based on these calculated values, a normative value for a can be determined for each solver, which can be used to make scaleability estimates for future simulations.

Drawing a correct conclusion from table 8.3 requires the results for the two largest time steps to be left out. These simulation times are so small that the results may easily be influenced by other processes.

	Solver	
Time step [s]	Iterative, no upd	Direct, no upd
0.01	~~0.01240~~	~~0.005200~~
0.005	~~0.00745~~	~~0.003450~~
0.002	0.00644	0.003700
0.001	0.00534	0.003390
0.0005	0.00511	0.003335
0.0002	0.004766	0.003118
0.0001	0.006011	0.003037

Table 8.3: a value calculation

The iterative solver shows some non-linear behaviour in the values of a. This may be caused by the iterative solver requiring a different amount of equilibrium equations in different time steps, therefore losing the direct relation between amount of calculations and the size of the time step. The direct solver has reasonably comparable values for a for nearly all time steps. This is a result of the amount of calculations being directly linked to the time step in a direct solver. If normative values are taken to be the average of the five remaining results then $a_{iterative} = 0.00553$, $a_{direct} = 0.00332$. By definition, the improvements can then be calculated as follows: $(a_{direct} - a_{iterative})/a_{iterative} = -40.0\%$.

8.2.3. Pantograph Velocity

In order to isolate the effects of the pantograph velocity with respect to the simulation times, it has been chosen to keep the locations at which the pantograph force is exerted on the catenary model the same. This situation is created by increasing the velocity and proportionally decreasing the time step and analysis time.

	Solver			
Load Velocity [m/s]	Iterative, no upd	Iterative, upd	Direct, no upd	Direct, upd
6	10.72	11.68	6.10	12.70
7.5	10.15	11.57	6.04	12.93
10	10.15	11.46	5.98	12.76
15	10.35	11.35	6.08	12.35
30	10.58	11.22	5.92	12.95
60	10.24	11.72	6.74	11.65
120	9.57	10.41	5.95	11.54

Table 8.4: Solver comparison by simulation time [s]

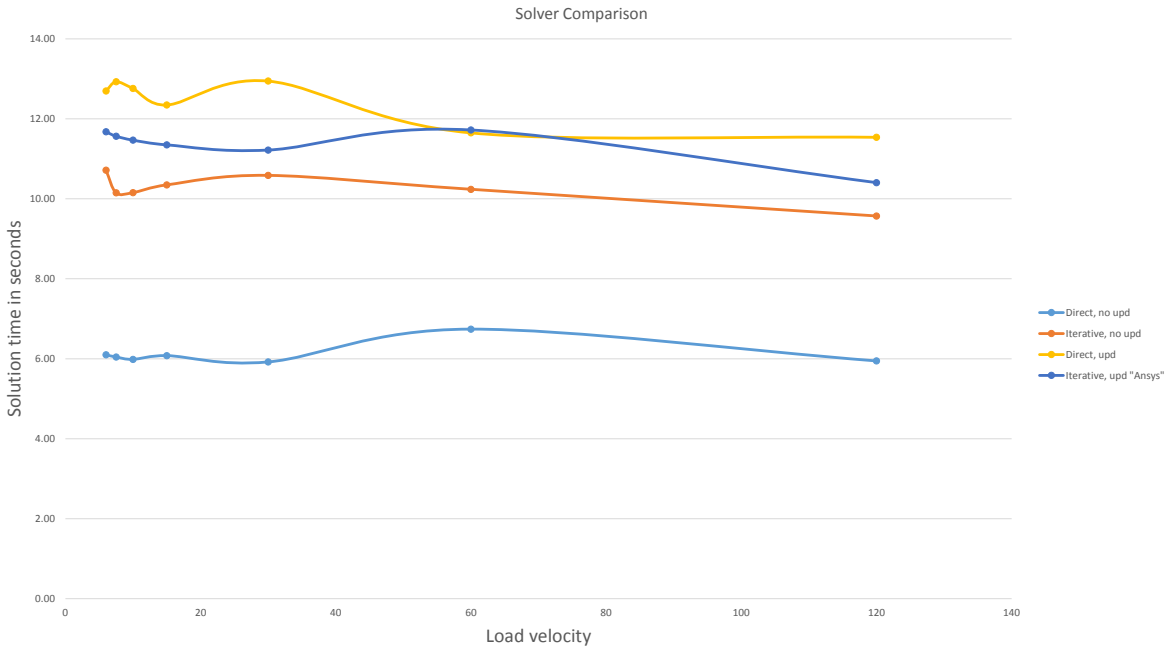

Figure 8.3: Solution times for all four solvers at different load velocities in m/s

From the data in table 8.4 and figure 8.3 it can be concluded that the pantograph velocity does not have significant influence on the simulation times. The hypothesis that a higher pantograph velocity would result in higher differences between equations and thus require more equilibrium equations is therefore *rejected*. The average improvement over all pantograph velocities, when moving from Iterative, no upd to Direct no upd is: 40.34%

8.2.4. Convergence criterion

Increasing the stringency of the convergence criteria slows down the simulation effort for the 'Ansys' like solver. The direct solver does not perform equilibrium equations, thereby it does not slow down as convergence criteria become stringent. The results for the simulations can be found in table 8.5 whereas the graphical representation of the results can be seen in figure 8.4.

	Solver			
Convergence criterion	Iterative, no upd	Iterative, upd	Direct, no upd	Direct, upd
10 * ||F||	3.16	2.9	6.08	12.89
1 * ||F||	10.10	11.28	6.04	12.85
0.1 * ||F||	9.79	10.79	5.85	11.86
0.01 * ||F||	10.26	11.49	5.95	12.39
0.001 * ||F||	11.71	14.98	5.92	11.08
0.0001 * ||F||	14.42	19.17	5.99	13.22
0.00001 * ||F||	16.81	21.94	5.91	12.61

Table 8.5: Solver comparison by simulation time [s], ||F|| denotes, norm of the external force

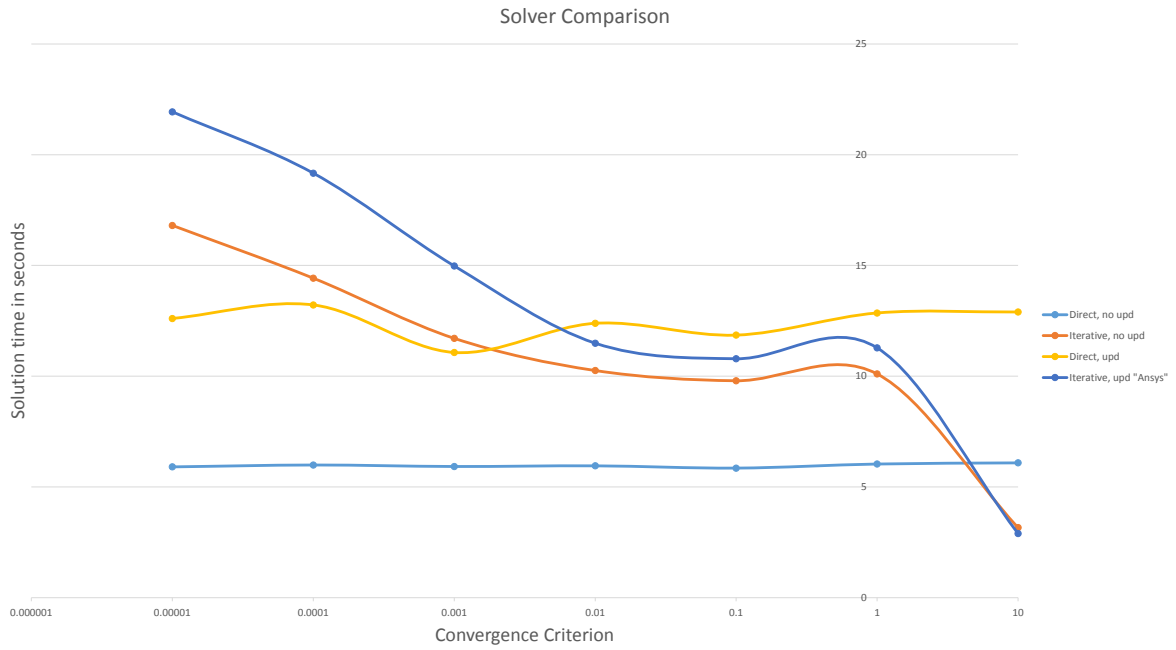

Figure 8.4: Solution times for all four solvers at different Convergence criteria (Logarithmic horizontal scale!)

Based on the data gathered from the convergence criteria the conclusion can be made that lowering the convergence criteria indeed increases the solution times of the iterative solvers. It can also be seen that the solution time only increases marginally with respect to the change in convergence criteria. This phenomenon can be described due to the quadratic convergence of the newton-rhapson iterative procedure, thus resulting in marginal simulation time increases. Furthermore it must be stated that, at 10 *|F|, both iterative solvers provide wrong results. Therefore, these simulation times, even though they are very impressive, should not be taken into account. Also, as convergence criteria become lower (≤0.001) the Direct solver with Matrix updates provides better results than the iterative solvers. Therefore it may be interesting to use such a solver when due to model size or complexity small convergence criteria are required. The average improvement over all time step sizes, when moving from Iterative, no upd to Direct no upd is: 45.26%. It can, however, also be stated that the base improvement of about 40%, which is observed for convergence criterion as low

as $0.01 * ||F||$, is not affected up until this value. After this value however, the improvements increase by 7-9% for every step, which results in the following equation:

$$Improvement_{CC*||F||} = (41 - 8 * (LOG^{10}(CC) + 2))\% \tag{8.2}$$

This equation will provide an acceptable approach to the actual improvement values whilst remaining within the current range of convergence criterion (≤0.01). As convergence values become smaller this relation will likely become inaccurate. Table 8.6 shows the measured improvements as well as the calculated improvements when comparing Iterative, no upd to Direct, no upd.

Convergence criterion	Improvements	Improvements Calculated: eq 8.2
10 * ||F||	+92.4%	-
1 * ||F||	-40.2%	-
0.1 * ||F||	-40.2%	-
0.01 * ||F||	-42.0%	(41%)
0.001 * ||F||	-49.6%	(49%)
0.0001 * ||F||	-58.4%	(57%)
0.00001 * ||F||	-64.9%	(65%)

Table 8.6: Solver comparison, Iterative, no upd to Direct, no upd , ||F|| denotes, norm of the external force

When reviewing the numbers in table 8.6 it can be concluded that equation 8.2 is a reasonable approximation of the measured values.

8.3. Solver implementation Conclusion

Based on the results from all four solver comparison analyses, the following conclusions can be drawn:

- The solution scales Quadratically with the mesh size for all solvers. The Direct solver without updating shows the fastest simulation times.
- The solution scales linearly with the inverse of the time step for all solvers. The Direct solver without updating shows the fastest simulation times.
- The solution does not scale noticeably with the velocity of the load for all solvers. The Direct solver without updating shows the fastest simulation times.
- The solution does not scale noticeable with the convergence criterion for Direct solvers. The solution scales inversely sub-linear with the convergence criterion. The Direct solver without updating shows the fastest simulation times.

Therefore, it can be concluded that in all comparisons, the Direct solver without updating shows the fastest simulation times, up to 50% improved with respect to the Ansys solver can be reached. However, overall it can be seen that an improvement of 40% is reached nearly always. Furthermore, the only comparison which shows clear differences in scaling between different solvers is the convergence criterion comparison. The variable in this comparison however, does not influence the direct solvers, thus it can be expected that as convergence criteria become stringent, the direct solvers become more favourable. This also results in the conclusion that the proposed solver (chapter 6) may turn out favourably in large simulations for which the direct solver without matrix updates lacks accuracy.

9

Contact model improvement results

9.1. Introduction

Ansys uses contact modules which can be applied to various complex contact problems. However, in the current work the contact is simple. Therefore, this chapter answers the question: Does replacing the Ansys contact module by another contact method result in lower simulation times, and do these represent a significant improvement with respect to the Ansys method.

Comparison can be made between two different implementations of a moving load:

- Application of a motion and a load through a contact element, upon which these boundary conditions are applied.
- Direct Application of the loads on different nodes at different load steps.

Both methods will be implemented to gain an understanding of the impact of the contact module on the simulation times. In the following sections each method is described briefly, along with the expected pros and cons. After analysis of the methods in Ansys the results will be compared and an estimate of the achievable improvements is made. The correct measurement of time is performed by recording the Ansys cpu time based on the WALL variable in the .MNTR file. This value is used for comparison of the contact models.

The model upon which this analysis is applied is a 2 span long, 100 meter catenary system, based on the Prorail B4 system, but altered to the point that the distance between droppers is 5m. An analysis is performed in which the load moves below the system at a speed of 5 m/s at analysis frequencies of 1 to 50 Hz. A second analysis is performed in which the load moves at 50 m/s at analysis frequencies of 10 to 500 Hz. Furthermore, the load is 150N in positive Z direction for every simulation. The analysis is outlined as follows:

- Let catenary come to resting position.
- In case of using Contact module, the contact needs to be initiated.
- Perform moving load analysis, whilst altering Contact method and Analysis frequencies.

Analysis frequencies are taken into account since certain modules may perform optimal at different frequencies. Frequencies are taken into account up to 50/500Hz to avoid prohibitive simulation times.

9.2. Simulation Results

The results for the contact model improvement are presented on the next pages. To clarify, one situation is presented per page. The corresponding Ansys result files are not saved, therefore, the process by which these results are produced is declared in appendix F

9.2.1. V = 5 m/s, 2 spans

The results for the contact model comparison analysis at 5 m/s are presented in table 9.1 and figure 9.1.

	Method		
Analysis frequencies	Contact module	Direct Application	Improvement in %
1hz 5m/step	26.43	21.66	-18.04%
5hz 1m/step	87.65	68.78	-21.53%
10hz 0.5m/step	147.5	128.54	-12.85%
50hz 0.1m/step	547.73	503.73	-8.03%

Table 9.1: Contact Method Simulations at 5 m/s and 2 spans, by simulation time [s]

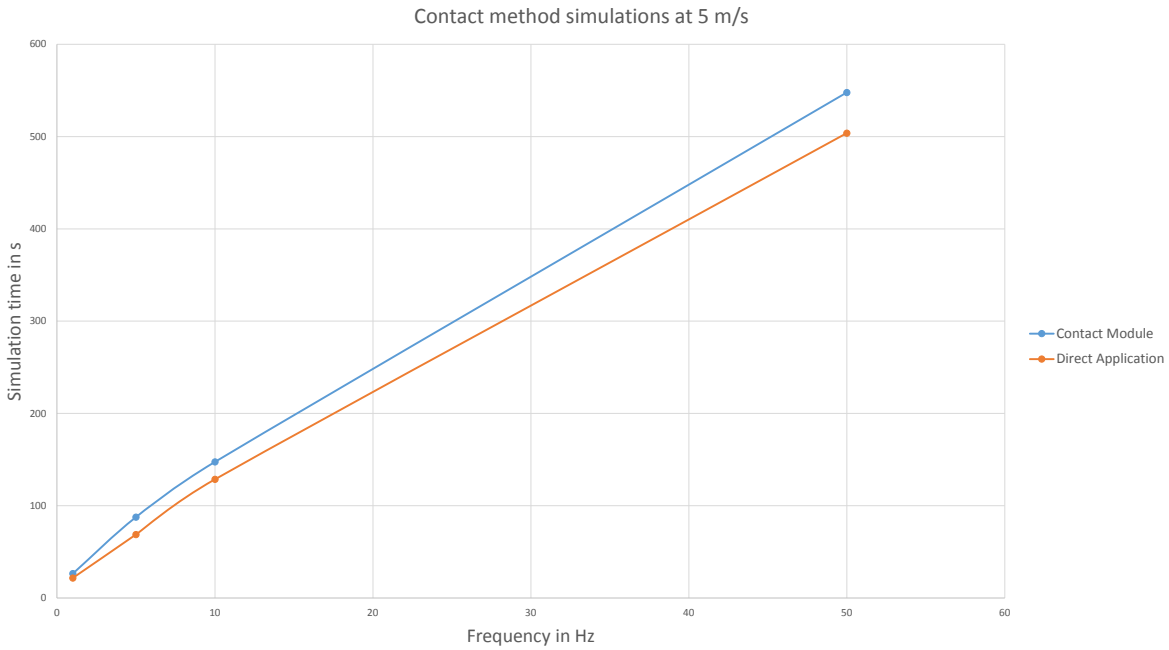

Figure 9.1: Solution times at various frequencies for v = 5 m/s and 2 spans

The 5 m/s simulation results show small differences between the Contact model and the Direct Application approach at higher frequencies. The explanation for this may be the low differences in energy between the time steps. Therefore both contact models allow the solver to converge almost directly. The lower frequency regions show higher differences of up to -21.53%, which is mainly due to slower convergence of the Contact Module method with respect to the Direct Application method.

9.2.2. V = 50 m/s, 2 spans

The results for the contact model comparison analysis at 50 m/s over 2 spans are presented in table 9.2 and figure 9.2.

	Method		
Analysis frequencies	Contact module	Direct Application	Improvement in %
10hz 5m/step	[not stable]	21.95	-%
50hz 1m/step	[not stable]	60.54	-%
100hz 0.5m/step	152.45 [not stable]	104.30	~~-31.59%~~
500hz 0.1m/step	483.05	386.80	-19.93%

Table 9.2: Contact Method Simulations at 50 m/s and 2 spans, by simulation time [s]

The 50 m/s simulation requires high sample frequencies for the catenary system to remain stable. Therefore the contact module only provides results for 100hz and 500hz. Based on the 100Hz results however, the system shows a beginning instability, from experience it is known that such instability will only increase. The main reason for the Direct Application approach staying stable is the fact that the force between 2 load steps is interpolated, rather than applied at another position.

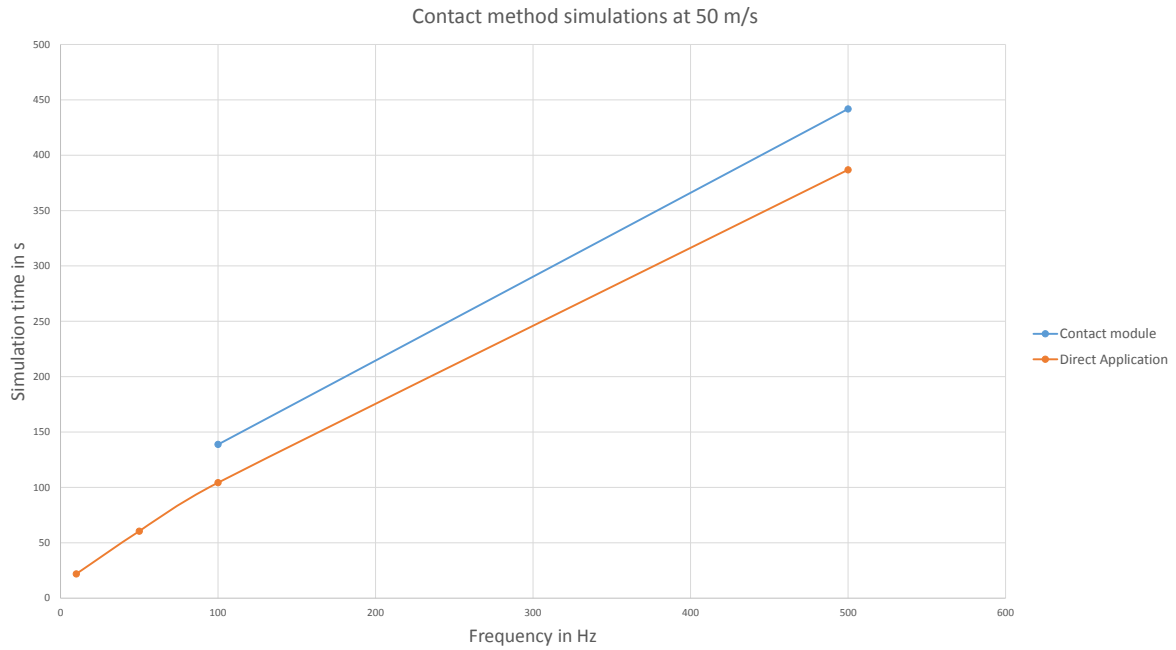

Figure 9.2: Solution times at various frequencies for v = 50 m/s and 2 spans

With respect to the 5 m/s results, the 50 m/s results show higher simulation time differences. This can be explained by the size of the energy differences between the time steps, slowing down the Contact Module method. The results for the 100 Hz simulation are noted. However, due to beginning instability which was observed in the simulation results, the -31.59% improvement may also be the result of the solver having difficulties with the system's oscillations.

9.2.3. V = 50 m/s, 4 spans

The 4 span model requires more load steps to achieve a resting position where the contact module does not overpenetrate. Furthermore, this model, whilst consisting of 4 spans, is only loaded on the first 2 spans.

	Method		
Analysis frequencies	Contact module	Direct Application	Improvement in %
10hz 5m/step	[not stable]	35.16	-%
50hz 1m/step	[not stable]	87.29	-%
100hz 0.5m/step	271.93 [not stable]	205.21	~~-24.54%~~
500hz 0.1m/step	891.82	580.11	-34.95%

Table 9.3: Contact Method Simulations at 50 m/s and 4 spans, by simulation time [s]

The Contact Module loses stability at a frequency between 500 and 100Hz. Adversely, the Direct application approach, which uses a less amount of interface locations remains stable, even at 10 Hz frequencies. When comparing the results of the 4 span system to the results of the 2 span system, it is observed that the simulation time improvements increase as the model becomes larger, but the amount of the model that is loaded remains the same. In order to check whether this improvement remains in simulations where the full system is loaded at all times, a comparable simulation needs to be performed. This is done in the form of a simulation of the same model, only loaded twice as long with the same load.

	Contact Module	Direct Application	Improvement in %
500hz, 0.1m/step, 4 sec	1740.24	1096.06	-37.02%

Table 9.4: Control simulation to check improvement at 4 spans, by simulation time [s]

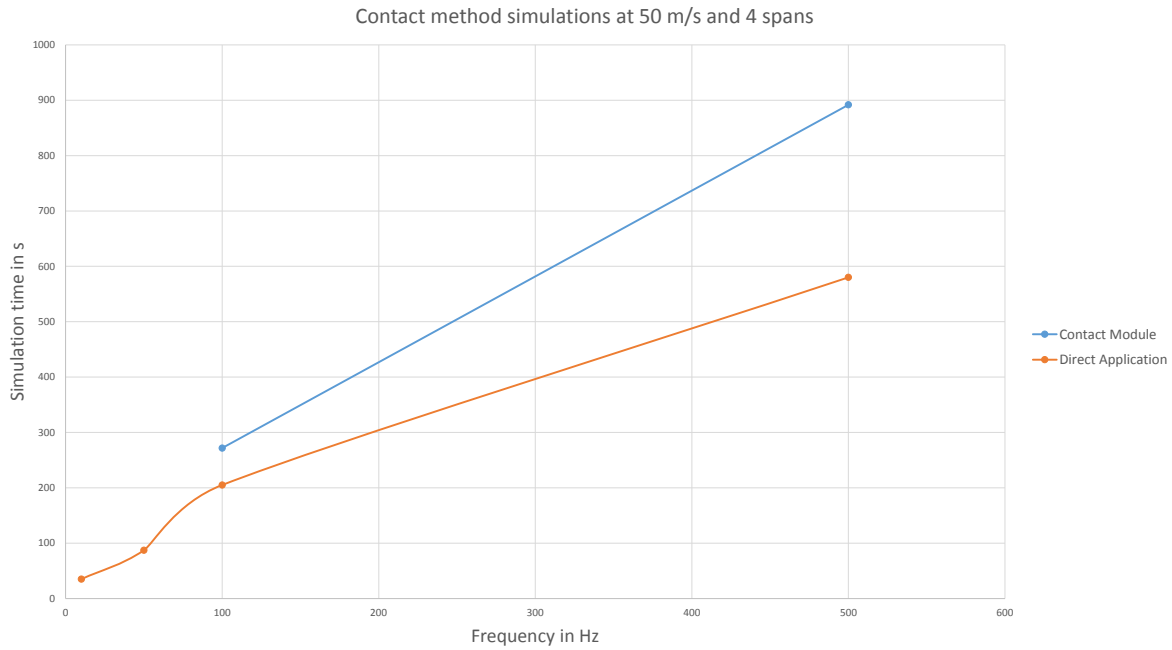

Figure 9.3: Solution times at various frequencies for v = 50 m/s and 4 spans

From the comparable 4sec simulation, due to the improvement in table 9.4 being comparable to the improvement in table 9.3, confidence is gained that the values presented in the contact method simulations provide a correct reflection of the simulation time improvements indeed.

9.2.4. V = 50 m/s, 6 spans

This model, even though it consists of 6 spans, is only loaded on the first 2 spans. As a consequence of the contact model losing stability at 100Hz in all previous simulations, the current simulation is only performed for the 500Hz situation, as a result of this no figure is provided.

	Method		
Analysis frequencies	Contact module	Direct Application	Improvement in %
10hz 5m/step	[not stable]	[not computed]	-%
50hz 1m/step	[not stable]	[not computed]	-%
100hz 0.5m/step	[not stable]	[not computed]	-%
500hz 0.1m/step	1164.55	717.18	-38.4%

Table 9.5: Contact Method Simulations at 50 m/s and 6 spans, by simulation time [s]

In comparison to the 4 and 2 span models and in line with the increase in improvements from the 2 span to the 4 span model, the 6 span model provides a small improvement in the simulation times. This provides certainty that the contact model improvements do not diminish with larger model sizes. As well as the 4 span model, the 6 span model is also loaded 4 and 6 seconds, which represents loading of respectively $2/3^{rd}$ and $3/3^{rd}$ of the model.

	Contact Module	Direct Application	Improvement in %
500hz, 0.1m/step, 4 sec	2339.95	1441.08	-38.4%
500hz, 0.1m/step, 6 sec	3439.6	2162.08	-37.1%

Table 9.6: Control simulation to check improvement at 6 spans, by simulation time [s]

The results in table 9.6 show that the calculated improvements remain constant when larger parts of the system are loaded. Therefore, simulation time improvements which result from table 9.5 are substantiated. Furthermore, due to the minor differences observed between the 4 and 6 span results, it is expected that the improvement limit will be 40%.

9.3. Contact improvement conclusions

The Direct Application approach performs op to -38% better than the Contact Module approach, when comparing at the same analysis frequency.

Moreover, improvements of up to -77% (ratio 1:4.3) can be achieved when comparing the stable Direct Application results at 100 Hz versus the stable Contact Module results at 500 Hz (4 span model).

Furthermore, confidence is gained that these improvements will scale to a full size model due to the sustained improvements as model sizes grow.

10

Conclusion / Discussion

10.1. Conclusion

A Pantograph-Catenary interaction model has been built which is deemed valid according to EN50318:2002. It has been found feasible that simulation times improve by means of a direct solver, which may result in improvements of 40%. Adversely, the rank-1 updating procedure of the iteration matrix inverse has not been found to improve simulation time for most situations. Furthermore, it has been found feasible that simulation times improve when simulations are executed by means of a modified contact model when analysis frequencies are kept equal this may result in improvements of up to 40% . In addition, it has also been found, that a modified contact model allows for lower analysis frequencies whilst the system remains stable, a result which is not observed when using the Ansys contact module. This can result in improvements of up to 77% based on the Direct Application results discussed in chapter 9. From these results, a potential improvement of the simulation times based on Contact Module and Solver improvement of [1:4.3](CM) * [3:5](SOLVER) = [6:43] can be achieved, speeding up a 24h simulation to a mere 3.4 hours. Lastly, the modal reduction which was proposed in this work, has not resulted in significant simulation time improvements. In conclusion, it can be said that the two main goals of the current work are accomplished. A validated model has been built. Moreover, a method has been found, which improves simulation times, whilst respecting dropper slackening, sliding contact, and wave propagation.

10.2. Discussion / Recommendations

Both goals set out in chapter 1 have been achieved. The Ansys model has been validated according to the norm EN50318:2002 and the reduction/improvement process has shown that significant time can be saved. Based on the different aspects of the research the following sections will discuss the results and consequently the conclusions.

EN50318 Model

- The valid EN50318 Ansys model is a reasonably slow model. This results from the fact that catenary systems are large systems, in addition, the interface between the Pantograph and the Catenary demands that element sizes remain small. Furthermore, wave propagation through the catenary results in wave reflection in short catenary systems, which produces erroneous results. To ensure simulation times to remain acceptable, it is important to use the Ansys model effectively. This may be achieved by minimising the catenary length whilst making sure end-effects are neglectable. Furthermore, time-step sizes may be optimized for certain catenary systems. 500 Hz has been found to be a frequency at which every catenary is stable, certain systems might however also be stable at lower frequencies.

- In extension to the currently validated EN50318 model, which builds a straight catenary system without custom features, a method may be applied, which automatically

implements custom features such as bridges, tunnels, current-less catenary locations and more.

- In order to future-proof the validated Ansys model, demands of the prEN50318:2016 may be inventoried and, if applicable, applied.
- One of the main issues resides in model stability. The current models that are known to be stable, may become unstable at the slightest change in model parameters. The catenary models are, by design, very compliant, which is expected to be the reason for this behaviour. This results in difficulties predicting whether a model, which has not been simulated before, will be stable. Research into stability of catenary FE models may provide further insights into how-and-why certain catenary systems lack stability with respect to other models.

Model improvements

General

- In extension to the current work, implementation of the found improvements may be applied to full systems consisting of multiple spans. Furthermore, pantograph models and force calculations may be implemented towards finding more precise improvement values.

Solver

- The Direct solver, which shows the largest simulation time improvements, is based on the Newmark solver for linear systems. This solver has been found to improve the simulation times by up to 40%, which is a reasonable improvement. It must, however, be stated that the solver is normally used in linear problems, whereas our simulation is not. This results in accuracy loss, mainly when the pantograph moves at very high velocities (>50m/s, >180 km/h). The bulk of Dutch catenary systems is built to allow a maximum speed of 160 km/h therefore this is not expected to be an issue. However, it must be noted that the solver should not be applied to dutch high speed train simulations. Furthermore, implementation of the improved solver in Matlab is found to be suboptimal. This is a consequence of the way Matlab files are executed. In order to actually improve the solution procedure, the improved solver will need to be implemented in another programming language, i.e. C++.
- Application of the Direct solver with its solution procedure in Ansys might be interesting since, it is also used in the valid EN50318 model. Performing such an analysis in Ansys, whilst taking advantage of the linear solver, requires for the system to first perform a large displacement transient analysis first, secondly a small displacement transient analysis must be performed. This needs to happen whilst saving the stress-state of the large displacement analysis. However, analysis types cannot be changed during a restart procedure, neither can the procedure be changed from large to small displacement between analyses. Another method would be to perturb the analysis, however the perturbation procedure does not cater in an option to perturb a non-linear transient analysis to another transient analysis [51]. Furthermore, even if a perturbation analysis allows the second analysis to be a transient analysis, the COMBIN39 element will no longer behave non-linearly [51]. Therefore, implementation of the improvements found in this work in Ansys, is not deemed feasible.
- The solver, which was originally proposed in chapter 6, has not been able to improve simulation times. However, its use may be found in the situation where stringent convergence criteria are applied in combination with a very fast load (>50m/s, >180 km/h), in which case the Iterative solvers are no longer an option due to the convergence issues, whereas the fast Direct solver lacks accuracy.
- The direct solvers, which have been compared in chapter 8, use different solution procedures. The Direct solver with iteration matrix updates is written in variational form, whereas the direct solver without iteration matrix updates is not. This is a result of the

dropper decoupling procedure and consequently the rank-1 updating procedure. The variational formulation is capable of handling iteration matrix updates, whereas the general (weak) formulation is not. This results in odd displacements when the general formulation is applied with iteration matrix updates. Future research may show that a non-variational formulation exists for the direct solver, which is able to cope with the iteration matrix updates. This may result in a method which is capable of improving speed whilst minimizing accuracy loss.

Contact Model

- By making clever use of the properties of a changed contact model, the speed improvements can not only be seen in the contact model, but also in the possibility of using a reduced amount of interface locations. The use of less interface locations allows the model to remain stable when loaded under high velocities and at lower frequencies. This in return allows the analysis of more models in the same amount of time, which is exactly the goal of the contact model change. Furthermore, lowering the amount of interface locations provides opportunities for Reduced Order Models, since less interface DOF leads to smaller Reduction Spaces resulting in smaller Reduced Order Models.

- The improvements calculated in chapter 9 exist between the Ansys Contact Module and an empty contact model called the Direct Application approach. This Direct Application approach does not contain any force calculation and therefore only applies a constant force on the FE model. Modifications to incorporate in-loop force calculations will slow down the Direct Application approach. Its impact is expected to be small but noticeable due to the force calculation being a reasonably simple one $F_{contact} = K_{contact} * (u_{z,panto} - u_{z,catenary})$.

- Moreover, the pantograph model is not modeled in either Contact Module and Direct Application approach. As a result, total simulation times will increase for both methods, which may have a leveling effect on the improvements. However, pantographs usually contain 3 DOF, whereas catenary systems' DOFs are several orders larger. Therefore, leveling effects are likely to diminish with respect to simulation times.

- In the Ansys environment the contact model possibilies have been found inferior. Two methods exist, which allow for a Contact Module to be circumvented. The first method entails all interface locations being equipped with time dependent force functions, all of which need to be evaluated in every time step. This is expected to cost significant amounts of simulation time. The question that is yet to be answered is whether these functions can be more than time dependent, and based on displacements in the previous time step. Therefore, this method is deemed inferior to in-loop calculation of the new contact force. The second method entails the solver solving one step at a time, after which results are loaded. The contact force is calculated and applied in a new load step, after which the solver calculates the next load step. This method is deemed inferior to the in-loop calculation due to the amount of operations, which are not part of the solution procedure. Therefore, implementation of a custom contact model has been found undesirable within the Ansys environment.

- The change of the contact model, whilst improving simulation times drastically, may introduce inaccuracies. It should therefore be applied with scrutiny. For instance, lowering the amount of interface locations requires interpolation of forces and displacements between nodes. The type of interpolation is of importance to the accuracy of the results. In the current work, this interpolation has not yet been performed. However, it is expected that a simple interpolation operation, i.e. Linear interpolation, will result in poor accuracy, whereas more advanced interpolation operations such as Hermite or Quadratic interpolation will provide good accuracy at the cost of lower simulation time improvements.

Reduced Order Model

- The modal reduction of the Pantograph-Catenary interaction model has not been found feasible due to Reduced Order Model sizes becoming prohibitively large, which results in diminishing improvements. The main drivers in determining the size of such reduced order models are the size of the full model, the frequency range of interest and the amount of interface DOF. Even though the transient modal simulation has not provided correct results, the modally reduced system has shown correct results in the static analysis. Therefore, it seems likely that a Reduced Order Model exists, which may be used in Transient dynamical analyses. Furthermore, dropper stiffness decoupling methods have been found applicable in modally reduced methods, therefore it is to be expected that this will also be the case for other reduction methods. Therefore, even though the modal reduction may not have provided useful results in the scope of this work, these findings may prove useful in future research.

- Related to the interface between pantograph and catenary is the in-loop conversion of the load vector from the physical to the modal domain. This conversion is required in every load step as a consequence of the movement of the load. Due to this operation, even though the modal system matrices might be significantly smaller than those of a full physical system, the modal system performs slower. In situations where the amount of interface DOF of the physical system are significantly lower than the total amount of DOF in the contact wire, load vectors may become smaller and the conversion operation may be improved.

- Substructuring of the model results in multiple smaller, easier to calculate systems. The current model improvements have been based on a FE approach in which multiple physical substructures have been connected via primal assembly. This work has shown that a reduction of the contact wire provides difficulties. However, the catenary system consists of more structures. Future research may focus on reducing structures other than the contact wire. Thereby, changing the messenger wire from a full physical base to a frequency base will likely provide less problems than the reduction of the contact wire, as a result of fixed interface locations and predictable loads.

Bibliography

[1] Technical specifications for interoperability relating to the 'energy' subsystem of the rail system in the Union., 1301/2014/EU,COMMISSION REGULATION (EU) No 1301/2014 of 18 November 2014 on the technical specifications for interoperability relating to the 'energy' subsystem of the rail system in the Union.COMMISSION REGULATION (EU) No 1301/2014 of 18 November 2014 on the technical specifications for interoperability relating to the 'energy' subsystem of the rail system in the Union.

[2] EN 50318, 2002, "Railway Applications - Current Collection Systems - Validation of Simulation of the Dynamic Interaction Between Pantograph and Overhead Contact Line," British Standard.

[3] P. Zdziebko en T. Uhl, "Finite element analysis of pantograph-catenary dynamic interaction", Archives of Transport, vol. 39, nr. 3, pp. 77–85, nov. 2016.

[4] G. Poetsch e.a., "Pantograph/Catenary Dynamics and Control", Vehicle System Dynamics, vol. 28, nr. 2–3, pp. 159–195, aug. 1997.

[5] A. Kumaniecka en J. Snamina, "Dynamics of the catenary modelled by a periodical structure", Journal of theoretical and applied mechanics, vol. 46, nr. 4, pp. 869–878, 2008.

[6] G. Galeotti, M. Galanti, S. Magrini, en P. Toni, "Servo Actuated Railway Pantograph for High-Speed Running with Constant Contact Force", Proceedings of the Institution of Mechanical Engineers, Part F: Journal of Rail and Rapid Transit, vol. 207, nr. 1, pp. 37–49, jan. 1993.

[7] V. Brandani, G. Galeotti, en P. Toni, "A FEM method combined with modal analysis for evaluating the dynamical performance of a pantograph", Advances in Engineering Software, vol. 14, nr. 3, pp. 171–177, jan. 1992.

[8] A. Beagles, D. Fletcher, M. Peffers, P. Mak, en C. Lowe, "Validation of a new model for railway overhead line dynamics", Proceedings of the Institution of Civil Engineers - Transport, vol. 169, nr. 5, pp. 339–349, okt. 2016.

[9] N. Cuartero, E. Arias, T. Rojo, F. Cuartero, en P. Tendero, "A Three-Dimensional Calculation for Dynamic Pantograph-Catenary Interaction", 2012.

[10] J. Ramos, M. Such, A. Carnicero, en C. Sánchez, "Dynamic simulation of the system pantograph-catenary-vehicle-track", in World Congress Railway Research, Lille France, 2011, vol. 9.

[11] Z. Liu, "Numerical study on multi-pantograph railway operation at high speed", KTH Royal Institute of Technology, 2015.

[12] S. Walters, A. Rachid, en A. Mpanda, "On modelling and control of pantograph catenary systems", 2011.

[13] Y. H. Cho, "Numerical simulation of the dynamic responses of railway overhead contact lines to a moving pantograph, considering a nonlinear dropper", Journal of Sound and Vibration, vol. 315, nr. 3, pp. 433–454, aug. 2008.

[14] L. Finner, G. Poetsch, B. Sarnes, en M. Kolbe, "Program for catenary–pantograph analysis, PrOSA statement of methods and validation according EN 50318", Vehicle System Dynamics, vol. 53, nr. 3, pp. 305–313, mrt. 2015.

[15] J. Ambrósio, J. Pombo, P. Antunes, en M. Pereira, “PantoCat statement of method”, Vehicle System Dynamics, vol. 53, nr. 3, pp. 314–328, mrt. 2015.

[16] Y. H. Cho, “SPOPS statement of methods”, Vehicle System Dynamics, vol. 53, nr. 3, pp. 329–340, mrt. 2015.

[17] P.-A. Jönsson, S. Stichel, en C. Nilsson, “CaPaSIM statement of methods”, Vehicle System Dynamics, vol. 53, nr. 3, pp. 341–346, mrt. 2015.

[18] A. Collina, S. Bruni, A. Facchinetti, en A. Zuin, “PCaDA statement of methods”, Vehicle System Dynamics, vol. 53, nr. 3, pp. 347–356, mrt. 2015.

[19] M. Ikeda, “‘Gasen-do FE’ statement of methods”, Vehicle System Dynamics, vol. 53, nr. 3, pp. 357–369, mrt. 2015.

[20] J.-P. Massat, E. Balmes, J.-P. Bianchi, en G. Van Kalsbeek, “OSCAR statement of methods”, Vehicle System Dynamics, vol. 53, nr. 3, pp. 370–379, mrt. 2015.

[21] N. Zhou, Q. Lv, Y. Yang, en W. Zhang, “Statement of methods”, Vehicle System Dynamics, vol. 53, nr. 3, pp. 380–391, mrt. 2015.

[22] C. Sánchez-Rebollo, A. Carnicero, en J. R. Jiménez-Octavio, “CANDY statement of methods”, Vehicle System Dynamics, vol. 53, nr. 3, pp. 392–401, mrt. 2015.

[23] M. Tur, L. Baeza, F. J. Fuenmayor, en E. García, “PACDIN statement of methods”, Vehicle System Dynamics, vol. 53, nr. 3, pp. 402–411, mrt. 2015.

[24] S. Bruni e.a., “The results of the pantograph–catenary interaction benchmark”, Vehicle System Dynamics, vol. 53, nr. 3, pp. 412–435, mrt. 2015.

[25] J. Ambrósio, J. Pombo, F. Rauter, en M. Pereira, “A Memory Based Communication in the Co-simulation of Multibody and Finite Element Codes for Pantograph-Catenary Interaction Simulation”, in Multibody Dynamics: Computational Methods and Applications, C. L. Bottasso, Red. Dordrecht: Springer Netherlands, 2009, pp. 231–252.

[26] W. H. Schilders, H. A. Van der Vorst, en J. Rommes, Model order reduction: theory, research aspects and applications, vol. 13. Springer, 2008.

[27] M. Géradin en D. J. Rixen, “A ‘nodeless’ dual superelement formulation for structural and multibody dynamics application to reduction of contact problems: A NODELESS DUAL SUPERELEMENT FORMULATION”, International Journal for Numerical Methods in Engineering, vol. 106, nr. 10, pp. 773–798, jun. 2016.

[28] M. Rewieński en J. White, “Model order reduction for nonlinear dynamical systems based on trajectory piecewise-linear approximations”, Linear Algebra and its Applications, vol. 415, nr. 2–3, pp. 426–454, jun. 2006.

[29] M. Rewienski en J. White, “A trajectory piecewise-linear approach to model order reduction and fast simulation of nonlinear circuits and micromachined devices”, IEEE Transactions on Computer-Aided Design of Integrated Circuits and Systems, vol. 22, nr. 2, pp. 155–170, feb. 2003.

[30] F. A. Lülf, D.-M. Tran, en R. Ohayon, “Reduced bases for nonlinear structural dynamic systems: A comparative study”, Journal of Sound and Vibration, vol. 332, nr. 15, pp. 3897–3921, jul. 2013.

[31] F. Bamer en C. Bucher, “Application of the proper orthogonal decomposition for linear and nonlinear structures under transient excitations”, Acta Mechanica, vol. 223, nr. 12, pp. 2549–2563, dec. 2012.

[32] T. Tamarozzi, G. H. K. Heirman, en W. Desmet, “An on-line time dependent parametric model order reduction scheme with focus on dynamic stress recovery”, Computer Methods in Applied Mechanics and Engineering, vol. 268, pp. 336–358, jan. 2014.

[33] ANSYS® Theory reference: Substructuring. https://www.sharcnet.ca/Software/Ansys/16.2.3/en-us/help/ans_thry/thy_anproc6.html#anpcms

[34] J. C. Simo en T. A. Laursen, “An augmented lagrangian treatment of contact problems involving friction”, Computers & Structures, vol. 42, nr. 1, pp. 97–116, jan. 1992.

[35] R. J. Guyan, “Reduction of stiffness and mass matrices”, AIAA Journal, vol. 3, nr. 2, pp. 380–380, feb. 1965.

[36] M. C. C. Bampton en R. R. Craig, Jr., “Coupling of substructures for dynamic analyses.”, AIAA Journal, vol. 6, nr. 7, pp. 1313–1319, jul. 1968.

[37] D. N. Herting, “A general purpose, multi-stage, component modal synthesis method”, Finite Elements in Analysis and Design, vol. 1, nr. 2, pp. 153–164, aug. 1985.

[38] D. Martinez, T. Carne, D. Gregory, en A. Miller, “Combined experimental/analytical modeling using component mode synthesis”, 1984.

[39] P. Benner, S. Gugercin, en K. Willcox, “A Survey of Projection-Based Model Reduction Methods for Parametric Dynamical Systems”, SIAM Review, vol. 57, nr. 4, pp. 483–531, jan. 2015.

[40] I. K. Fodor, “A survey of dimension reduction techniques”, Lawrence Livermore National Lab., CA (US), 2002.

[41] A. Chatterjee, “An introduction to the proper orthogonal decomposition”, Current Science, vol. 78, nr. 7, pp. 808–817, 2000.

[42] G. Kerschen, J. Golinval, A. F. Vakakis, en L. A. Bergman, “The Method of Proper Orthogonal Decomposition for Dynamical Characterization and Order Reduction of Mechanical Systems: An Overview”, Nonlinear Dynamics, vol. 41, nr. 1–3, pp. 147–169, aug. 2005.

[43] IMAC, Proceedings of the 35th IMAC, a Conference and Exposition on Structural Dynamics 2017. Volume 4: Dynamics of coupled structures. “Chapter Eighteen: Falco, Marco et al. Nonlinear Substructuring Using Fixed Interface Nonlinear Normal Modes” Cham: Springer, 2017.

[44] V. Lenaerts, G. Kerschen, en J.-C. Golinval, “Identification of a continuous structure with a geometrical non-linearity. Part II: Proper orthogonal decomposition”, Journal of Sound and Vibration, vol. 262, nr. 4, pp. 907–919, mei 2003.

[45] G. Berkooz, P. Holmes, en J. Lumley, Turbulence, Coherent Structures, Dynamical Systems and Symmetry–Cambridge Monographes in Mechanics. Cambridge Universtity Press, UK, 1996.

[46] S. N. Voormeeren, “Dynamic Substructuring Methodologies for Integrated Dynamic Analysis of Wind Turbines”, Delft University of Technology, 2012.

[47] S. Jain, P. Tiso, J. B. Rutzmoser, en D. J. Rixen, “A quadratic manifold for model order reduction of nonlinear structural dynamics”, Computers & Structures, vol. 188, pp. 80–94, aug. 2017.

[48] D. D. Klerk, D. J. Rixen, en S. N. Voormeeren, “General Framework for Dynamic Substructuring: History, Review and Classification of Techniques”, AIAA Journal, vol. 46, nr. 5, pp. 1169–1181, mei 2008.

[49] J. Sherman en W. J. Morrison, “Adjustment of an Inverse Matrix Corresponding to a Change in One Element of a Given Matrix”, The Annals of Mathematical Statistics, vol. 21, nr. 1, pp. 124–127, mrt. 1950.

[50] Ansys Solver theory reference: https://www.sharcnet.ca/Software/Ansys/17.0/en-us/help/ans_thry/thy_anproc2.html#thyeq2systemsnov2001

[51] Ansys Perturbation analysis theory reference: https://www.sharcnet.ca/Software/Ansys/16.2.3/en-us/help/ans_cmd/Hlp_C_PERTURB.html

[52] MATLAB Release 2016b, The MathWorks, Inc., Natick, Massachusetts, United States.

[53] ANSYS® Academic Teaching Advanced, Release 18.1

[54] Ricardo Netherlands Hya:628576,628575

Appendices

A

Modelling method discussion

Since the pantograph-catenary interaction model consists of 2 components, which are to be modeled in a completely different way, the ideal modeling programs for these models are also different. In addition to this, the system will be simulating a dynamic situation which is created by a motion of the two models with respect to each other. For the Catenary, the most accurate modeling practice is the finite element method. For the Pantograph, a multi body dynamics model would be the best, simplified lumped mass-spring-damper models are however provided and can be used. The relative motion can be modeled relatively easy. However the finite element analysis software does not like this. In order to make a choice of how to model and simulate the system to the best accuracy, the best method will have to be isolated. This includes looking into combining methods and programs. Possible ways of modeling and simulating the pantograph-catenary interaction are provided below, as well as the main argument in favour of this method and secondly the main argument against this method. After this list, the different options are discussed to a deeper extent.

- Matlab
  - All possible calculations, modeling and simulation requirements can be coded.
  - Since everything will have to be made in code, the process of creating such program will be very time consuming.
- Ansys
  - FE-model of the catenary can be modeled in Ansys, removing a lot of coding work. Model can be visualised in Ansys.
  - Uncertainty wether or not the available Ansys 18.1 Mechanical APDL is capable of dynamic simulation and loads.
- Matlab + Ansys co-simulation
  - FE-model of the catenary will not need to be ’hard coded’
  - co simulation package is not available at Ricardo, Possible use of Ansys As a server.
- Simpack
  - Pure dynamical modeling increases the speed.
  - Since FE model of catenary is very important to retain model accuracy the FE model will need to be made in Simpack. This can be achieved with Simbeam, however, this is not available at Ricardo.
- Simpack + Ansys co-simulation

  - Dynamic simulation done by the Simpack program, FE simulation done by the Ansys program. Both programs run at the same time, increasing the resulting accuracy significantly
  - Probably requires an additional module, which currently does not exist.

- Simpack + Ansys (FE2FBI/FMI load in to Simpack)
  - Dynamic simulation and FE simulation Done by the Simpack program. Modeling of the catenary still done in Ansys and loaded into Simpack. No interaction between two programs should increase simulation speed.
  - Absolutely no guarantee whether or not this will work.

Determining which option is best requires determining which solution provides the best chance for success. This is based on findings in literature and on modeling techniques of which it is considered they can accurately model the situation. Time constraints are also taken into account. Last but not least, the stake of Ricardo Netherlands B.V. should be evaluated. Certain software is already available in house. These options require no extra investment. Some packages require extra toolboxes or add ons to allow for the intended modeling and simulation option.

To ensure the best possible method is used for simulation, a simple grading criterion is created, every method is awarded a grade for its usability as pre- and post-processor, as well as a grade for its usability as solver, in the current research.

- 0, is awarded if a method is not usable for the desired purpose at all.
- 1, is awarded if a method might be usable but might require additional modules, or programming.
- 2, is awarded if the method is usable but might require more work than necessary
- 3, is awarded if the method is usable and efficient.

Note that co-simulation methods are not incorporated in this grading process since they all require additional programmes or toolboxes in order to work. Pleas also note that this is a subjective way of choosing the final method. The result might not be the absolute best method. It does however keep in mind the competences of the researcher and the facilities at Ricardo.

A.1. C/C++/CSHARP

C/C++/CSHARP is a versatile programming language. It benefits from a long history of libraries with which all kinds of calculations can be done. Documentation for these libraries might lacks precision. As a pre- or post-processor, the C language would be useful. The knowledge of C at Ricardo however, seems to be less than the knowledge of Matlab. It is also less intuitive than Matlab. It does however not run directly from the code such as matlab, therefore time profits can be gained from porting to C if pre- and post-processing times become slow. The C language, for now does not seem interesting to pursue. The corresponding decision values reside in table A.1.

C/C++/C#	Decision value
Pre- and post-processor	1
Solver	1

Table A.1: Decision C/C++/C#

A.2. Matlab

The Matlab program allows for a high level of flexibility and functionality. In Matlab every calculation which is required can be done. The dynamical simulation can be implemented relatively easy. It does however require, that all calculations are written in code, including the finite element analysis. Performing finite element analysis in Matlab is possible. It does however not provide an intuitive environment for this type of calculations. Also the FE calculations, which have to be written in code, will probably never be as good (with respect to accuracy as well as computation time) as the calculations done by any commercial or open source FEA package. With respect to pre-processing, the Matlab environment provides plenty of opportunities for automating the modeling process, therefore it is very useful. With respect to the solver, an FE library will need to be found. Creating the FE solver from nothing would be too expensive and does not provide any guarantees that results will be correct, therefor this would be a risky choice. Post-processing in Matlab can profit from the same benefits as pre processing.The corresponding decision values reside in table A.2.

Matlab	Decision value
Pre- and post-processor	3
Solver	1

Table A.2: Decision Matlab

A.3. Ansys

Using only Ansys allows for a full Finite element model of both pantograph and catenary. Full transient dynamic analyses can be run in Ansys [8]. The finite element method used in Ansys also allows a good representation of the catenary system. The Ansys Parametric design language is a serial language and is very well automated through creation of text files in another programming language. Therefore, interfacing between programmes is not necessary. Modeling in Ansys however is time consuming. Post processing does not allow a lot of changes to the signals. Therefore it is very suitable to be used as solver, but not as pre- or post-processor. The question that remains unanswered is which part of Ansys is used for these results and whether these modules are installed at Ricardo Netherlands. The corresponding decision values reside in table A.3.

Ansys	Decision value
Pre- and post-processor	2
Solver	3

Table A.3: Decision Ansys

A.4. Matlab + Ansys co-simulation

In [25] a method is described for co simulation of 2 programmes, one being a FEA model and one being a MBD model. The biggest pro for such a 2 sided model is, that each model can do what it does best. Since it is to be expected that the Ansys system will provide us with an accurate catenary model and the Matlab system can model lumped mass damper models, the expectation is that the this combination can meet the simulation goals within reasonable time.

A.5. Simpack

Pure simpack simulation means using rigid bodies and model reduced flexible bodies. This will not work positively for the catenary simulation. Using simpack as pre- or post-processor is therefore also not applicable, since the pre- and post-processing abilities are tailored specifically to data created by the Simpack solver. The corresponding decision values reside in table

A.4.

Simpack	Decision value
Pre- and post-processor	0
Solver	0

Table A.4: Decision Simpack

A.6. Simpack + Ansys co-simulation

As in [25] this systen uses a MBD model for the pantograph and an FE model for the catenary. Dynamic time integration is no problem in Simpack. The interface between Ansys and Simpack will need to be acquired. This is however the method of choice for Ricardo Netherlands. Therefore this option will be looked at further. This is the preferred method, since it is already widely used at the company and people understand the way the program works. Also it can be extended reasonably easily to incorporate rail-car interactions and car dynamics in future iterations of the method. All in all it can therefore be said, that this method will be preferred, under the condition that the required packages and toolboxes can be acquired.

A.7. Simpack + Ansys (FE2FBI/FMI load in to simpack)

This option Models the catenary in Ansys and loads this model using FEMBS into Simpack. This reduces the model however to a situation, where the actual simulation is no longer done in an FE model, but in a reduced model. This results in a less desirable situation since all current methods use FE models.

B

Modelling of EN50318 Model

B.1. Summary

The simulation to support this research will be done in Ansys. The process of modeling the Pantograh-Catenary dynamics is fully described in appendix C, throughout this chapter references will be made to this Appendix. In this chapter the modeling choices and methods which are used in the final model will be discussed, the way these methods were derived will only be discussed briefly. Therefor, for a full explanation of the modelling process please read Appendix C, in addition to this chapter.

B.1.1. General model

There are three main catenary systems, which should be modeled, as defined in the Norm prEN50318:2016 [2] (this version is not used for validation!).These models are: AC Simple, AC Stitched and DC simple. More systems do exist, they will however not be treated as separate systems since small changes may be made to the three defined systems to create the other systems. These models contain reasonably similar elements, their geometry and material properties may vary. The Ansys program, in combination with a Matlab pre-processing code, allows for easy modelling and editing of models. Ansys provides a pre existing contact model, removing the necessity for creating such model. Ansys can also run off code (APDL) allowing for automation. It is usable for all the above models, and allows for Automation in future use.

B.1.2. Elements

The elements of which the model consists are as follows:

- Beam188, Timoshenko beam
  The Beam188 element is a 2 node 6-7 DOF per node beam element which follows the Timoshenko Beam theory, it represents the mechanical properties of the Catenary wire, the contact wire and the steady arms.
- Combin39, Non-linear spring-damper
  The Combin39 element is a 2 node 6 DOF Non linear spring element, which represents the dropper cables in the catenary system. These elements do not have any mechanical properties beyond the non-linear stiffnesses, and therefore do not describe the complete dropper behaviour.
- Mass21, Mass-inertia in x,y,z,rotx,roty,rotz
  The Mass21 element is a 6DOF Mass element, it represents all discrete masses such as the Dropper and Steady arm clamps, but is also used to divide the dropper masses over the contact and catenary wire, They are also used to represent the masses in the pantograph
- Conta176, Line-line contact

- Targe170, 3D Target element

- Combin14, Linear spring-damper

Stress stiffening.

The previous examples assume that the bending stiffness of the beam remains the same throughout the bending. This is accurate as long as the small-deflection assumption holds. This means the deflection of the beam should be relatively small to the original form, in which case the stiffness matrix is determined by the stiffness of the original shape for all calculations.

The actual contact line however is not only loaded in bending but also in tension. which means that the system deflects axially and transversally. These two can impact eachother's stiffnesses and therefore require further research. The axial load that is applied, is relatively large and therefore the expectation is that the deflection in the axial direction will also be reasonably large, in which case the small displacement assumption will no longer hold. In order to test this effect, the model of the simply supported beam will be improved and the tension in the cable will be applied on the right side support, the resulting model can be seen in figure C.4. This results in a system which should bend less in the Z direction.

The assumption of small displacements as described previously simplifies the situation too much. The solution to this problem is, to do a (non linear) large displacement analysis. This analysis does not assume the stiffness matrix to remain the same. The stiffness matrix is updated in every step and therefore the influence of the axial load can be incorporated. The value for UZ at node 6 has reduced to 0.000330 m. This seems more accurate for a simply supported beam under tension where the axial load is much larger than the transversal load.

Now that we know intuitively that the large displacement solution is better than the small displacement solution. We need to calculate whether or not the values that are output by the large displacement solver are accurate. The easiest way to do this is to calculate the 'sag' of the wire by use of the catenary equation. The sag of the wire is defined as being the largest deflection in the negative Z direction, when a cable is under tension and carrying its own weight. This is easier than using the normal beam equations, since those all assume one load and do not couple the transversal and axial loads. Also, our 'simply supported beam' actually is a catenary wire, under tension and only carrying its own weight. In these conditions the catenary equation applies.

The error between the calculation in formula C.12 and the UZ value from the large displacement solver is only 0.21% or $6.95 * 10^{-7}$ meter as can be seen in formula C.15. This error is well below the desired precision of the model (0.1 mm) and therefore, we can conclude that the large displacement solver has calculated the deflection in the tensioned cable sufficiently accurate. The remaining error can be attributed to numerical error and rounding error in the calculations. It can also be attributed to the inclusion of shear stress in the calculation of the Timoshenko beam.

B.2. Contact modelling in Ansys

Modeling a Contact in ansys can be done through the available contact and target elements. In our case the Line-to-Line Conta176 element is available. This element can model crossed beam sliding contact. In order to determine contact the Conta176 Element will be coupled to a Targe170 Element through a common set of real constants. These real constants contain all parameters necessary to determine the contact. The Conta176 Elements will be overlaid on the BEAM188 elements which represent the ocl's material and geometrical properties. The Target170 element will be RIGID by determining it between nodes (not over element nodes). This results in a rigid-deformable contact pair which will be used in the simulation. The contact however encounters some difficulties, which originate from the Contact elements

B.3. Possible future problems

Connection Between Contact wire and steady arm is locked and does not allow independent rotation. Investigation of this 'problem' resulted in the conclusion that it does not influence the model in a significant manner. Induced moments in the system were up to 0.8 nm, A simple calculation of the moments tells us the lift created by this is no more than 0.7 N.

Constraint locked with modes. Locked modes: x 1:2 z 3:4 beta 19:20 gamma 5:13

B.3.1. Dynamic modelling problems

Ansys modeling Has successfully resulted in a correct static model of the A simple variety. This model has been statically validated with the values in the norm EN50318:2016 The step towards dynamic analysis was a big one. Problems were instability of the system when scaling up from 2 or 4 spans to 10 or more spans. This problem occurred due to too large solver constraints. To ensure correct convergence the values have been changed to F 0.0001 INF M 0.0001 INF U 0.0001 INF ROT 0.0001 INF

Secondly the system output after simulation was problematic. This was the result of too coarse meshing. The model was meshed too an extent where it was not possible to bend the contact wire sufficiently at the point of contact. This resulted in very high(and low) peaks in the system. due to the discontinuities at the interface of the elements (elements behave linearly). This was improved upon by increasing the amount of elements in the cable. Until the discontinuities no longer form a big part of the end result.

Lastly the peak forces were a little big at points where the cable had a high amount of bending (mostly around the first and last dropper). This was resolved by lowering the contact stiffness.

B.3.2. Contact force issues

The Resulting model shows us that whilst displacements might be within the expectable ranges this might not be true for the Forces. This is highly probably the result of mesh refinement and especially the lack of element refinement.

Refinement

In the situation of low mesh refinement the system does not represent the true situation well. This results in very noisy results as can be seen in figure C.9b

Contact issues

If the refinement is high enough another issue presents itself. The contact model, which usually only sees one contact element, now sporadically sees multiple contact elements. These elements will both have a contact relationship with the target element, this results in a discontinuity in the contact relation. Which then results in an erroneous force. This phenomenon is clearly visible in figure C.9. The 2 lines represent the force of 1 pantograph on a catenary system with 2 contact wires.

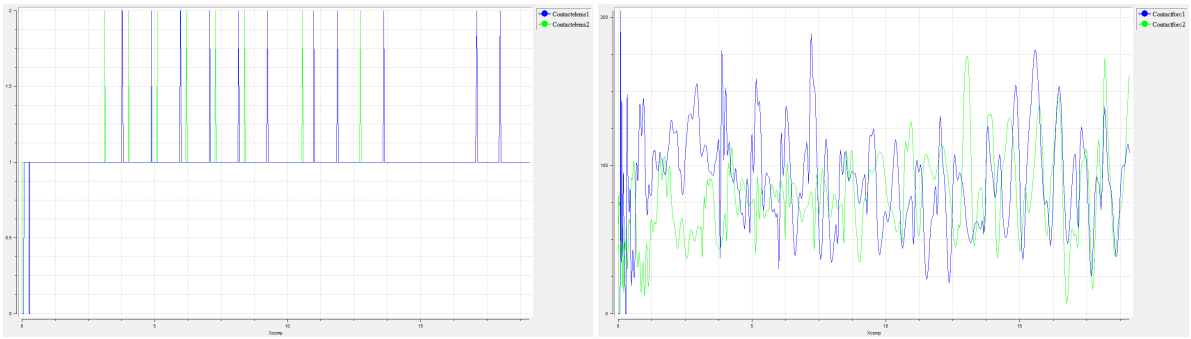

(a) Amount of elements in contact (b) Contact force

Figure B.1: Contact force output showing unwanted peaks in the amount of contacts found

These contact issues were eventually solved by switching the target and contact elements, since if there is only 1 contact element, there can be only 1 contact. This step however, is not recommended by the ansys program since the most rigid part should be the target.

This solution has also introduced another problem, which can be eliminated by improving the mesh. For the issue is speed and refinement related formula B.1 was made. It represents the frequency at which elements are being passed. This frequency needs to be above 20HZ in order to be filtered away. In order to keep some safety margin, and be absolutely sure that the error is filtered out, a boundary of 40hz is chosen.

$$\frac{\frac{LongestDistanceBetweenDroppers}{REFINEMENT}}{V_{sim}} < 0.025s \tag{B.1}$$

Formula B.1 uses the geometry, refinement and desired simulation velocities to determine whether the simulation which is done is valid. If the result of this calculation ends up to be false, the refinement value can be increased to accomodate the desired simulation velocity.

If the simulation velocity is between 0 and 40Hz the results will need to be checked manually for noise due to the element lay-out. At very low speeds the noise may be irrelevant, this can however not be assumed.

B.3.3. Automated Ansys modelling

In order to create a model which can be easily used by others, it is a requirement that the model can be created without needing to go through the process of finding out how to make it. With this in mind, it is important that the modeling turns into a simple process, where settings are changed and the model is made. Also, the simulation process should be automated. These 2 will result in a simple (enough) process for everyone with some basic ansys and matlab knowledge to run a full simulation with his or her OCL model or pantograph.

The automated modeling process will be done through a Matlab code. The basic geometry of the OCL model will be input through a matlab file. In this file all the necessary geometric and material properties can be entered. A second matlab file is used to enter the Pantograph model, For both these files the running will result in a .mat file which is saved in the current directory. If the models are required for future use they do not need to be entered anymore but can be loaded from file.

The main .m file will then create the ansys code. Some basic settings such as amount of spans, pantographs and simulation speed can be entered and the Running will result in 4 text files, which can be entered into Ansys to run the full simulation. After the simulation is finished, results will be extracted and processed in the Post processor .M file. This process is visualised in the flow chart as can be seen in figure C.10. Therein the names of the .m Files and their version numbers can be found.

B.3.4. Large Model Simulation issues

During the process of modeling the system. The models with which simulations were run became significantly larger. This induced an issue which was not of importance in smaller models. The large system, using the same settings as smaller systems, becomes unstable. This is not a result of the model, but instead a result of the solver settings. The solver would find a converged situation where in reality the system became gradually more unstable. After some research it was found to be the result of too loose convergence criterion (L2) Changing to an infinite criterion, where every DOF needs to converge resulted in a stable system.

Model clarity

The reference models as defined in the norm EN50318:2016 lack some small parts of information. Therefore sometimes results are inadequate. For instance steady arm inclinations are not defined in the Reference models. After several attempts it was found that ten degrees of inclination provides a static situation closest to the values described in the EN50318:2016 norm.

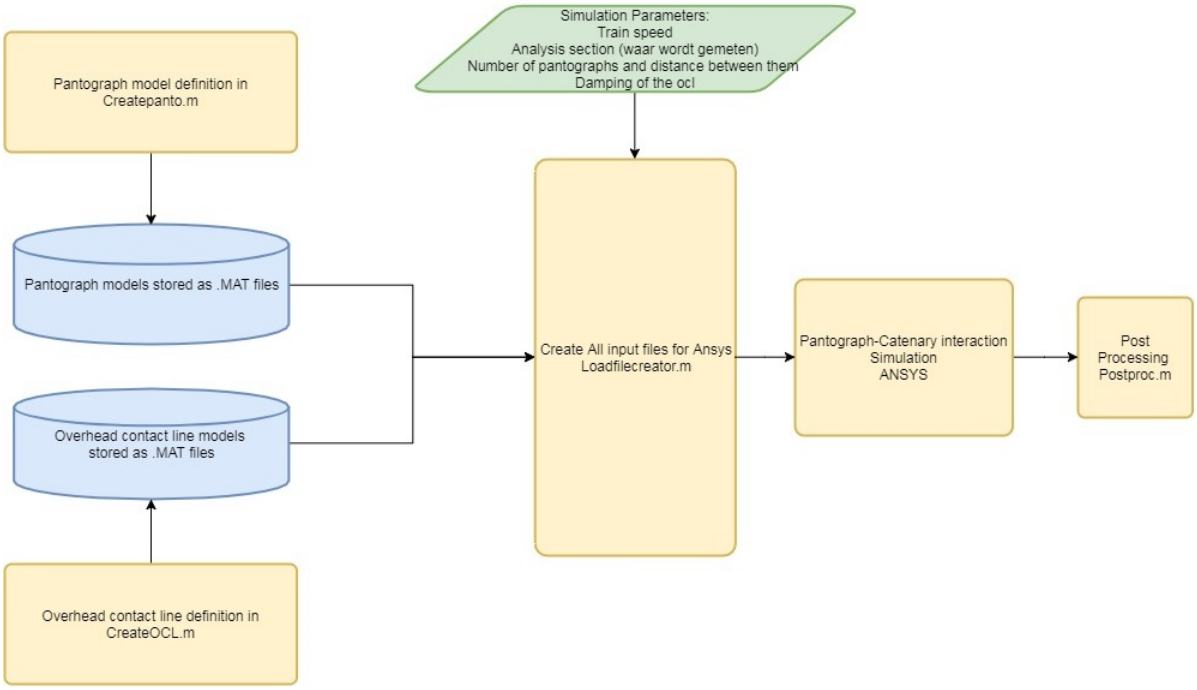

Figure B.2: Automated simulation flow chart

Further Reading

As the modeling process is complicated and not all steps of which it consists can be seen in the final model. Some steps, mostly initial validations of the correct workings of beam elements and other modeling elements, are left out in this section. For a full summary of the modelling process, please refer to appendix C

C

Ansys modelling log

Read first

This appendix is the unedited log of the modeling process in Ansys. From deciding upon beam theories up to the static validation of reduced models. Furthermore it contains directives toward certain ansys applications. It is meant as a collection of knowledge, a way to reconstruct certain behaviour in ansys. It will not be edited, even though certain parts could use it, in order to keep all information. It may be referenced to determine wether or not certain processes have been executed correctly. It is however in no way part of the report and should therefore not be addressed as such.

The Modelling of the catenary will be done in the multi body dynamics package simpack. This version of Simpack that will be used is version 9.7.

Since Co-simulation between Ansys and Simpack is not possible (Ansys <->Adams is possible) The modeling will have to be done with ansys and the simulation in SimPack. This requires the creation of .Sub and .cdb files in Ansys. These files do in no case directly work when loaded into Simpack and therefore require some formatting.

Firstly the FE model will need to be validated. This is done step by step in a manner which allows validation of the elements used, but also it allows s for validation of the load step and the solver options.

Beam Theories

There are 2 theories that can be used, The Euler-Bernouilli (or classical beam theory), and the Timoshenko beam theory. The classical theory assumes the cross section is always perpendicular to the centerline, no shear stresses are included in this theory. Timoshenko beam theory assumes that shearing is possible and therefore the cross section is not necessarily perpendicular to the centerline. In theory it can be found that both theories approach each other as the thickness to length ratio becomes small. Therefore a simple beam deflection situation will be calculated which represents the geometry of the contact wire and model this with a BEAM188 Timoshenko beam in Ansys. Comparison of these results will determine whether the results are related (they should be). Secondly the BEAM188 will be modeled in Ansys and compared to analytical calculations. This will be done to see, whether indeed the differences between the models become negligible if the t:l ratio becomes small. If this happens the models can be assumed to be valid in the static situation.

The reason Timoshenko beams are used in this section is as follows. The overhead contact line that has to be modeled can be seen as a long and slender beam. It is under a bending load as well as under an axial tension and it will be used to perform a dynamic analysis. The Timoshenko beam is for such a situation the beam that will result in the most accurate model. Transverse shear stress is taken into account in this element, this would not be necessary since the beam is a (very) slender beam with thickness:length ratio of 0.001333

which is well below the 0.1 value which is normally assumed the value below which shear deformations can be neglected.

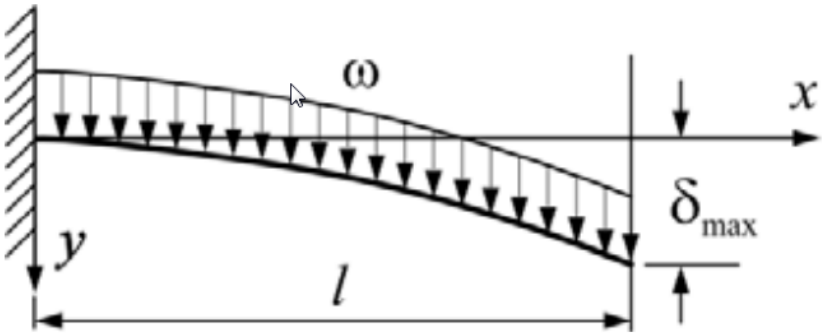

Figure C.1: Simple Cantilever Beam under a uniformly distributed load

Calculating the deflection of a cantilever beam by using Beam-Deflection formula's with one side completely constrained and one side freely moving:

$$\delta_{(x)} = \frac{qx^2}{24EI}(x^2 + 6L^2 - 4Lx) \quad \text{(C.1)}$$

$$\text{Location of maximum deflection: } x = L \quad \text{(C.2)}$$

$$\delta_{(Max)} = \frac{qL^4}{8EI} \quad \text{(C.3)}$$

$$\text{E Modulus Copper: 124 gPa} \quad \text{(C.4)}$$

$$\text{Bending moment solid cirular cross-section: } I_y = \frac{\pi r^4}{4} = 1.8065710^{-9}\text{m}^4 \quad \text{(C.5)}$$

$$q = \rho * A * g = 13.2435N/m \quad \text{(C.6)}$$

$$\text{Fill in for L = 2m : } \delta_{Max} = 0.11824\text{m} \quad \text{(C.7)}$$

Modeling the exact same beam in Ansys should approach the same result as the analytical solution. Since Snsys uses numerical methods to approach the analytical solution, the solution which it gives will approach the actual value, but it will not be exactly the same. Improving the precision of the calculation can be done by increasing the amount of nodes and elements in the simulation. The model of the cantilever beam can be seen in figure C.1.

The Results of solving this model should approach the result of equation C.7. In figure C.2a The maximum deflection is found to be 0.11896 Meter. This is within 0.61% of the analytical result in equation C.7. This difference can be expected since the analytical solution does not take into account shear stresses, and therefore should result in slightly less deformation as compared to the Ansys result. As an extra check the rotation at the end point can be calculated with the following formula:

$$\theta_{Max} = \frac{qL^3}{6EI} = 0.078665 \text{ Rad} \quad \text{(C.8)}$$

$$\theta_{Ansys} = 0.079041 \text{ Rad} \quad \text{(C.9)}$$

This value can also be compared to the result from the Ansys model in figure C.2b The difference between these values is just below 0.48% This can be attributed to the shear deformation and numerical error. Therefore it is concluded that modeling in Ansys with the Beam 188 element and the Linear Elastic isotropic material model produces accurate results.

To approach the static situation of the full contact wire, it will not only be enclosed at one side. But rather will it be modeled as a simply supported beam. Therefore the Ansys model will be extended to implement 2 supports, one which restricts all Translational DOF's and one which only restricts the y and z translations but allows for x direction motion. Taking

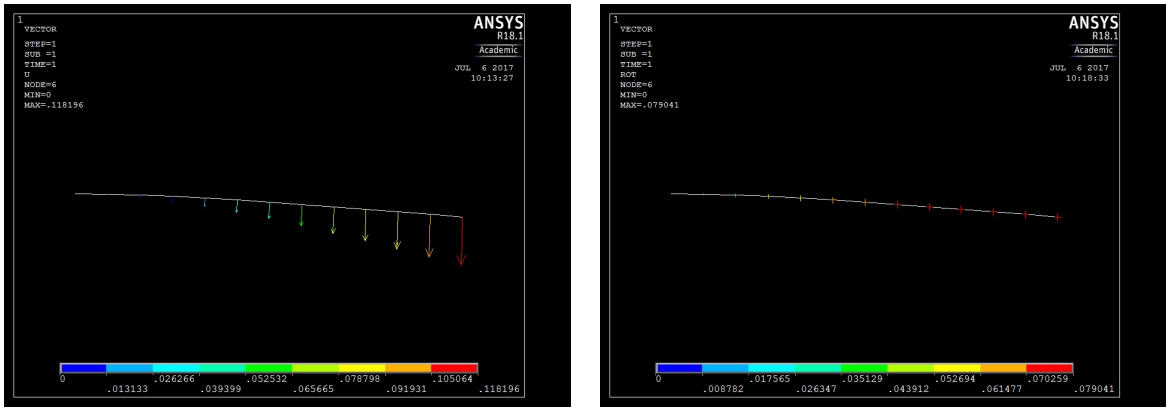

(a) Displacements (b) Rotations

Figure C.2: Results of the static analysis for a cantilever beam

the deflection equation for such a beam and taking L = 2 gives :

$$\delta_{Max} = \frac{5qL^4}{384EI} = 0.01231\text{m} \tag{C.10}$$

$$\theta_{x=0} = tan(\frac{qL^3}{24EI}) = 0.01970434\text{Rad} \tag{C.11}$$

The images show the deflection of the simply supported beam as it is modeled, the values resulting from the simulation correspond to the analytically calculated values.

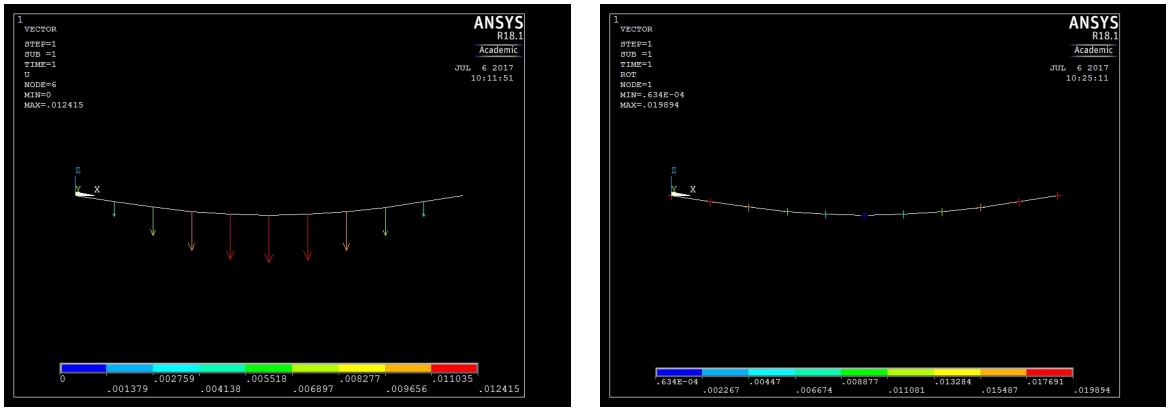

(a) Displacements (b) Rotations

Figure C.3: Results of the static analysis for a simply supported beam

Stress stiffening.

The previous examples assume that the bending stiffness of the beam remains the same throughout the bending. This is accurate as long as the small-deflection assumption holds. This means the deflection of the beam should be relatively small to the original form, in which case the stiffness matrix is determined by the stiffness of the original shape for all calculations.

The actual contact line however is not only loaded in bending but also in tension. which means that the system deflects axially and transversally. These two can impact eachother's stiffnesses and therefore require further research. The axial load that is applied, is relatively large and therefore the expectation is that the deflection in the axial direction will also be reasonably large, in which case the small displacement assumption will no longer hold. In order to test this effect, the model of the simply supported beam will be improved and the

tension in the cable will be applied on the right side support, the resulting model can be seen in figure C.4. This results in a system which should bend less in the Z direction.
If we assume small displacements, the nodal results of the solver are in the following output

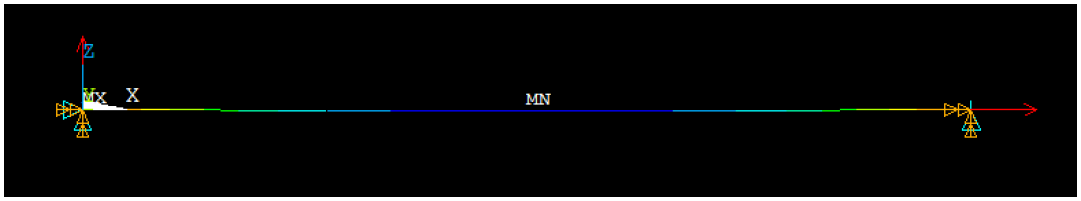

Figure C.4: Simply supported Beam under a uniformly distributed load with axial tension T =20000N

list. It can be seen that the value for UZ at node 6 equals -0.012415 m. This is equal to the UZ in the same beam without an axial load. The expectation would however be that the deflection becomes less due to the stress stiffening effect.

Small Deflection

```
 PRINT U      NODAL SOLUTION PER NODE

  ***** POST1 NODAL DEGREE OF FREEDOM LISTING *****

 LOAD STEP=       1   SUBSTEP=     100
  TIME=      100.00        LOAD CASE=     0

  THE FOLLOWING DEGREE OF FREEDOM RESULTS ARE IN THE GLOBAL COORDINATE SYSTEM

    NODE        UX            UY            UZ            USUM
       1    0.0000        0.0000        0.0000        0.0000
       2   0.21426E-003   0.0000       -0.38785E-002  0.38844E-002
       3   0.42853E-003   0.0000       -0.73481E-002  0.73606E-002
       4   0.64279E-003   0.0000       -0.10073E-001  0.10093E-001
       5   0.85706E-003   0.0000       -0.11810E-001  0.11841E-001
       6   0.10713E-002   0.0000       -0.12415E-001  0.12461E-001
       7   0.12856E-002   0.0000       -0.11834E-001  0.11903E-001
       8   0.14999E-002   0.0000       -0.10109E-001  0.10220E-001
       9   0.17141E-002   0.0000       -0.73797E-002  0.75762E-002
      10   0.19284E-002   0.0000       -0.38764E-002  0.43296E-002
      11   0.20355E-002   0.0000        0.0000        0.20355E-002

 MAXIMUM ABSOLUTE VALUES
 NODE          11            0             6             6
 VALUE    0.20355E-002   0.0000       -0.12415E-001  0.12461E-001
```

The assumption of small displacements as described previously simplifies the situation too much. The solution to this problem is, to do a (non linear) large displacement analysis. This analysis does not assume the stiffness matrix to remain the same. The stiffness matrix is updated in every step and therefore the influence of the axial load can be incorporated. The value for UZ at node 6 has reduced to 0.000330 m. This seems more accurate for a simply supported beam under tension where the axial load is much larger than the transversal load.

Large Deflection

```
 PRINT U      NODAL SOLUTION PER NODE
```

***** POST1 NODAL DEGREE OF FREEDOM LISTING *****

LOAD STEP= 1 SUBSTEP= 15
TIME= 100.00 LOAD CASE= 0

THE FOLLOWING DEGREE OF FREEDOM RESULTS ARE IN THE GLOBAL COORDINATE SYSTEM

NODE	UX	UY	UZ	USUM
1	0.0000	0.0000	0.0000	0.0000
2	0.21458E−003	0.15920E−022	−0.11347E−003	0.24273E−003
3	0.42917E−003	0.33754E−022	−0.20722E−003	0.47657E−003
4	0.64376E−003	0.36471E−022	−0.27476E−003	0.69995E−003
5	0.85837E−003	0.37939E−022	−0.31582E−003	0.91463E−003
6	0.10730E−002	0.39348E−022	−0.33039E−003	0.11227E−002
7	0.12876E−002	0.40799E−022	−0.31846E−003	0.13264E−002
8	0.15022E−002	0.43011E−022	−0.28002E−003	0.15281E−002
9	0.17168E−002	0.53262E−022	−0.21492E−003	0.17302E−002
10	0.19314E−002	0.31468E−022	−0.11916E−003	0.19351E−002
11	0.20386E−002	0.0000	0.0000	0.20386E−002

MAXIMUM ABSOLUTE VALUES

NODE	11	9	6	11
VALUE	0.20386E−002	0.53262E−022	−0.33039E−003	0.20386E−002

Now that we know intuitively that the large displacement solution is better than the small displacement solution. We need to calculate whether or not the values that are output by the large displacement solver are accurate. The easiest way to do this is to calculate the 'sag' of the wire by use of the catenary equation. The sag of the wire is defined as being the largest deflection in the negative Z direction, when a cable is under tension and carrying its own weight. This is easier than using the normal beam equations, since those all assume one load and do not couple the transversal and axial loads. Also, our 'simply supported beam' actually is a catenary wire, under tension and only carrying its own weight. In these conditions the catenary equation applies.

$$T = \frac{qL^2}{8d} \quad \text{T: axial tension, q: load, L: length, d: sag} \tag{C.12}$$

$$20000 = \frac{13.2435 * 2^2}{8d} \tag{C.13}$$

$$d = 0.0003310875 \text{ m} \tag{C.14}$$

$$\text{Error} = \epsilon = \frac{UZ - d}{d} = 0.21\% \tag{C.15}$$

The error between the calculation in formula C.12 and the UZ value from the large displacement solver is only 0.21% or $6.95 * 10^{-7}$ meter as can be seen in formula C.15. This error is well below the desired precision of the model (0.1 mm) and therefore, we can conclude that the large displacement solver has calculated the deflection in the tensioned cable sufficiently accurate. The remaining error can be attributed to numerical error and rounding error in the calculations. It can also be attributed to the inclusion of shear stress in the calculation of the Timoshenko beam.

Coupling of 2 beams

The next phenomenon we verify is, whether the sag of multiple connected beams with a support in the middle does also follow the rules. For this check a model is made which consists of 1 beam supported at 3 locations. The middle support is connected to node 11 of the beam. In order to be able to use the beam equations, the axial load is removed.

It is proposed that if an Ansys beam model with 3 supports holds, the model can be

extended to an infinite amount of middle supports and the validation will not need to be done again.

In figure C.5, the model shows the contact wire up until the second dropper location X = 10.5 m. The middle support is located at X=5 m. With this setup, the sag of both wires can be calculated.

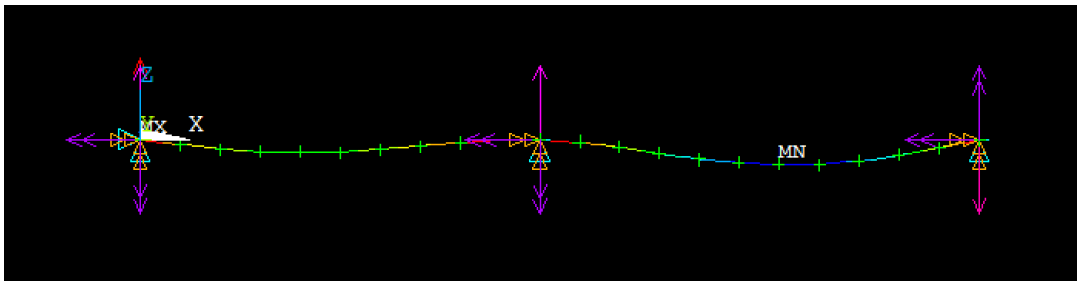

Figure C.5: Triple support beam under a uniformly distributed load

The sag is calculated without Axial load with the small-deflection assumption. In section C we have validated, that this method provides us with good results. Therefor, it can be used for the deflection calculations in the following validation.

Since this is less straightforward than both previous calculations the validation will be done as follows.

1. Solve the Ansys model;
2. Read the moment/torqua on node 11;
3. Calculate the sag caused by the moment/torque on both (partial) beams, using the beam deflection formula's (in Matlab);
4. Superpose the self-weight sag and moment sag over each other;
5. Compare to the UZ value of the Ansys model.

The solution of the Ansys model provides the following moments on the 11^{th} and 12^{th} node.

ELEM=	144	MX	MY	MZ
	11	0.28435E−016	45.572	−0.31572E−015
	12	−0.28435E−016	−24.888	0.31572E−015

The moment returned by Ansys is entered into a Matlab calculation file **??** which calculates the 3^{rd} and 4^{th} step of the list.
For the 5 m beam the calculated maximum UZ = 0.1734 m
For the 5.5m beam the calculated maximum UZ = 0.3284 m

The Ansys model returns a minimum UZ = 0.17102 m at node 37, UZ = 0.32572 m at node 17.

$$\text{Error: } \epsilon_{5m} = \frac{0.17102 - 0.1734}{0.1734} = 1.37\% \tag{C.16}$$

$$\text{Error: } \epsilon_{5.5m} = \frac{0.32562 - 0.3284}{0.3284} = 0.7515\% \tag{C.17}$$

These errors seem to be non negligible. But they do show that the ansys model is 2.38mm off at the 5 m beam and 2.68mm off at the 5.5m beam compared to the calculations which were made by hand. since the Modeled elements are 0.5m long the sag is calculated at 8 points in the first beam and at 9 points in the second beam. this might be too little to catch

the exact minimum caused by the added moment. The error could also lie with the beam deflection formula's not being completely accurate for this situation since there might be some additional forces and moment working on the system. The curvature of the beams also is of importance in this derivation. The previous calculations have all had reasonably low curvatures compared to the curvature of this beam at the middle support. Since the Timoshenko beam theory takes into account the shear stresses in the beam, these stresses (due to the high amount of curvature) are likely to play a role in the calculation Ansys has made. The classical beam theory which is used for the analytical calculations does not incorporate these effects. Furthermore, the analytical calculations are applicable to systems with small deflections in them, as the stifness is not updated. This calculation is clearly no longer a small displacement, therefore the analytical calculations can be expected to show larger errors. In contrast to the first calculations the classical beam theory does no longer hold, the analytical calculations should be done by means of the Timoshenko beam theory,

Difference between Euler-Bernoulli and Timoshenko beam theory in practice

In order to validate the Ansys model a matlab program was written which calculates deflections and slopes, for both a cantilever beam as well as a simply supported beam. The calculation is done twice, once with Euler-Bernoulli Beam theory and once with Timoshenko beam theory. The resulting deflections and slopes are plotted for both theories and they are compared through their differences (error). These results can be seen in figure C.6 and figure C.2b.

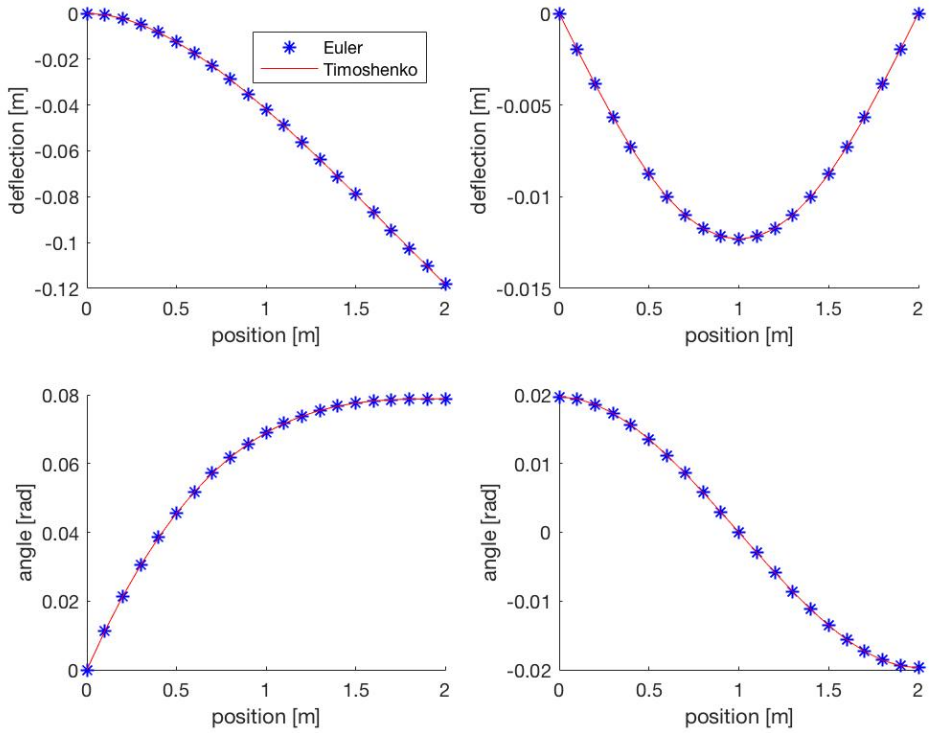

Figure C.6: Analytical deflection results for Euler-Bernoulli and Timoshenko beams

The chosen beam188 element in Ansys should represent reality well, to support this expectation the choice is validated through table C.1. The comparison between the Ansys and Timoshenko calculation shows errors of up to 1%. These errors find their origin in the capacities of the applied analytical formulas. Analytical bending equations are very accurate for small displacements, and they assume beams are loaded only in bending. As the beams which are used in catenary systems are however very slender, using these theories will result

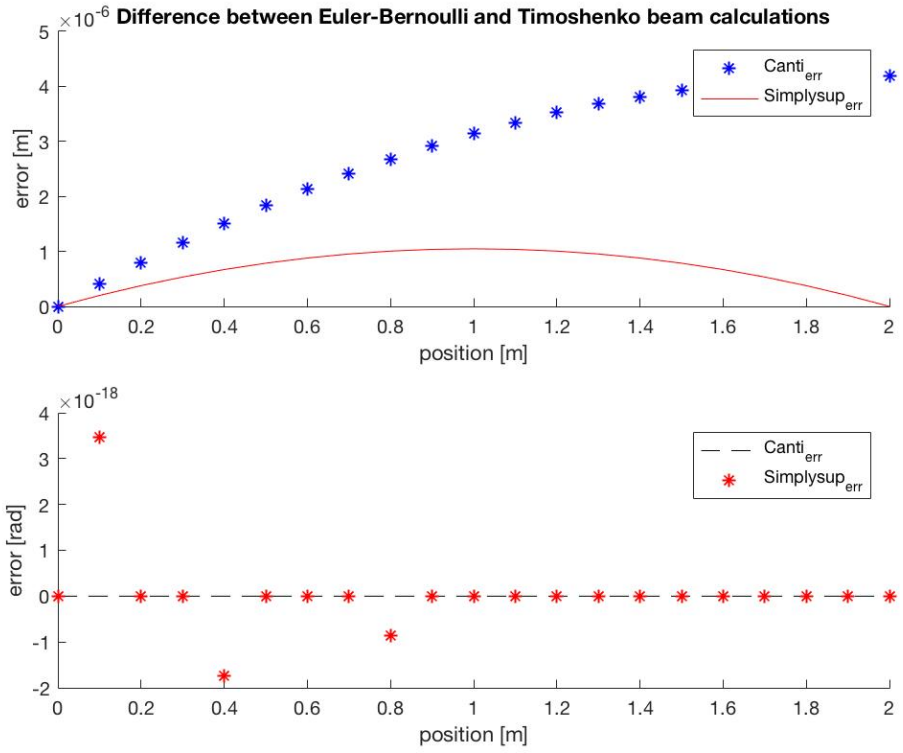

Figure C.7: Analytical errors between Euler-Bernoulli and Timoshenko beams

in high displacements, in which case the beam theory loses accuracy. The Ansys system does not suffer this problem, therefore as bending increases the error will also increase. To prove that the error does converge as the beam becomes stubbier, the short ss beam has been added for comparison. The displacements remain in the 1E-05m range where the errors become less than 0.1%. From this it is reasoned that, these increasing errors occur from shortcomings in the analytical solution. **This leads to the conclusion that the Ansys model with the BEAM188 element provides sufficiently accurate deflection characteristics even when large displacements occur.** Furthermore the cable will be loaded in bending as well as in tension, therefore the tensioned ss beam deflection was calculated. Comparable results were observed between the analytical result and the Ansys model with a relative error of 0.2107% resulting in an absolute error of 0.0006975mm. For the final simulation, vertical resolution of 0.5mm is required, which is about 1% of the total vertical bandwith. The acquired results in this calculation will allow these expectations to be met. Therefore it can be stated that:**the comparison of the Ansys model to analytically calculated deflections under tension provides sufficiently accurate results with the BEAM188 element and the large displacement solver.**

Dynamical response and substructuring

Since the catenary system is the most complicated sytem in the simulation it is of the essence that it is modeled correctly as well as substructured correctly. Since it has been shown that the statical results for the system are accurate. The dynamical responses can be investigated. Eigenmodes and eigenfrequencies will be determined for a model which consists of three spans (180m). This has been chosen since the contact wire is not constrained at the ends, which results in a response in the middle span which will approach the reaction in a full length span (minus the wave propagation). Multiple analyses will be done, some will include all droppers and some will be done minus droppers on some locations to determine the responses and respectively the best way to model the system.

	Euler		Timoshenko		Error	
	Deflection	Angle	Deflection	Angle	Eu-Tim deflection	Eu-Tim angle
Cantilever beam	0.1182	0.0788	0.1182	0.0788	4.1901E-06	0
Simply supported beam	0.0123	0.0197	0.0123	0.0197	1.0475E-06	3.4694E-18
Extended ss beam	0.3284					
	Ansys BEAM188		Timoshenko		Error	
	Deflection	Angle	Deflection	Angle	Relative	Absolute
Cantilever beam	0.118398	0.078929	0.1182	0.0788	0.1675%	0.198mm
Simply supported beam	0.012415	0.019655	0.0123	0.0197	0.8530%	0.105mm
Extended ss beam	0.325932		0.3284		0.7515%	2.468mm
	Simpack		Ansys BEAM188		Error	
	Deflection	Angle	Deflection	Angle	Relative	Absolute
Cantilever beam			0.118398	0.078929		
Simply supported beam			0.012415	0.019655		
Extended ss beam			0.325932			
	Catenary eq		Ansys BEAM188	tensioned	Error	
	Deflection	Angle	Deflection	Angle	Relative	Absolute
Tensioned ss beam	0.00033039		0.0003310875		0.2107%	0.0006975mm
Short ss beam	4.817E-05		4.815E-05		0.0415%	0.00002mm

Table C.1: Difference between analytical and numerical deflection calculations

Modal Analysis

Analysis of the Eigen frequencies and corresponding modes of the system provides knowledge of the way the system will move under certain excitation frequencies. This knowledge can then be used to determine which modes and frequencies are essential for simulation, and which mode shapes will not be of such essence, therefor allowing an even more simplified model and faster computation times. The Ansys mechanical environment provides us with several possibilities for modal analysys

- Static condensation/Guyan Reduction
- Block Lanczos
- PCG Lanczos
- Supernode
- Subspace
- Unsymmetric
- Damped
- QR Damped

Since Ansys provides multiple options for modal analysis, an understanding of the different options should be available in order to determine which of the different options provides the most accurate results. In order to describe the dynamic behavior of the system properly, the Mass participation factors need to be calculated. These values represent the amount of energy/mass divided by the total energy/mass is available in one mode. Therefore, if a mode has a high mass participation factor for a certain mode, this mode must be important for describing the total dynamical behaviour of the system, in the direction which is described by this value. Whereas modes with low mass participation factors influence this direction less. Modes with low mass participation factors in X direction might however be important in the Y, Z, ROTX, ROTY, ROTZ directions. And therefore, for each direction. Important modes must be chosen which together, sum up to a Mass participation ratio of between 0.8 and 0.9.

The OCL model has a lot of non linearities, however, none of the modal analyses accounts for these nonlinearities.

Substructuring in ansys can be done one of four ways. the goal of the substructuring process is reduction of the complete model in order to reduce computation time. It should however reduce the model as well as retain as much information as possible. Therefor an analysis of the different substructuring processes is necessary to determine the best choice for our model. The ansys program provides the following options for substructuring:

- Substructuring
- Component mode synthesis - fixed-interface
- Component mode synthesis - free-interface
- Component mode synthesis - residual-flexible free-interface

These respectively translate to Guyan, Craig-Brampton, Herting and Martinez methods.

Guyan [35] reduction - also known as static condensation is a technique for reduction of the systems which does not take into account inertial terms.....

Craig-Brampton [36] reduction determines the eigenvectors and eigen modes with all the master degrees of freedom constrained (interfaces fixed). This reduction is not useful for reduction of this system since the modes of the system need to be determined for entire system and the lowest modes are neglected when the master DOF's are fixed in place.

Herting [37] reduction Free-interface substructuring is useful for systems where large displacements are in effect. In this system it is particularly useful since it does not constrain the interfaces (master DOF's).

Martinez [38] reduction Residual-Flexible Free-Interface substructuring is useful towards a system where large displacements.

Validation of the Eigenmode reduction in Ansys

To ensure the correct workings of the final system. It is necessary to determine whether the eigenmodes are calculated correctly, or at least in a manner where logical derivation would result in the same eigenmodes. Therefore a system has been conceived in which the first representative eigenmode analysis can be done. It consists of three spans of the EN50318 overhead contact line. Where the middle span is completely built to spec, whereas the outer two spans have fixed points to ensure the model is sufficiently constrained. The drawbacks of this system will therefore be created by the fact that it is not a full length system, causing the fixed points to be relatively close to the analysis section (middle section). Determining whether Ansys correctly applies reduction to a model, and which reduction provides the best result can be determined without application to a full model.

Implicit Dynamics

The reduction of the system allows for an interesting option. Modeling the complete system in Ansys is no problem since it is designed to cope with a very high amount of degrees of freedom. SimPack however is not created for high DOF systems. This is why reduction of the model is necessary. In order to remove as much DOF's as possible it is possible to reduce the system to (explicitly) only exist of the contact wire, since this is the point where the pantograph and the catenary system interface during simulation. To make sure the system reduction does not leave out the relevant dynamics the pre-reduction system is a full catenary system. In this case the dynamics of the full system will be taken into account (implicitly) in the reduced contact wire system.

Validation of Flexible Modelling techniques in SimPack

In order to determine whether or not the model that was made in ansys and was validated in ansys remains correct in SimPack after the reduction and FBI file creation process is an important Factor. The SimPack Flexible body needs to do (exactly) the same as the Ansys model. This is important since the Ansys results have been validated. Small differences, if and when they occur, should be evaluated to see whether they are avoidable or within acceptable margins. Expected differences might occur due to the Ansys model being a full FE model whereas the Simpack wire is a Substructured and reduced model.

this validation will also be used to find the correct way of substructuring an Ansys model. Minute differences might occur while substructuring, it is therefore necessary to determine carefull, for every simulation in Simpack, whether the error occurs due to Simpack or due to the substructuring process in Ansys.

Modeling issues

EN50318 states that the supports should be fixed points, it also states that for both the contact wire and the messenger wire the tension forces should be constant. For the contact wire, this should not pose an issue, since it is attached to the support by means of the registration arm. The end point of this arm is fixed, therefor the cable itself can be tensioned.

Renewed EN50318:2016

During the creation of the EN50318:2002 model. A newer version of the Norm was released (only preliminary) This norm states much clearer, to which extent a model has to conform to the reference in order for it to be usable.

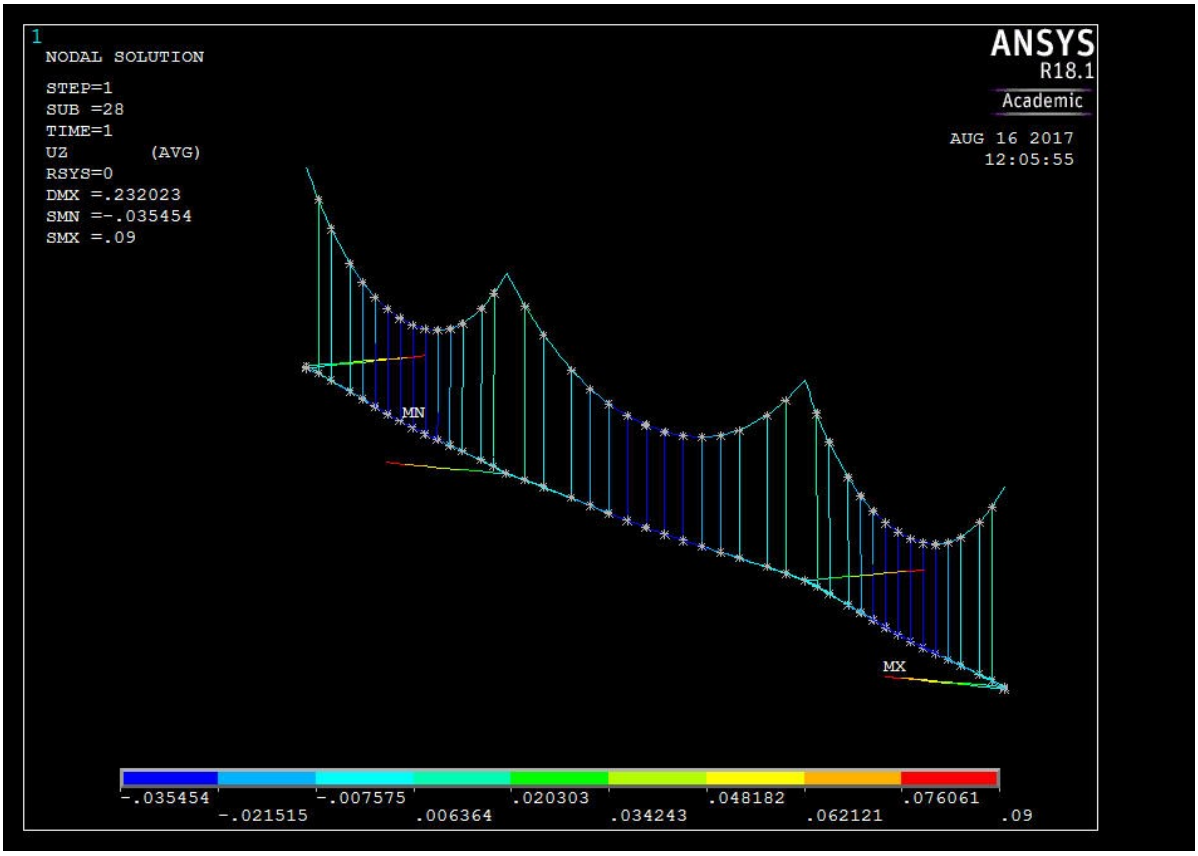

Figure C.8: Three spans

Stress stiffening for a reduced 3 portal model.

In order to correctly introduce a FE model into Simpack the following process was followed. The Model was made in Ansys, modeling the nodes so they would be at their desired position when at rest. This position calculation can be found in the respective XLS file. Elements are determined, materials consist of Linear isotropic properties, densities, and damping coefficients as determined in the Norm.

Real constants determine the dropper stiffness.

With the large deflection static calculation the static situation of the system is calculated.

When this is done. the solution environment is closed and reopened. The analysis type tab is opened and Restart is selected. This will show the last LS and substep number, these

will be remembered and the dialog will be closed.

The command line is fed with the folliwing info

——-

ANTYPE„RESTART,LSnumber,SSnumber,PERTURB

PERTURB,SUBSTR

SOLVE,ELFORM

——-

Next go Analysis type > Analysis opts Fill in the options below!

Which CMS opts are used (28-8-2017)

RFFB(this ensures the model does not need to come to rest in simpack)
300
0
100
Automatic
0
TCMS Transformn mx
YES
Port2016
STIFF+MASS+DAMP
LOADVECT+MATRIX
YES
YES
nothing[RIGID]

Next run SOLVE >current LS

This will create a SUB (and a TCMS if using free interface (not recommended)) file, A third file is needed and this is the CDB file. In order to produce this file go Preprocessor>ArchiveModel>Write.

Go to the correct directory and copy the SUB, TCMS and CDB file to the Simpack computer.

Loading Into simpack

After the substructuring process is complete, the ansys program will have created 2 files necessary for creating the SimPack flexible body. These are The modelname.CDB and the modelname.SUB files. In simpack the FBI (flexible body) file can be generated with the following process. go to Utilities>FBI Files>Generation, use the + sign and select the modelname.CDB and the modelname.SUB files (it might be necessary to change the extension search in the drop down menu next to the path in order to see the files) open them, they will now show in the dialog window. Then define the path for the .FBI file. Check both the Convert recovery matrix and the retain rotational dofs boxes. and generate the .FBI file.

Next a body can be created of the Flexible type and the FBI file can be entered into this body. Modes will need to be calculated (fmin=0 nmodes=150) Next all modes with odd shapes (mostly ydirection modes) will need to be turned off. Markers can be generated with the position connection type in the last tab, after applying all changes there should now be a flexible body in the viewer (zoom fit).

The model that is currently in SimPack is not the exact replica of the model which was created in ansys. This is a result of some shortcomings in the modeling and reduction process.

The first difference is the end influences, Since a 2 portal model will always have some influences at the end of the system. To counteract these influences the contact wires have an applied force and moment at their first and last nodes. The values of this force and moment are chosen in such a way that they mimic the situation had there been another portal after it. In SimPack therefore these forces should be counteracted when two or more of the same model are connected to each other.

The second difference is the dropper non-linearity. Whilst the full ansys model uses non linear droppers, this can not be said for the reduced model. The reduced model uses the

100000N/m stiffness for tension and compression. Since there is no way to change this in the reduction process. The now linear behaviour will have to be compensated. This is done by introducing a Non-linear force element which does nothing in tension (tension should be 100000N/m) and which has a stiffness of -100000N/m in compression (counteracting the implicit stiffness of 100000N/m in compression).

The combination of two models into one is done by using multiple substructures. These substructures will need to be connected to the Reference system markers. these markers will, in case of 56m spans, need to be offset 112m in the X-direction. After joining the Substructure bodies to their respective Reference system marker, they should now be behind each other. At this point there is however still no interaction between the different substructures. In order to join the contact wires of the first structure to those of the second structure, a force element (bushing) is defined between the corresponding markers (1 for each wire). This bushing has very high stiffness in x,y,z,al,be,ga directions. Therefore linking the two markers solidly together.

Contact modeling in Ansys

Modeling a Contact in ansys can be done through the available contact and target elements. In our case the Line-to-Line Conta176 element is available. This element can model crossed beam sliding contact. In order to determine contact the Conta176 Element will be coupled to a Targe170 Element through a common set of real constants. These real constants contain all parameters necessary to determine the contact. The Conta176 Elements will be overlaid on the BEAM188 elements which represent the ocl's material and geometrical properties. The Target170 element will be RIGID by determining it between nodes (not over element nodes). This results in a rigid-deformable contact pair which will be used in the simulation. The contact however encounters some difficulties, which originate from the Contact elements

Possible future problems

Connection Between Contact wire and steady arm is locked and does not allow independent rotation. Investigation of this 'problem' resulted in the conclusion that it does not influence the model in a significant manner. Induced moments in the system were up to 0.8 nm, A simple calculation of the moments tells us the lift created by this is no more than 0.7 N.

Constraint locked with modes. Locked modes: x 1:2 z 3:4 beta 19:20 gamma 5:13

Dynamic modelling problems

Ansys modeling Has successfully resulted in a correct static model of the A simple variety. This model has been statically validated with the values in the norm EN50318:2016 The step towards dynamic analysis was a big one. Problems were instability of the system when scaling up from 2 or 4 spans to 10 or more spans. This problem occurred due to too large solver constraints. To ensure correct convergence the values have been changed to F 0.0001 INF M 0.0001 INF U 0.0001 INF ROT 0.0001 INF

Secondly the system output after simulation was problematic. This was the result of too coarse meshing. The model was meshed too an extent where it was not possible to bend the contact wire sufficiently at the point of contact. This resulted in very high(and low) peaks in the system. due to the discontinuities at the interface of the elements (elements behave linearly). This was improved upon by increasing the amount of elements in the cable. Until the discontinuities no longer form a big part of the end result.

Lastly the peak forces were a little big at points where the cable had a high amount of bending (mostly around the first and last dropper). This was resolved by lowering the contact stiffness.

C.0.1. Contact force issues

The Resulting model shows us that whilst displacements might be within the expectable ranges this might not be true for the Forces. This is highly probably the result of mesh refinement and especially the lack of element refinement.

Refinement

In the situation of low mesh refinement the system does not represent the true situation well. This results in very noisy results as can be seen in the following figure.

Contact issues

If the refinement is high enough another issue presents itself. The contact model, which usually only sees one contact element, now sporadically sees multiple contact elements. These elements will both have a contact relationship with the target element, this results in a discontinuity in the contact relation. Which then results in an erroneous force. This phenomenon is clearly visible in figure C.9. The 2 lines represent the force of 1 pantograph on a catenary system with 2 contact wires.

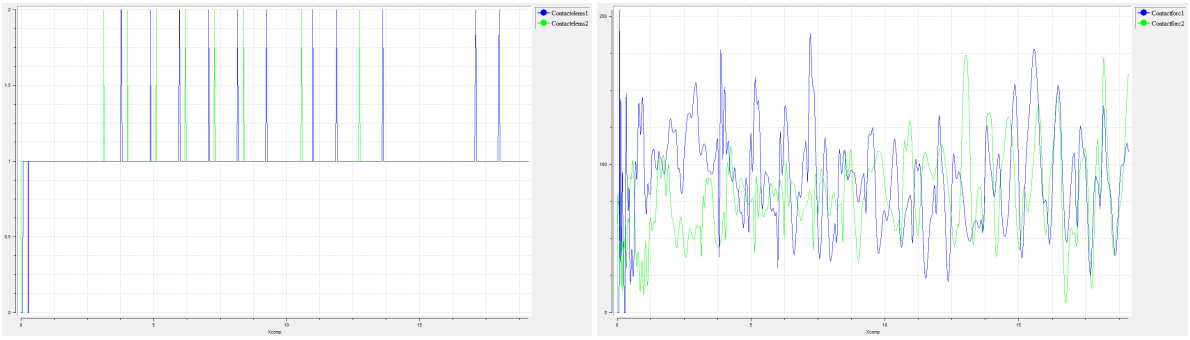

(a) Amount of elements in contact (b) Contact force

Figure C.9: Contact force output showing unwanted peaks in the amount of contacts found

C.0.2. Automated Ansys modeling

In order to create a model which can be easily used by others, it is a requirement that the model can be created without needing to go through the process of finding out how to make it. With this in mind, it is important that the modeling turns into a simple process, where settings are changed and the model is made. Also, the simulation process should be automated. These 2 will result in a simple (enough) process for everyone with some basic ansys and matlab knowledge to run a full simulation with his or her OCL model or pantograph.

The automated modeling process will be done through a Matlab code. The basic geometry of the OCL model will be input through a matlab file. In this file all the necessary geometric and material properties can be entered. A second matlab file is used to enter the Pantograph model, For both these files the running will result in a .mat file which is saved in the current directory. If the models are required for future use they do not need to be entered anymore but can be loaded from file.

The main .m file will then create the ansys code. Some basic settings such as amount of spans, pantographs and simulation speed can be entered and the Running will result in 4 text files, which can be entered into Ansys to run the full simulation. After the simulation is finished, results will be extracted and processed in the Post processor .M file. This process is visualised in the flow chart as can be seen in figure C.10. Therein the names of the .m Files and their version numbers can be found.

C.0.3. Large Model Simulation issues

During the process of modeling the system. The models with which simulations were run became significantly larger. This induced an issue which was not of importance in smaller models. The large system, using the same settings as smaller systems, becomes unstable. This is not a result of the model, but instead a result of the solver settings. The solver would find a converged situation where in reality the system became gradually more unstable. After some research it was found to be the result of too loose convergence criterion (L2) Changing to an infinite criterion, where every DOF needs to converge resulted in a stable system.

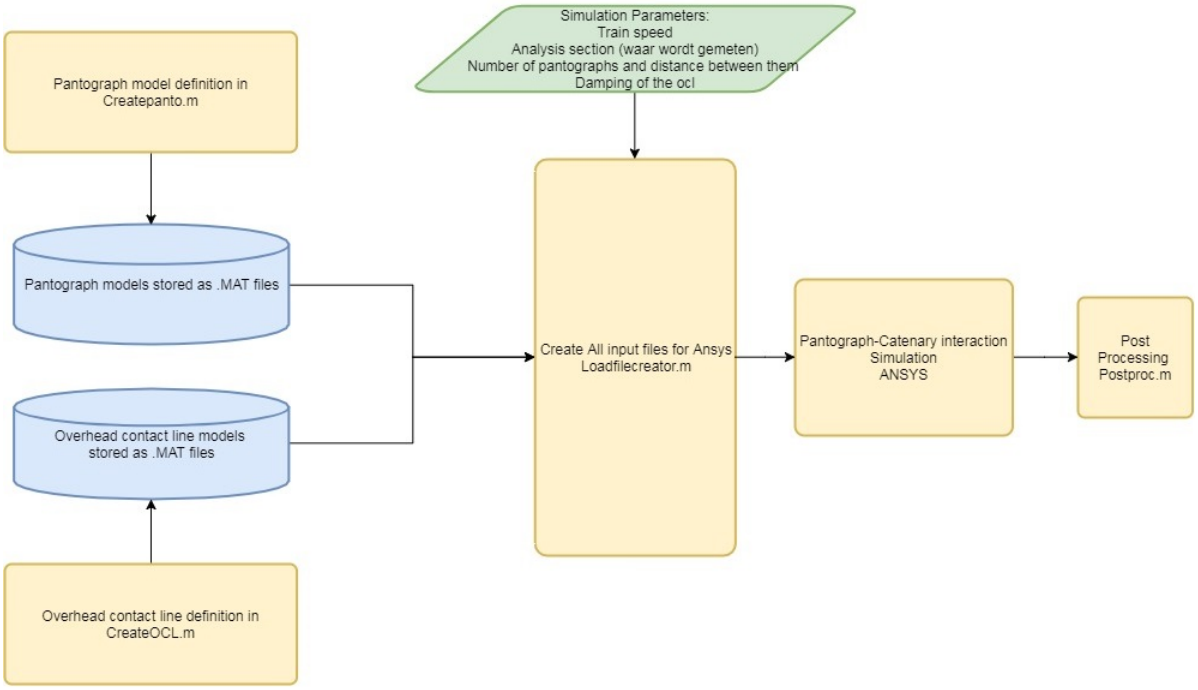

Figure C.10: Automated simulation flow chart

Model clarity

The reference models as defined in the norm EN50318:2016 lack some small parts of information. Therefore sometimes results are inadequate. For instance steady arm inclinations are not defined in the Reference models. In the end ten degrees of inclination are used, since this results in the best pre-sag (read closest to the reference).

D

Spring Decoupling and Time-history analysis on Modal system

D.1. Introduction

In this chapter, the modal reduction is performed on the full physical system. In section D.2, spring decoupling is to be tested in the modal domain. In section D.3, Time history analysis results are presented for a small amount of analyses. Further time history analyses have not been performed due to unpromising results in the early stages of time-history analysis of these models. Therefore, the modally reduced method is deemed inapplicable, w.r.t. simulation time improvements, to the Pantograph-Catenary simulation model. Furthermore, section D.5 contains the validation of the eigenmodes, the modes calculated in Matlab are compared to the eigenmodes calculated by Ansys. Where beam elements are represented by BEAM4 elements, and spring elements by COMBIN14 elements. BEAM4 elements do not allow linear perturbation analyses, these are calculated without pretension.

D.2. Dropper Decoupling in the Modal domain

In order to ensure quick time history iterations in Matlab it is essential that the non-linear dropper behaviour is added to the system without having to invert the entire admittance matrix. Adaptation of the Modal basis to ensure correct dropper behaviour needs to be studied. In figures D.1 and D.9b the first and sixth eigenmode of a fully coupled system, as well as a system with the first non-linear spring decoupled are shown. The modes specific to the decoupled spring, as they are found here in a controlled and small model, seem to show very local behaviour linked to a frequency which is not found in the fully coupled system. From this the preliminary conclusion can be drawn that the decoupled spring behaviour can easily be isolated from the rest of the system response. A test is done in which a fully coupled modal space V_c is used to perturb a 1-spring-decoupled stiffness matrix Z_{dc} in figure D.3b, as well as a 1-spring-decoupled modal space V_{dc} to perturb a fully coupled stiffness matrix Z_c in figure D.4a. To clarify, the control tests V_c, Z_c is in figure D.3a, V_{dc}, Z_{dc} is in figure D.4b.

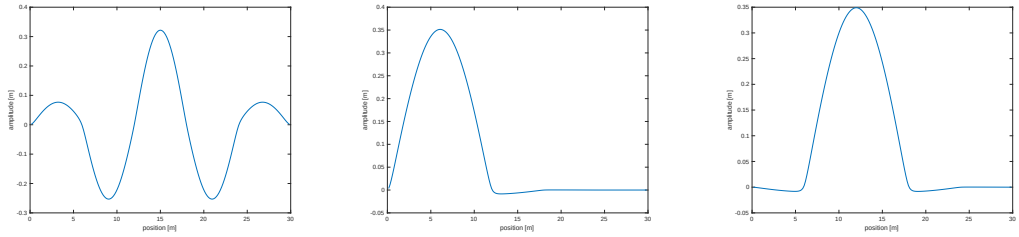

(a) all springs coupled $\omega = 26.33$ rad/s

(b) first spring decoupled $\omega = 13.29$ rad/s

(c) second spring decoupled $\omega = 13.29$ rad/s

Figure D.1: Mode 1

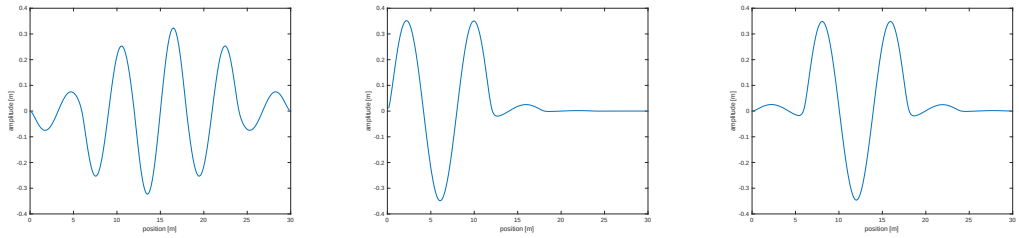

(a) all springs coupled $\omega = 54.19$ rad/s

(b) first spring decoupled $\omega = 40.66$ rad/s

(c) second spring decoupled $\omega = 40.66$ rad/s

Figure D.2: Mode 6

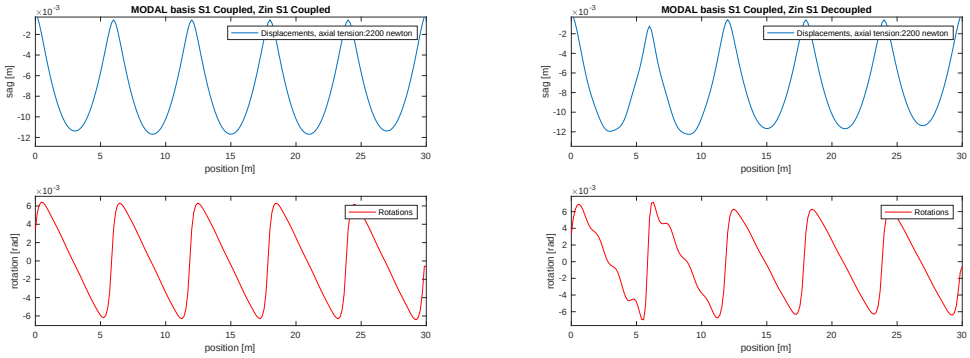

(a) Coupled Stiffness matrix (b) Decoupled Stiffness matrix

Figure D.3: Modal basis based on COUPLED stiffness matrix

Figure D.3b shows that when the modal basis does not incorporate movement at the decoupled dropper location, the movement is not observed. Therefore, simply changing the stiffness matrix is no longer sufficient when dealing with decoupling of droppers. In figure D.4a it shows that in a decoupled modal basis, changing only the stiffness matrix provides a result which approaches the fully coupled system V_C, Z_C from figure D.3a very close. Therefore, it can be concluded that decoupling, in a modal basis, does not work properly when the modal basis itself is not altered. However, it can also be concluded that coupling, in a modal basis, does work properly when the modal basis is not altered. For a validation of the eigenmodes as they are calculated by matlab, a comparison is made to Ansys eigenmodes in appendix D. The comparison is done for the non-pretensioned model. For the pretensioned model, a comparison is not fully representational since the large axial load the Ansys model will calculate axial strains as well, which is impossible for the Matlab model. Of this comparison it can be said that modal shapes and frequencies are alike, however not the same. A check of the proposed approach is in order, therefore a static simulation is done based on the first 40 modes of the fully coupled system, augmented with the 4 first modes of the decoupled system, therefore resulting in a 44 DOF system. Effectively using these modes involves interpolating between them every time step in order to create a continuously moving mode. In figure D.5 an interpolation procedure is shown, this interpolation takes place between the first eigenmode of the decoupled dropper numbers 2,3 and 4.

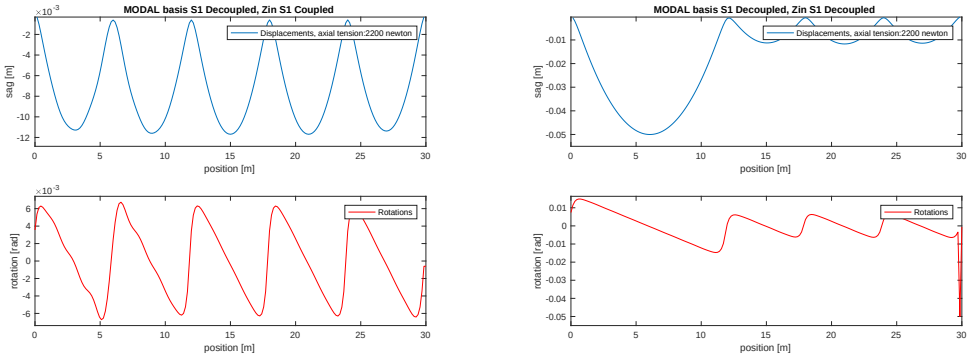

(a) Coupled Stiffness matrix (b) Decoupled Stiffness matrix

Figure D.4: Modal basis based on DECOUPLED stiffness matrix

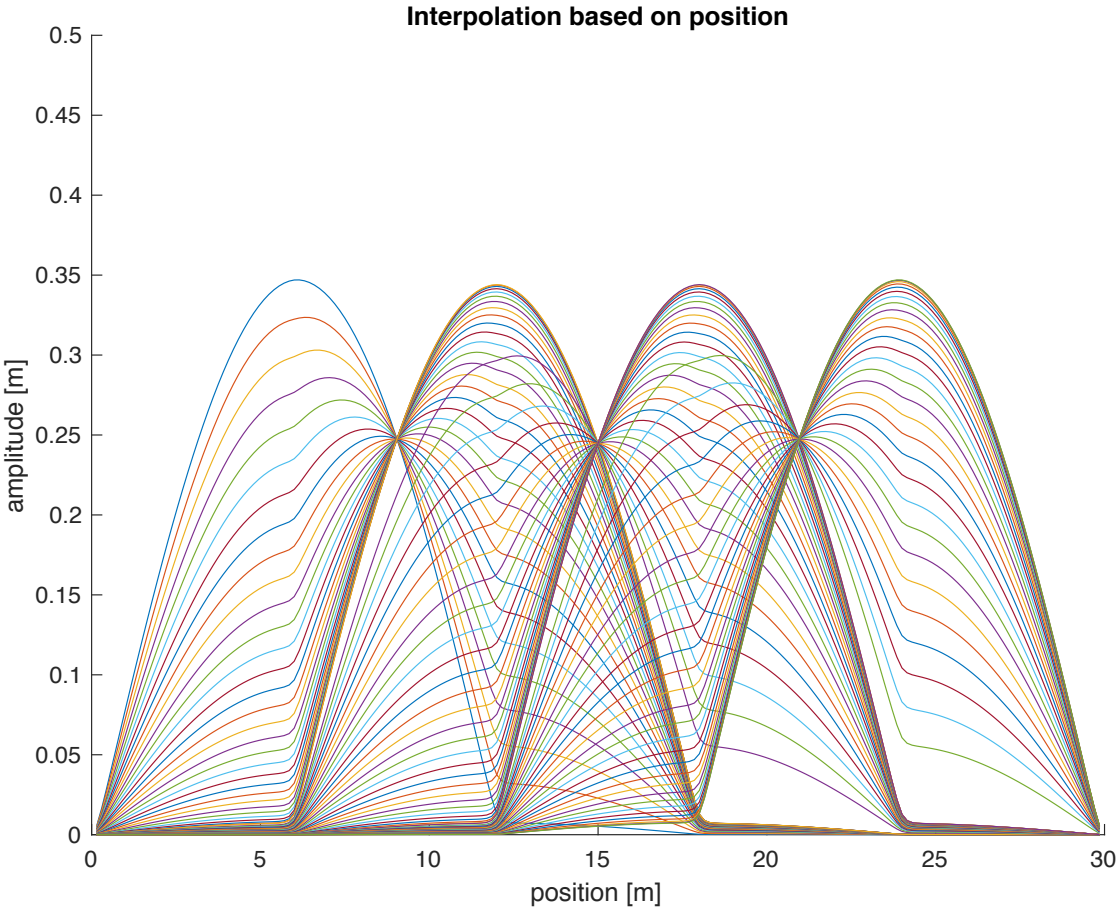

Figure D.5: Interpolation between the first decoupled modes, for neighbouring droppers

The interpolation, as shown in figure D.5, is performed using Hermite polynomials 1 and 3 (translational). This choice was made since these are also used to create the full FE matrices and thus the newly interpolated mode retains important properties such as mass and stiffness orthogonality with respect to the rest of the modes [32]. Furthermore, interpolation between two modes, if not done correctly, may result in energy dissipation. An initial check shows that the area encompassed by all interpolated modes remains the same between dropper 2 and 3. Towards dropper 4 a small decrease of 1.8 % is observed due to that mode being closer to the support, thus lacking a 'tail'.

D.3. Time history analysis of a modally reduced OCL model

In order to check whether the Modal reduction performs as desired, it is compared to the full system in a time history analysis over 30 meters of catenary. Dropper-decoupling is not incorporated in this analysis. Firstly, the full system simulation is performed at 200 elements (398 DOF), after which a reduction to 44 and 34 Vibration Modes is performed. At 34/44 Vibration modes, the modally reduced system shows reasonably good accuracy. Secondly, the full system simulation is performed at 400 elements (798 DOF), after which a reduction to 88 and 68 Vibration Modes is performed. Finally, the full system simulation is performed at 600 elements (1198 DOF), after which a reduction to 132 and 102 Vibration Modes is performed. The analyses are performed on exactly the same system every time, therefore, a modal reduction to 34 DOF will, in this method always suffice. However, generally systems will increase in size, thus increasing the amount of interface locations and required Vibration Modes is necessary. This increase is simulated by increasing the modal base linearly with the size of the full system. The results of these simulations are presented in table D.1.

	Method		
Elements	Full Physical system	Reduced	Reduced
200	0.86	1.12 (34 modes)	1.2 (44 modes)
400	3.03	5.04 (68 modes)	5.84 (88 modes)
600	12.08	14.74 (102 modes)	17.66 (132 modes)

Table D.1: Modal reduction simulations, by simulation time [s]

Inclusion of the dropper-decoupling in the modal analysis will require a re-projection of the stiffness matrix onto the modal basis. This will result in an increasing simulation time delay versus the times presented in table D.1.

D.4. Conclusion

During a time history analysis the system is excited by a moving load. The amount of interface DOFs is determined by the amount of locations where this excitation is applied. When using a pure modal basis, $V_m = [\phi_1 \phi_2 ... \phi_m]$ the movement of the system is based on free vibration shapes only. Very local excitations are not easily described by such systems. As a result, the pure modal basis V_m does not provide correct and accurate results when looking at the very near field. Far field results are accurate starting from 30 Vibration Modes for a 30m long system. The results have not shown significant simulation time improvements in this early stage and do not seem to scale favorably to larger models.

Furthermore, improving the modal base by adding Residual Attachment Modes to improve near-field behaviour, would require a RAM at every interface location (assuming non-parametric Residual Attachment Modes). With simulations easily spanning 5 or more seconds per run, at frequencies of 200-500 Hz this results in an added 1000 to 2500 or even more DOFs. Assuming the Residual Attachment Modes may be executed parametrically, this number could be improved. Unfortunately, the need to transform the load vector to the modal domain to provide input, as well as the back transformation of the results to the physical domain for visualisation purposes, provide high calculation overhead slowing down the model to a situation where modal reduction is not interesting (see results in table D.1). Further research will therefore no longer focus on modal reduction.

D.5. Validation of Vibration Modes

On the following pages, the Vibration Mode calculated in matlab are compared to the VM calculated in Ansys, see figures D.6 up to D.9. It can be seen that all VM are of similar shape. Therefore it is concluded that the calculated modes are correct.

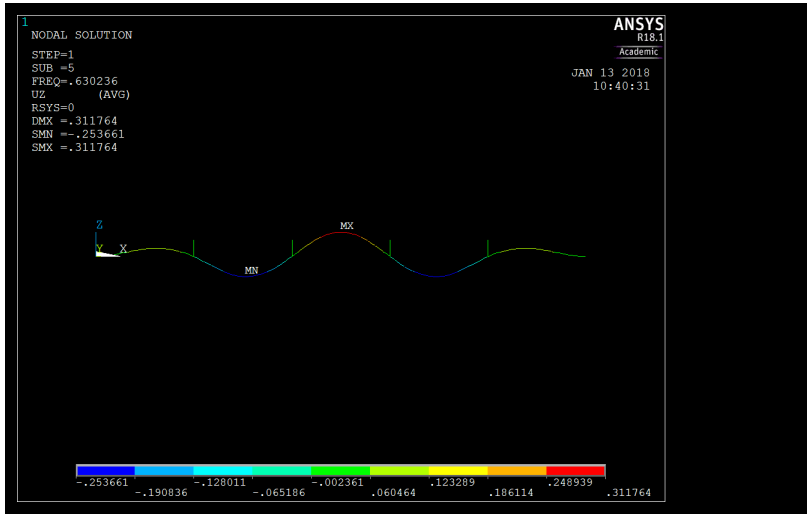

(a) first spring decoupled
ω = 3.95 rad/s

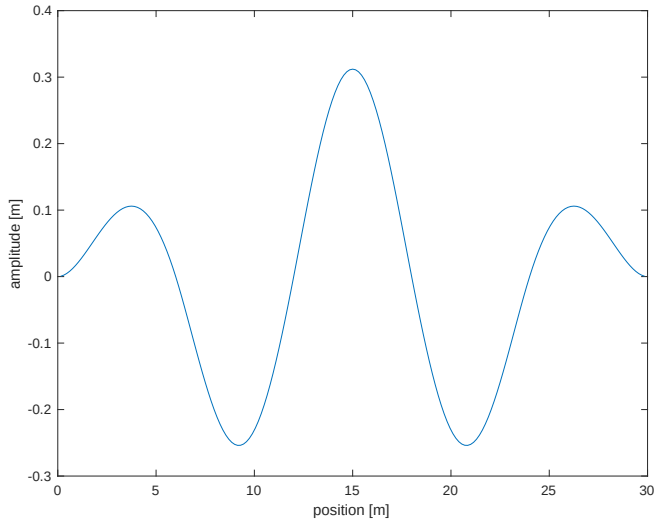

(b) All coupled
ω = 3.96 rad/s

Figure D.6: Mode 1 without axial load

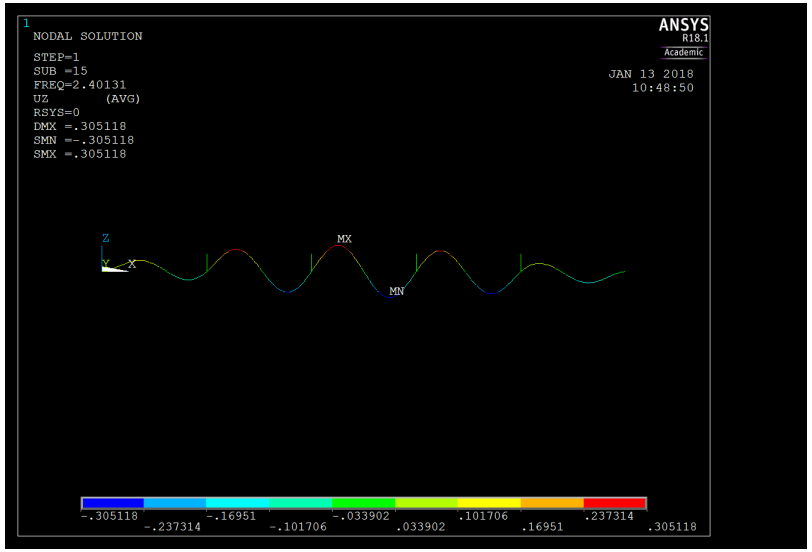

(a) first spring decoupled $\omega = 15.08$ rad/s

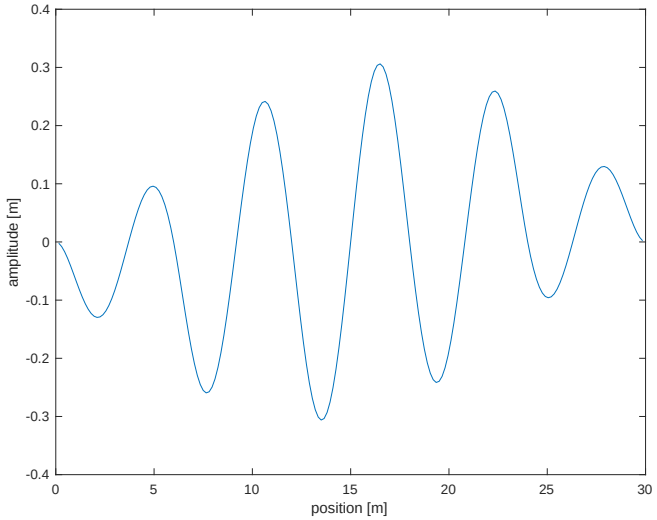

(b) All coupled $\omega = 15.13$ rad/s

Figure D.7: Mode 6 without axial load

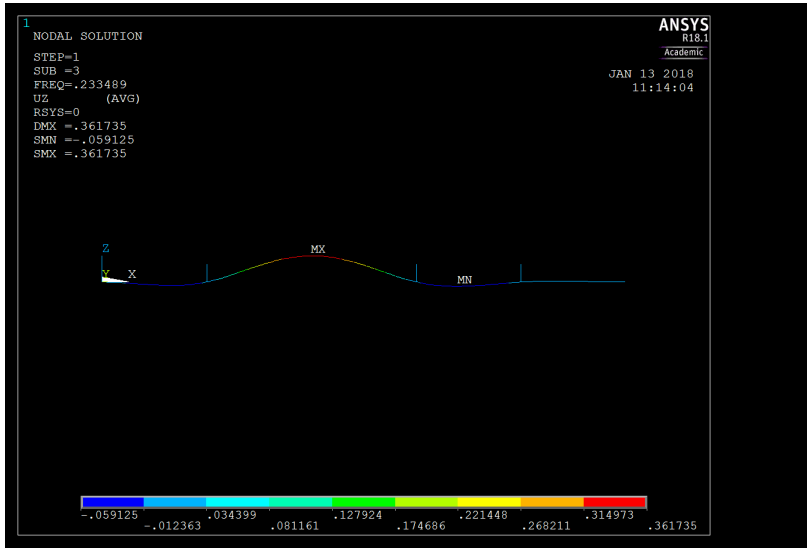

(a) first spring decoupled
ω = 1.46 rad/s

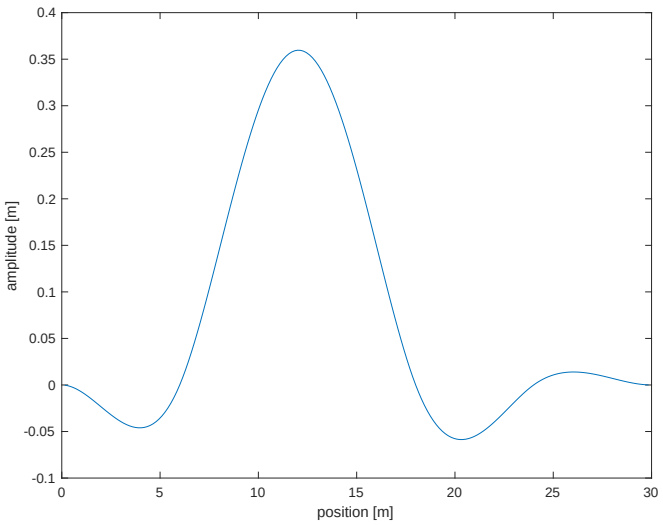

(b) second spring decoupled
ω = 1.46 rad/s

Figure D.8: Mode 1 without axial load

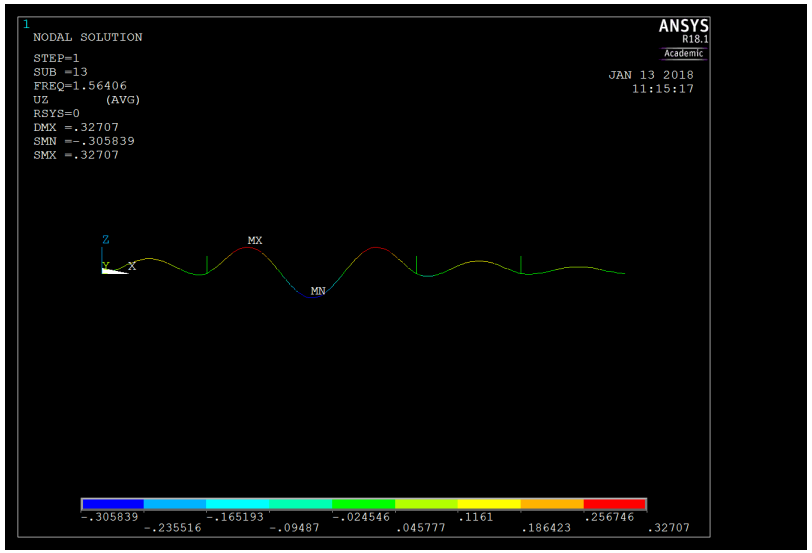

(a) first spring decoupled $\omega = 9.83$ rad/s

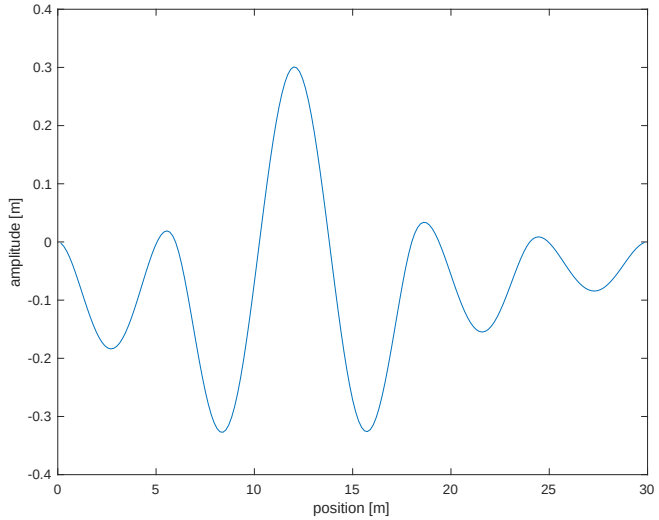

(b) second spring decoupled $\omega = 9.80$ rad/s

Figure D.9: Mode 6 without axial load

E

Simulation results for comparison

it,0	it,1	impl,0	impl,1
200			
5.44	5.65	3.47	6.08
5.21	5.16	3.22	5.16
5.42	5.12	3.29	4.78
400			
19.04	25.64	13.23	29.76
17.86	22.2957	11.526	25.3048
21.90	17.3871	11.5558	25.0213
600			
53.16	51.45	26.18	59.91
53.28	51.64	25.05	58.9696
52.54	51.84	24.837	56.12
600			
it,0	it,1	impl,0	impl,1
53.16	51.45	26.18	59.91
53.28	51.6419	25.0578	58.9696
52.54	51.84	24.837	56.12
800			
96.54	101.6018	42.27	123.01
105.2856	105.9863	42.56	121.92
108.4528	110.821	44.59	130.21
1000			
208.68	214.27	74.26	224.16
203.5068	211.60	79.73	230.62
207.148	214.72	73.40	222.81
1200			
314.935	317.08	130.5325	353.69
299.577	306.74	140.8493	350.83
313.27	305.48	133.1515	358.21
1400			
466.6155	477.16	237.12	575.75
455.5616	447.0093	238.26	547.96
460.13	487.73	224.15	592.49

Table E.1: Mesh scaleability in seconds [s]

0	it,0	it,1	impl,0	impl,1
0.01	1.14	1.22	0.53	1.7417
0.005	1.68	1.56	0.6845	1.2482
0.002	3.33	3.0179	1.82	2.8045
0.001	5.32	5.77	3.274	5.06
0.0005	10.15	10.3217	6.34	10.112
0.0002	25.20	25.9404	17.57	24.8093
0.0001	52.96	53.75	32.48	47.2271
0	it,0	it,1	impl,0	impl,1
0.01	1.3431	1.68	0.49	0.7923
0.005	1.42	1.63	0.71	1.1833
0.002	3.16	3.2018	2.10	2.89
0.001	5.29	5.35	3.76	5.05
0.0005	10.28	10.18	6.82	10.74
0.0002	21.73	22.28	14.78	22.47
0.0001	63.197	43.36	29.18	42.09
0	it,0	it,1	impl,0	impl,1
0.01	1.52	1.5238	0.62	0.98
0.005	1.45	1.61	0.68	1.14
0.002	3.29	2.85	1.65	2.82
0.001	5.30	5.25	3.29	5.10
0.0005	10.13	10.17	7.12	9.63
0.0002	26.05	21.56	14.68	21.19
0.0001	57.73	44.03	29.70	42.68
0	it,0	it,1	impl,0	impl,1
0.01	0.97	1.18	0.43	0.69
0.005	1.39	1.56	0.67	1.14
0.002	3.09	3.24	1.82	2.93
0.001	5.42	5.18	3.25	5.07
0.0005	10.30	10.15	6.37	9.59
0.0002	22.31	21.85	15.33	22.60
0.0001	66.54	44.17	30.10	44.58

Table E.2: Time Step scaleability in seconds [s]

vsim	it,0	it,1	impl,0	impl,1
6	13.2658	11.45	5.84	11.7
7.5	10.11	11.49	5.97	12.88
10	10.15	11.4678	5.98	12.76
15	10.49	11.67	6.15	10.92
30	10.1096	11.19	5.94	13.17
60	9.80	11.09	6.11	9.86
120	9.34	10.51	5.87	10.17
	it,0	it,1	impl,0	impl,1
6	10.07	11.71	6.28	13.39
7.5	9.97	11.46	6.16	12.93
10				
15	10.05	11.25	6.4	12.75
30	9.25	11.02	5.92	12.94
60	12.31	12.29	5.97	11.93
120	9.66	10.22	5.94	10.19
	it,0	it,1	impl,0	impl,1
6	9.38	11.89	6.22	12.81
7.5	10.37	11.75	6	12.97
10				
15	10.41	11.23	5.88	12.7
30	9.99	11.3	5.94	13.04
60	10.3903	11.76	8.69	10.93
120	9.89	10.05	5.92	12.91
	it,0	it,1	impl,0	impl,1
6	10.15	11.65	6.05	12.89
7.5				
10				
15	10.44	11.25	5.88	13.02
30	12.99	11.37	5.88	12.63
60	8.44	11.75	6.18	13.88
120	9.39	10.84	6.05	12.88

Table E.3: Velocity scaleability in seconds [s]

CC	it,0	it,1	impl,0	impl,1
10	3.13	2.87	5.78	13.61
1	9.89	11.27	6.06	13.04
0.1	10.1655	11.06	5.89	13.28
0.01	10.53	11.89	5.77	12.95
0.001	12.17	15.38	5.98	11.02
0.0001	14.7	17.43	5.84	13.2
0.00001	16.05	21.04	5.9	12.97
10	2.93	2.89	6.42	12.24
1	10.07	11.08	5.92	12.04
0.1	9.65	10.87	5.8	10.67
0.01	10.03	11.66	6.17	10.93
0.001	12.19	15.11	5.89	10.89
0.0001	14.66	19.75	6.01	13.11
0.00001	15.71	24.47	5.91	12.96
10	3.43	2.94	6.06	12.84
1	10.14	11.24	6.07	13.15
0.1	9.69	9.91	5.89	10.8
0.01	10.31	10.44	5.88	12.79
0.001	10.66	15.32	5.95	11.22
0.0001	14.79	19.68	5.85	13.7
0.00001	17.78	21.26	5.87	13.04
10				
1	10.31	11.53	6.09	13.18
0.1	9.66	11.31	5.82	12.67
0.01	10.14	11.97	5.99	12.88
0.001	11.81	14.1	5.87	11.16
0.0001	13.54	19.8	6.26	12.85
0.00001	17.68	20.97	5.94	11.45

Table E.4: Convergence criterion scaleability in seconds [s]

F

Contact model comparison simulation process

In order to reduce the amount of files that need to be saved, the process for reproduction of the results presented in chapter 9 is explained in the following sections.

NOTE that the exact same results will likely not be found twice since simulation performance is dependent of the hardware as well as other circumstantial variables.

F.1. Contact model simulation process

This process is described compactly, therefore measures to ensure stability are not shown here. It is assumed that people attempting to replicate this test are known with the Ansys software and will take their own preventive measures if instability occurs.

1. Run LOADFILECREATOR_V_0_0_2 with settings and models
    - OCLTYPE: B4+
    - OCLVER: CONTACT
    - PANTOVER: Generic
    - PANTOTYPE: Panto
    - PANTOAMOUNT: 1
    - SPANS: 1/2, input value times 2 is the amount of spans that are made.
    - REFINEMENT: 10
    - CARRYREFINEMENT: 4
2. Note that a file named ”1run.txt” is made
3. Open ANSYS 18.1 and >file>read input from> 1run.txt,
4. Copy and paste the following in to the command window
    - d,10,uz,0
    - /SOL
      !*
      OUTPR,ALL,ALL,
      ANTYPE,4
      NLGEOM,1
      DELTIM,0.00001,0.0000000001,0.1
      OUTRES,ERASE

OUTRES,NSOL,ALL
OUTRES,RSOL,ALL
OUTRES,V,ALL
OUTRES,A,ALL
OUTRES,ESOL,ALL
OUTRES,NLOA,ALL
OUTRES,STRS,ALL
OUTRES,EPEL,ALL
OUTRES,EPTH,ALL
OUTRES,EPPL,ALL
OUTRES,EPCR,ALL
OUTRES,FGRA,ALL
OUTRES,FFLU,ALL
OUTRES,MISC,ALL
ALPHAD,0.8
KBC,0
TIME,10
CNVTOL,U„0.000001,0
CNVTOL,ROT„0.000001,0
CNVTOL,F„0.000001,0
CNVTOL,M„0.000001,0
OUTPR,ALL,ALL,
NLHIST,pair,contactFORCREAR,cont,pres,10
NLHIST,pair,contactELEMSREAR,cont,ELCN,10
NLHIST,nsol,xcompREAR,u,x,10
nlhist,nsol,REARHEIGHT,u,z,10
NLHIST,pair,contactFORCFRONT,cont,pres,11
NLHIST,pair,contactELEMSFRONT,cont,ELCN,11
NLHIST,nsol,xcompFRONT,u,x,20
nlhist,nsol,FRONTHEIGHT,u,z,20

- LSWRITE,1
- ALPHAD,0.0125
- DELTIM,0.01,0.01,0.01 ! this value may be changed according to the frequency of interest
- ddele,10,uz F,11,FZ,287.34 D,10,VELX,50

5. TIME,10.1
6. Then choose to load the system in 1 step or in multiple steps

- LSWRITE,4,
  TIME,10.2
  LSWRITE,5,
  TIME,10.3
  LSWRITE,6,
  TIME,10.4
  LSWRITE,7,
  TIME,10.5
  LSWRITE,8,
  TIME,10.6

LSWRITE,9,
TIME,10.7
LSWRITE,10,
TIME,10.8
LSWRITE,11,
TIME,10.9
LSWRITE,12,
TIME,11
LSWRITE,13,
TIME,11.1
LSWRITE,14,
TIME,11.2
LSWRITE,15,
TIME,11.3
LSWRITE,16,
TIME,11.4
LSWRITE,17,
TIME,11.5
LSWRITE,18,
TIME,11.6
LSWRITE,19,
TIME,11.7
LSWRITE,20,
TIME,11.8
LSWRITE,21,
TIME,11.9 LSWRITE,22,
TIME,12
LSWRITE,23,

- TIME,12 LSWRITE,2,

7. Then run either LSSOLVE,1,23,1
8. Or LSSOLVE,1,2,1
9. after the solver is finished, investigate the Jobname.MNTR file, there the WALL variable shows the elapsed time at every Load- and sub-step.

F.2. Direct approach simulation process

1. Run LOADFILECREATOR_V_0_0_2 with settings and models
    - OCLTYPE: B4+
    - OCLVER: CONTACT
    - PANTOVER: Generic
    - PANTOTYPE: Panto
    - PANTOAMOUNT: 1
    - SPANS: 1/2, input value times 2 is the amount of spans that are made.
    - REFINEMENT: 10
    - CARRYREFINEMENT: 4
2. Note that a file named ”1run.txt” is made

3. Open ANSYS 18.1 and >file>read input from> 1run.txt,
4. Copy and paste the following in to the command window

- d,10,uz,0
- /SOL
  !*
  OUTPR,ALL,ALL,
  ANTYPE,4
  NLGEOM,1
  DELTIM,0.00001,0.0000000001,0.1
  OUTRES,ERASE
  OUTRES,NSOL,ALL
  OUTRES,RSOL,ALL
  OUTRES,V,ALL
  OUTRES,A,ALL
  OUTRES,ESOL,ALL
  OUTRES,NLOA,ALL
  OUTRES,STRS,ALL
  OUTRES,EPEL,ALL
  OUTRES,EPTH,ALL
  OUTRES,EPPL,ALL
  OUTRES,EPCR,ALL
  OUTRES,FGRA,ALL
  OUTRES,FFLU,ALL
  OUTRES,MISC,ALL
  ALPHAD,0.8
  KBC,0
  TIME,10
  CNVTOL,U„0.000001,0
  CNVTOL,ROT„0.000001,0
  CNVTOL,F„0.000001,0
  CNVTOL,M„0.000001,0
  OUTPR,ALL,ALL,
  NLHIST,pair,contactFORCREAR,cont,pres,10
  NLHIST,pair,contactELEMSREAR,cont,ELCN,10
  NLHIST,nsol,xcompREAR,u,x,10
  nlhist,nsol,REARHEIGHT,u,z,10
  NLHIST,pair,contactFORCFRONT,cont,pres,11
  NLHIST,pair,contactELEMSFRONT,cont,ELCN,11
  NLHIST,nsol,xcompFRONT,u,x,20
  nlhist,nsol,FRONTHEIGHT,u,z,20
- LSWRITE,1
- ALPHAD,0.0125
- DELTIM,0.01,0.01,0.01 ! this value may be changed according to the frequency of interest
- TIME,10.1
  FDELE,100001,FZ
  F,100011,FZ,150

```
LSWRITE,2,
TIME,10.2
FDELE,100011,FZ
F,100021,FZ,150
LSWRITE,3,
TIME,10.3
FDELE,100021,FZ
F,100031,FZ,150
LSWRITE,4,
TIME,10.4
FDELE,100031,FZ
F,100041,FZ,150
LSWRITE,5,
TIME,10.5
FDELE,100041,FZ
F,100051,FZ,150
LSWRITE,6,
TIME,10.6
FDELE,100051,FZ
F,100061,FZ,150
LSWRITE,7,
TIME,10.7
FDELE,100061,FZ
F,100071,FZ,150
LSWRITE,8,
TIME,10.8
FDELE,100071,FZ
F,100081,FZ,150
LSWRITE,9,
TIME,10.9
FDELE,100081,FZ
F,100091,FZ,150
LSWRITE,10,
TIME,11
FDELE,100091,FZ
F,100101,FZ,150
LSWRITE,11,
TIME,11.1
FDELE,100101,FZ
F,100111,FZ,150
LSWRITE,12,
TIME,11.2
FDELE,100111,FZ
F,100121,FZ,150
LSWRITE,13,
TIME,11.3
FDELE,100121,FZ
F,100131,FZ,150
LSWRITE,14,
```

```
TIME,11.4
FDELE,100131,FZ
F,100141,FZ,150
LSWRITE,15,
TIME,11.5
FDELE,100141,FZ
F,100151,FZ,150
LSWRITE,16,
TIME,11.6
FDELE,100151,FZ
F,100161,FZ,150
LSWRITE,17,
TIME,11.7
FDELE,100161,FZ
F,100171,FZ,150
LSWRITE,18,
TIME,11.8
FDELE,100171,FZ
F,100181,FZ,150
LSWRITE,19,
TIME,11.9
FDELE,100181,FZ
F,100191,FZ,150
LSWRITE,20,
TIME,12
FDELE,100191,FZ
F,100201,FZ,150
LSWRITE,21,
```

5. run LSSOLVE 1,21,1
6. after the solver is finished, investigate the Jobname.MNTR file, there the WALL variable shows the elapsed time at every Load- and sub-step.